

A STUDY OF THE STRENGTH OF TUNGSTEN
CARBIDE-COBALT ALLOYS FROM A FRACTURE
MECHANICS VIEWPOINT

THESIS FOR THE DEGREE
OF Ph. D

MICHIGAN STATE UNIVERSITY

ROY CARL LUETH

1972

This is to certify that the

thesis entitled

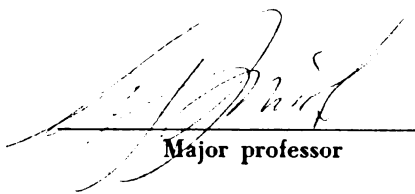
A STUDY OF THE STRENGTH OF TUNGSTEN CARBIDE -
COBALT ALLOYS FROM A FRACTURE MECHANICS VIEWPOINT

presented by

ROY C. LUETH

has been accepted towards fulfillment
of the requirements for

Ph.D. degree in Metallurgy


Major professor

Date 12 May 72

ABSTRACT

A STUDY OF THE STRENGTH OF TUNGSTEN CARBIDE-COBALT ALLOYS FROM A FRACTURE MECHANICS VIEWPOINT

By

Roy Carl Lueth

The critical strain energy release rate and stress intensity parameter have been determined for nine tungsten carbide-cobalt alloys by a wedge loaded double cantilever beam test. The nine alloys studied had uniform average grain sizes ranging from 1.5 to 8 microns, and cobalt contents from 3 to 15 wt. percent. The implications of these data have been discussed as they affect the theories of strength of cemented carbides.

The critical strain energy release rate depends on the energy absorbed in the area adjacent to the tip of a metastable crack in the material. The energy absorbed at the tip of the crack depends on the amount of plastic work done on the binder contained in the plastic yield zone, as no flow was detected in the tungsten carbide

particles. The amount of plastic work done on the binder in the yield zone is dependent on the volume of binder which plastically flows, which in turn is dependent on the binder film thickness, and the number of grains (and binder films) the plastic zone includes. As a result, the critical strain energy release rate generally increases as the binder film thickness increases. The mode of fracture of a tungsten carbide-cobalt alloy varies widely depending on several compositional and microstructural factors. If the plastic zone radius is less than one grain diameter, then the alloy will fail through the binder, regardless of the carbide grain size. If the plastic zone size is large enough to include several grains, then the failure mode will depend on the carbide grain strength; the larger grained alloys (weak grains) will fail through grain fracture, the smaller grained alloys will fail through ductile binder failure. Medium grain size alloys with large plastic zone sizes will fail with various amounts of the above modes, depending on cobalt content and grain size. The larger the cobalt content and the larger the grain size the more fracture will tend to be transgranular.

The strength of these alloys in tension depends on the inherent flaw size, yield strength, and fracture toughness. The shape of the transverse rupture strength versus binder film thickness curve is a necessary result of these factors. The compressive strength of these alloys is dependent on carbide grain strength and dislocation density in the binder at the failure stress. The stress imposed on the grains of tungsten carbide-cobalt alloys has been found to be constant for a given grain size regardless of cobalt content, and as a result the compressive strength will rise as the binder film thickness goes down for a given grain size.

A STUDY OF THE STRENGTH OF TUNGSTEN
CARBIDE COBALT ALLOYS FROM A FRACTURE
MECHANICS VIEWPOINT

By

Roy Carl Lueth

A THESIS

Submitted to
Michigan State University
in partial fulfillment of the requirements
for the degree of

DOCTOR OF PHILOSOPHY

Department of Metallurgy,
Mechanics and Materials Science

1972

575778

© Copyright by
ROY CARL LUETH
1972

ACKNOWLEDGMENTS

The author would like to express his gratitude to Dr. A. J. Smith for his assistance during this work, and also to the staff of the Hard Metals Research section of the General Electric Metallurgical Products Department, especially Mr. William A. Powell who supplied the test material; and Dr. E. W. Goliber and Mr. T. E. Hale for many helpful and stimulating discussions.

A special appreciation is expressed to G. F. Paluch who conducted most of the test work and R. J. Wills who did all of the microscopy and photographic work, and to Dr. Robert Little who contributed a great deal more than technical assistance to this project.

TABLE OF CONTENTS

INTRODUCTION -----	1
THEORY OF STRENGTH OF TUNGSTEN CARBIDE-COBALT ALLOYS -----	12
SUBJECT RESEARCH -----	43
EXPERIMENTAL PLAN -----	44
COMPLIANCE CALIBRATION -----	46
LOAD MEASURING SYSTEM -----	46
DISPLACEMENT MEASURING SYSTEM -----	47
MEASUREMENT OF DATA AND TREATMENT -----	48
EFFECT OF MODULUS ON COMPLIANCE -----	51
TEST PROCEDURE -----	54
RESULTS AND DISCUSSION -----	58
CONCLUSIONS -----	83
BIBLIOGRAPHY -----	85
APPENDIX I THE DOUBLE CANTILEVER BEAM TEST --	87
APPENDIX II MATERIALS USED -----	122
APPENDIX III APPARATUS AND SETUP -----	126
APPENDIX IV FRACTOGRAPHS -----	129

LIST OF TABLES

Table		Page
I	Strength of Tungsten Carbide-Cobalt Alloys Assuming Cobalt to Govern, No Size Effect, Carbide Infinitely Strong	32
II	Physical Property Data	59
III	The Effect of Plastic Zone Size on Mode of Fracture	65
IV	Compressive Strength Data	73
V	Material Structure Data	122

LIST OF FIGURES

Figure		Page
1	System W-Co-C Section at 1400°C (2550°F)	9
2	Quasi-Binary WC-Co Diagram	11
3	Transverse Rupture Strength Versus Mean Free Path	17
4	Effect of Test Procedure Upon Relationship Between Compressive Strength and Hardness for Various WC-Co Alloys	20
5	Diagrammatic Representation of Thermal Stresses in Carbide and Cementing Phases of WC-Co Alloys	22
6	Dislocation By-Pass Model for Calculating Orowan's Stress	28
7	A Comparison of the Observed Yield Stresses in Shear of WC-Co Alloys with the Theoretical Values for the Dispersed Particle Strengthening	30
8	Effects of Carbon Content on the Strength of WC 10% Co Alloy Having Mean Grain Size of 2.2 Microns	35
9	Compressive Strength as a Function of Percent WC (Gurland)	39

Figure		Page
10	Compliance Versus Crack Length	50
11	Stress Strain Curve for 15% Co 1.5 Micron Grain Size Alloy in Compression	57
12	Critical Strain Energy Release Rate Versus Binder Film Thickness for WC-Co Alloys	61
13	Compressive Stress Versus the Fourth Root of Plastic Strain	69

APPENDIX III

Figure		
1	Test Sample and Calibration Wedge	126
2	Test Apparatus	127
3	Apparatus for Calibration of Instrumented Wedge	128

LIST OF SYMBOLS

μ	-	Microns
γ	-	Surface Energy
σ	-	Normal Stress
τ	-	Shear Stress
F	-	Force
$\Delta\delta$	-	Displacement
λ	-	Compliance
P	-	Load
G	-	Shear Modulus
E	-	Modulus of Elasticity
G_{Ic}	-	Critical Strain Energy Release Rate
K_{Ic}	-	Critical Stress Intensity Parameter
ν	-	Poisson's Ratio
ϵ	-	Strain
v	-	Crack Opening Displacement

INTRODUCTION

Tungsten carbide-cobalt alloys are liquid-phase sintered compacts consisting of 3 to 25% cobalt, the remainder being tungsten monocarbide. The cobalt appears as a thin binder film 0.1 to 1.0 μ thick between irregularly shaped tungsten monocarbide particles 1 to 5 μ in diameter. This type of composite enables many of the best properties of each component to be realized--the result being an extremely hard, strong material, the major disadvantage being the brittle or semibrittle nature of the fracture.

The cobalt in these alloys, because of the restraint which this phase sees, remains in an F.C.C. configuration at room temperature rather than in its equilibrium H.C.P. structure. It also contains percentages of carbon and tungsten in solution, the amounts depending on process variables. The tungsten monocarbide, which is an H.C.P. structure with the carbon arranged in the interstices, is virtually free of dissolved cobalt.

These materials have the highest compression strength of any commercially available material. Because of their strength and their extremely good wear resistance, they are without equal as materials for rock drilling and similar

applications. These composites, because of their strength, hardness and relatively good toughness over a large temperature range, have found great use in other fields such as metalcutting and metalforming operations. They have become and will continue to be the prime materials where this combination of properties of wear resistance, hardness and strength can best be exploited in industry.

The fracture mechanisms are not well understood in these alloys. Such things as failure criteria, initiation points, and fracture paths have been the subject of much research; however, a large number of conflicting ideas are in evidence in the literature. If these mechanisms and criteria were better understood, the alloys could be used more effectively as this would come into play during the design stage of industrial equipment. Furthermore, the proper existing grade best used in any specific application could be better selected using the design data of existing equipment.

Many theories have been advanced which propose to elucidate the mechanisms of fracture in tungsten carbide-cobalt alloys--these have met with varying success in attempting to fit experimental data. The main theories will be dealt with at some length. First, however, to

gain some awareness of the complex nature of these alloys, the process variables and how they can affect the results of any mechanical test, and thus any theory to explain these mechanical test results, will be explored.

There are two main areas where processing variables can enter into the resultant mechanical properties.

First, consider the mechanical preparation of the alloys.

Prior to sintering, the material is in a powder form. The preparation of this powder is critical to the final product. During processing of the raw powders contamination is the greatest danger. This contamination consists of foreign materials getting into the raw powders. Also contamination occurs in storage drums, pickup of iron, etc. After the raw powder has been prepared, a fugitive binder is added to facilitate compaction of the powder. This binder is usually paraffin and is mixed with the tungsten carbide-cobalt powder. This can be a critical step, as without careful control, the powder could be put into lumps which will be very detrimental to the pressing operation. Also this procedure creates heat and, due to the powder's low oxidation resistance, if the powder is exposed to air this can cause oxidation. The powder is then screened and granulated for better flow in the

automatic presses. Here care again must be taken to avoid contamination. The granules must also be of a certain "hardness"--if they are too "hard" they will not flow properly and during pressing voids may result. The high cobalt materials are less sensitive to flaws during the mechanical handling processes and, in general, produce better compacts. It is harder to get a good compact with low cobalt grades. The finer the powder the poorer the flowing characteristics--shrinkage is greater and they are harder to compact, and thus more susceptible to voids. The fine powders sinter better as there is a greater surface area to volume ratio and thus a greater driving force. They do shrink more, however, due to pressing difficulties. The coarse powders during sintering will shrink approximately 15%, the fine about 18%. It can be seen from this very brief discussion that getting a mechanically sound (free from macroflaws) product can be difficult and that the difficulties increase with alloys of lower cobalt content and finer grain size (finer tungsten carbide powders). Thus in comparing the failure characteristics of alloys of different compositions, it should be recognized that there may be a systematic variation in soundness of the material (freedom from flaws).

The other area which is critical for good mechanical properties is the chemical and metallurgical interactions during sintering. The development of a dense, strong material in the tungsten carbide-cobalt system is accomplished via liquid phase sintering. In tungsten carbide-cobalt alloys, the eutectic reaction between tungsten carbide and cobalt forms the liquid as the temperature is raised; the position of this eutectic depends on such things as composition, free carbon, etc. This liquid penetrates between the tungsten carbide particles due to capillary action. The driving force for this effect is the reduction of surface free energy. The penetration of the liquid is dependent on the differences in free energy of the various surface interfaces, such as gas solid, liquid solid, solid solid. This can be expressed as the angle of contact of the liquid with the solid. The smaller the angle the larger the reduction in free energy by replacing a solid gas interface with a liquid solid interface. The angle of contact of a liquid solution of tungsten carbide and cobalt with solid tungsten carbide is essentially zero. This is a major factor in achieving up to 99.9 theoretical density. All other sintering mechanisms still operate, however, such as solution and reprecipitation, volume

diffusion, etc., but they play a more or less secondary role in the densification. A much more complete discussion of sintering mechanisms and processes can be found in reference (1) (Schwartzkopf).

There are several phenomena which may be observed in the final product which are detrimental to good mechanical properties. First consider several types of porosity. By convention the industry refers to porosity as being one of three types. The first type is termed "A" porosity and is observed as pores less than 10μ in diameter. This type of porosity can have several causes. It can result from incomplete penetration of the liquid between the particles of carbide and can be alleviated by raising the sintering temperature, thereby reducing the contact angle of cobalt on tungsten carbide, thus increasing the activity of the liquid. The second, a so-called "B" type porosity, refers to holes larger than 10μ . "B" type porosity may be a gross version of "A" type porosity. If caused by incomplete penetration of the liquid phase, it could be corrected by remilling to break down the aggregates or by increasing the sintering temperature. "B" type porosity may also be due to gas pockets formed at liquid phase sintering temperatures. Other causes are large oxide patches and pressing

voids which have partially closed. The last type of porosity to be discussed is type "C". It is not really porosity but rather precipitated graphite, much like that which occurs in cast iron. This morphology appears when the free carbon is above 0.05%. For free carbon below 0.05%, it occurs in clusters on cooling, frequently outlining the cobalt grain boundaries.

Even with elimination of porosity in the sintering process, the final product may not be acceptable. Segregation of the cobalt may appear. This is termed "binder laking", and appears in conjunction with rounded carbide grains. If we continue to "soak" the compact the mobility of the binder is increased and more tungsten carbide goes into solution. This allows the binder to flow properly, and laking will be eliminated. As the compact cools, the tungsten carbide will precipitate on existing grains and they will become more angular. When laking is eliminated and tungsten carbide crystal growth advanced, the properties are found to be in the optimum range for that particular grade. Soaking for too long a time can cause excessive grain growth to the point of being detrimental to properties. Further heating will cause density to drop off as bloating of the compact occurs due to residual gases and increased

binder activity. Both of these can affect mechanical properties in a negative manner.

Carbon control is another extremely important parameter in the sintering operation. As can be seen from a ternary isothermal section of the equilibrium phase diagram (Figure 1), the system cobalt-tungsten carbide-carbon is quite complex containing several different phases. For tungsten carbide-cobalt alloys, the narrow region connecting tungsten carbide to cobalt is the working area of the diagram. The region of equilibrium for tungsten carbide-cobalt is very narrow, and above this region (toward the C corner) free carbon will exist; with tungsten carbide-cobalt alloys, below this region several carbon deficient phases exist. The only one of interest to tungsten carbide-cobalt alloys is eta phase, as any one of the other three are observed only in rare occasions, and then only when the sintering process has gone far from the desirable one. Eta phase is $\text{Co}_3\text{W}_3\text{C}$ and is a member of the M_6C family. Eta phase grows in an uncontrolled manner at the expense of the binder phase and appears in macroscopic proportions. Eta phase does show good corrosion resistance but is extremely detrimental to mechanical properties. A vertical quasi-binary diagram taken through the tungsten carbide-cobalt

region is shown in Figure 2. The reactions occurring during sintering are discussed in detail by Schwartzkopf, and will not be given here. To produce a quality carbide, precise carbon control must be exercised. From our previous discussion it can be observed that a deviation of $\pm 0.06\%$ carbon can have great consequences with respect to mechanical properties. This can also cause surface effects which will change the normal strength characteristics.

Considering all of the above factors in any testing program, especially those which involve surface, strength such as transverse rupture testing, care must be taken not only to evaluate the quality of the general microstructure but surface conditions as well. When comparing the fracture characteristics of alloys of different composition the greater susceptibility of some composition ranges to porosity, etc., must be carefully appraised and such matters as binder migration within the test specimen must be avoided. All of these factors must be considered in any explanation of testing phenomena.

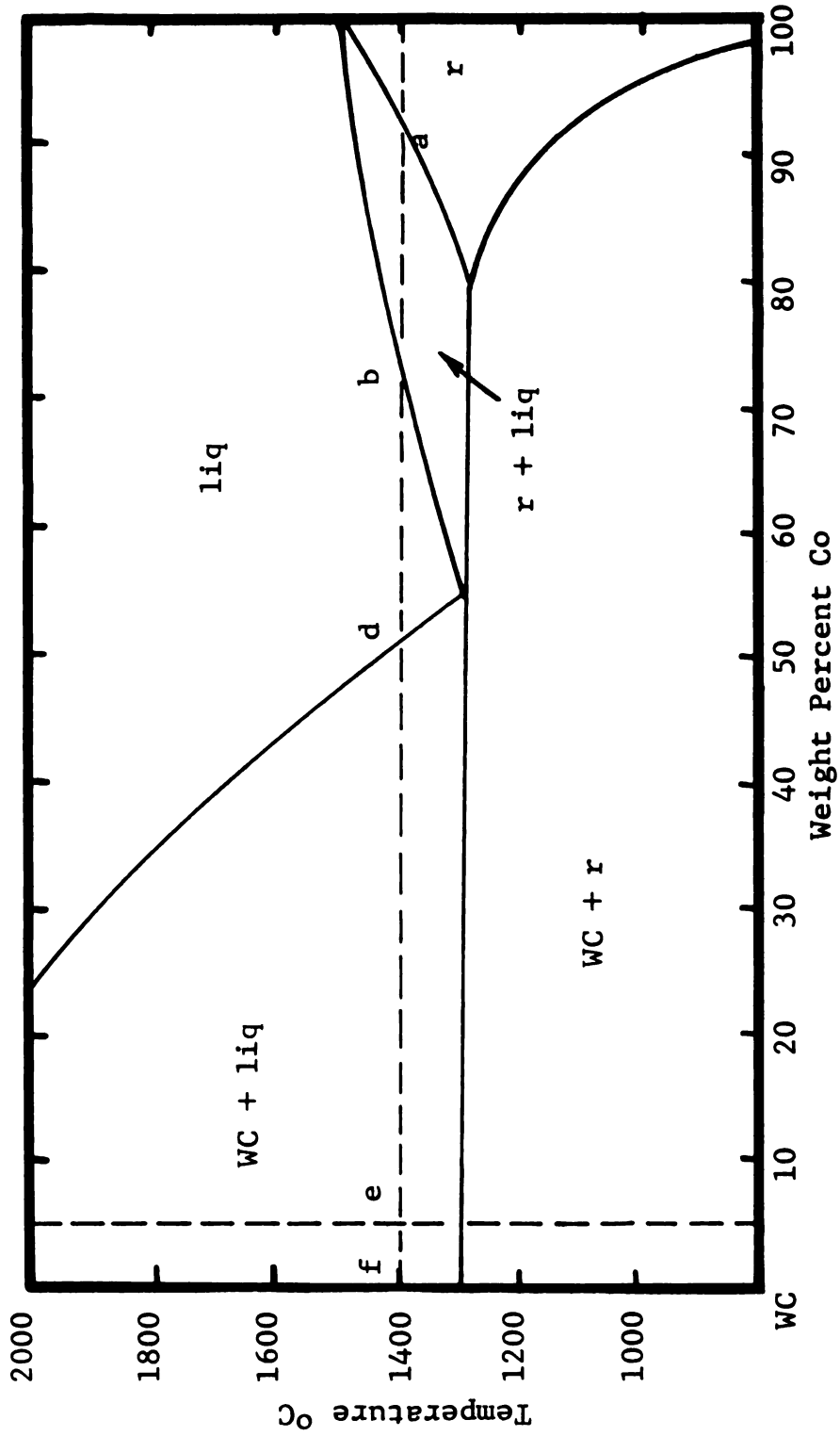


FIGURE 2
QUASI-BINARY WC-Co DIAGRAM

THEORY OF STRENGTH OF TUNGSTEN CARBIDE-COBALT ALLOYS

The earliest attempt to formulate a theory of strength for tungsten carbide-cobalt alloys was that of Dawihl(2). He postulated that in view of the fact that tungsten carbide-cobalt alloys of less than 6% cobalt retained their shape and partially their strength after leaching with boiling HCl, the strength of the normal tungsten carbide-cobalt alloy was due to the formation of a continuous carbide skeleton in the compact. An inconsistency in this theory arises, however, when one considers the fact that the same investigation revealed that compacts with 11 wt. % Co or greater, when leached in HCl, were reduced to a powder with no apparent skeleton. This would indicate that if Dawihl's theory were correct there should be a large change in strength characteristics of the alloys between 6% and 11%; no such change has been observed. The transverse rupture vs. cobalt content curve and the compression vs. cobalt content curve are both smooth in this region with no inflection points indicating the same load bearing mechanism to be operating both below and above 11%.

Ivensen, Eiduk and Pivovavov(3) have attempted to refine this idea. These authors consider the effect of cobalt content on the yield strength of tungsten carbide

cobalt alloys. Since in the range of the alloys they studied the compressive strength of the alloy differs from the yield by approximately the same magnitude for all cobalt contents, the conclusions they drew would be applicable to ultimate compressive strength also. These authors determined the completeness of the tungsten carbide skeleton by metallographically measuring the decrease in relative "contact surface area" of the carbide grains with increase in cobalt content. The authors show that the yield strength of tungsten carbide-cobalt alloys in this cobalt range (6%-20% wt.) is approximately proportional to the size of the "contact surface" as determined by the number of zones of approach of tungsten carbide grains intersected by a random straight line on a metallographic section. It is assumed that the tungsten carbide grains approach zones are true tungsten carbide-tungsten carbide boundaries rather than very thin cobalt interlayers, as well as that there exists a continuous carbide skeleton, whose degree of coherence diminishes with increasing cobalt content. Based on metallographic observations, Ivensen concludes that "the deformation of any WC grain is due to the pressure exerted by the neighboring crystal in the zone of direct contact between the two crystals." With an increase

in cobalt content and resulting decrease in the size of the "contact surface" of its carbide grains, this would mean that plastic deformation of a tungsten carbide-cobalt alloy would begin with deformation of the tungsten carbide phase. Ivensen explains this conclusion as follows: Due to the difference in thermal expansion coefficient between tungsten carbide and cobalt, the tungsten carbide is in compression and the cobalt in tension after cooling from the sintering temperature; thus at the beginning of compressive deformation the tensile stresses in the cobalt decrease, while the compressive stresses in the carbide are superimposed on the applied stress, thereby increasing it. The result being the flow stress of the carbide is attained before the cobalt begins to flow. Suzuki, Hayashi and Kawakatsu(4), however, report that by using procedures such that the alloys remain on the low side of the stoichiometric carbon range, so that a greater amount of tungsten is retained in solution in the cobalt (thereby raising the binder yield point), the strength of all alloys investigated was raised. If Ivensen's theory were correct, this would hardly be possible, as an increase in binder strength would not affect the yield strength of the alloy because it is not the binder which yields first but the

tungsten carbide according to the theory. It would seem then that the binder itself is responsible for strength or weakness of commercial grades of tungsten carbide-cobalt alloys and not a skeleton of tungsten carbide.

The hypothesis that tungsten carbide-cobalt alloys consist of a continuous matrix phase supporting tungsten carbide inclusions and that tungsten carbide-tungsten carbide contacts occur only infrequently was first put forward by Gurland and Norton(5). With this hypothesis explanations can be given for various other phenomena observed in tungsten carbide-cobalt alloys, such as the linear dependence of hardness on cobalt content in these alloys, and the fact that the temperature dependence on hardness is similar to that of cobalt. Although there have been numerous studies of various kinds, conclusive proof of the presence or absence of a carbide skeleton or a continuous matrix has not been offered.

None of the above theories explains the dependency of transverse rupture strength on cobalt content or the compression strength on cobalt content curves. (See Figure 3) In recent years Gurland has advanced a theory purported to explain this behavior. Essentially, Gurland maintains that the degree of coherence of the carbide

FIGURE 3
TRANSVERSE RUPTURE STRENGTH
VERSUS MEAN FREE PATH

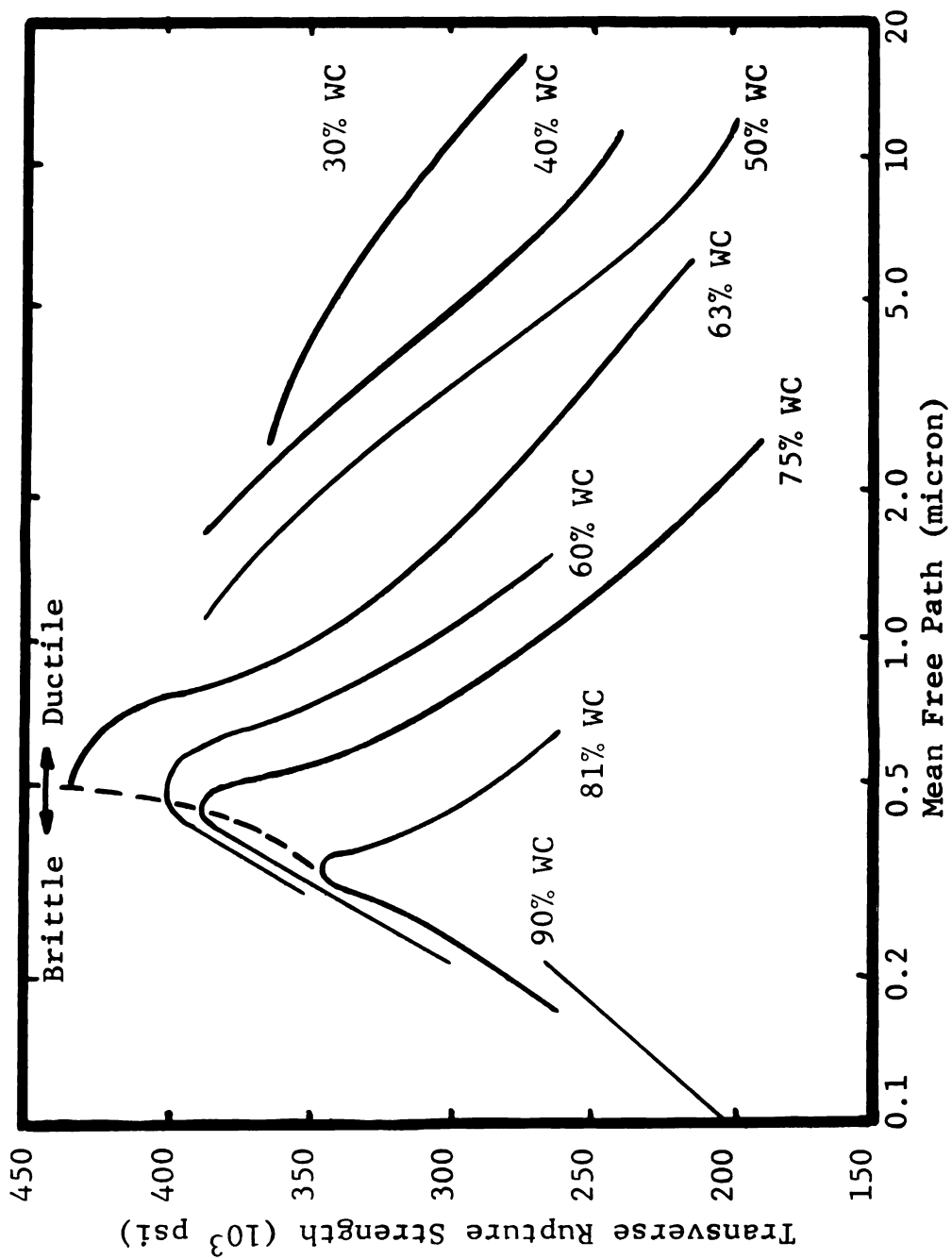


FIGURE 3

grains in tungsten carbide-cobalt alloys as a function of cobalt content changes steadily from a continuous carbide skeleton in sintered tungsten carbide free of the cementing phase. Dilatometric cooling curves plotted by Gurland indicate the absence of a continuous carbide skeleton in an alloy with 6% wt. cobalt; in higher cobalt grades he believes there are still partial tungsten carbide skeletons. Such a structure is thermodynamically possible if two faces of crystallographically favorable traces (low free energy) came together, then γ_{11} may be less than γ_{12} . Such crystallographically favorable pairs are found in tungsten carbide-cobalt alloys but not frequently enough to lead to a carbide skeleton. Most supporters of the skeleton theory regard it as a source of strength, whereas Gurland attributes the low strength of tungsten carbide-cobalt alloys on the left hand side of the TR vs. cobalt curve to a tendency for the failure path to preferentially proceed through the brittle carbide grains as a result of increased coherence of the grains. Many investigations have researched the path of fracture in tungsten carbide-cobalt alloys and there is fairly common agreement that in fine grain alloys the crack travels in the cobalt phase regardless of cobalt content. This would seem to be a serious objection to

FIGURE 4
EFFECT OF TEST PROCEDURE UPON RELATIONSHIP BETWEEN
COMPRESSIVE STRENGTH AND HARDNESS FOR VARIOUS WC-Co ALLOYS

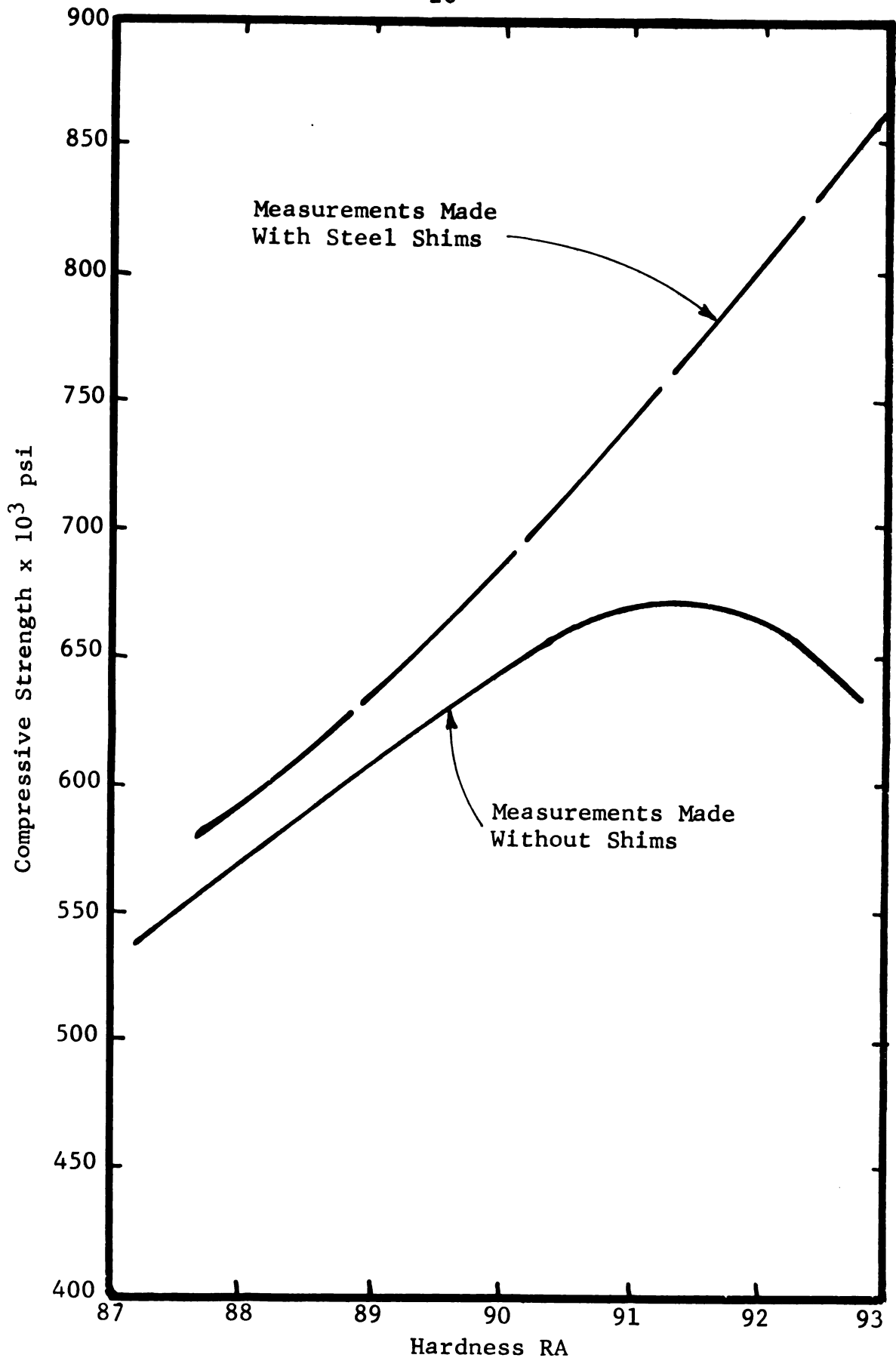


FIGURE 4

Gurland's theory. The fracture paths of coarse grained alloys are generally thought to travel through the tungsten carbide phase as well as the cobalt phase, but the decrease of ultimate strength with decrease in cobalt is found to be very similar to the fine grained alloys, thereby throwing further doubt on this theory.

A theory for the strength of tungsten carbide-cobalt alloys based on rather different premises is presented by Spath(6). He modeled tungsten carbide-cobalt alloys as cylinders of tungsten carbide surrounded by cobalt (see Figure 5). From this model he calculates the thermal stresses set up in the two phases during cooling from sintering temperatures due to the difference in the thermal coefficients of expansion. From this treatment, the phenomena likely to occur in tungsten carbide-cobalt alloys are illustrated in Figure 5. The tungsten carbide grains are represented by circles, while the lines between them indicate the thickness of the cobalt regions. When these regions are very thin (low cobalt content), very high tensile stresses, shown in Figure 5 by arrows pointing downward, are generated in them. Conversely, low stresses of the opposite sign, designated by arrows pointing upward, act in the tungsten carbide grains. When the regions of the

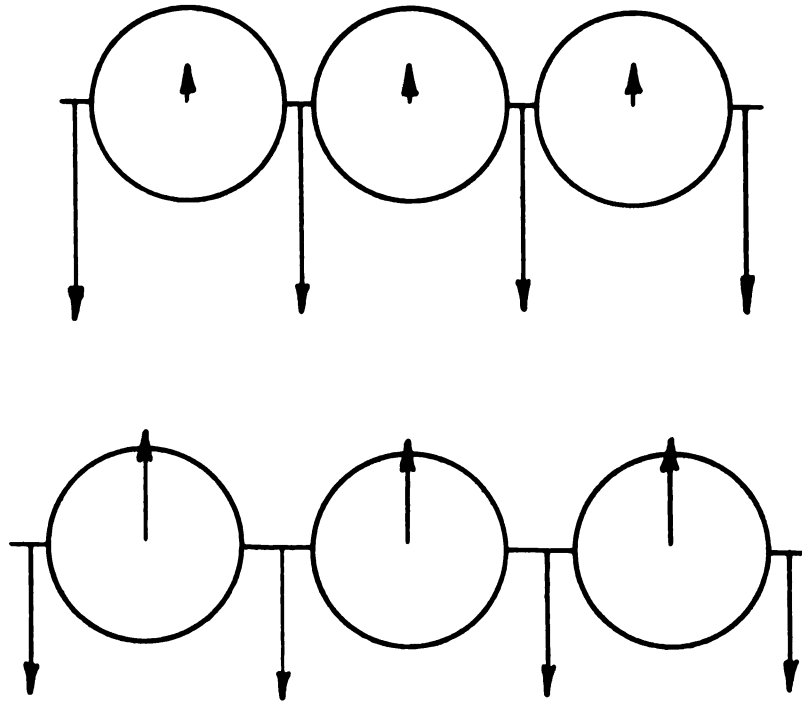


FIGURE 5

DIAGRAMMATIC REPRESENTATION OF THERMAL STRESSES
IN CARBIDE AND CEMENTING PHASES OF WC-Co ALLOYS

cementing phase are large (Figure 5 bottom) the stresses in the binder are much lower, while those in the tungsten carbide grains are larger. On the basis of this Spath concludes that external load alone does not give a correct picture of the stress distribution in a tungsten carbide-cobalt alloy. When external compressive loads are applied, the tensile stresses prevailing in the cobalt phase must be neutralized before compressive stresses can be generated. The tungsten carbide grains have a very high compressive strength, thus the cobalt phase may be expected to rupture first. For this reason, high external compressive loads are required to rupture tungsten carbide-cobalt alloys. This leads to the conclusion that the maximum compressive strength of a tungsten carbide-cobalt alloy must be exhibited by those alloys with the minimum cobalt content. Until recently this has not been observed. However, Lueth and Hale(7) found that by using proper techniques to obtain better uniaxial compression the material with the lowest cobalt also exhibited the highest compressive strength. Spath concludes that, the situation is reversed for tensile or transverse rupture loading as the internal and external loads are superimposed and the ultimate strength is surpassed at quite low external stresses. This explains the

large difference in strength of hard alloys in compression and bending. The inflection in the transverse rupture vs. cobalt curve is due to the fact that with increasing cobalt content the tensile thermal stresses diminish, thus the strength goes up to a limiting point at which point the thermal stresses are less important than the bulk properties of the cobalt.

If this phenomenon indeed occurs, then the compressive strength of low cobalt alloys may be expected to decrease with a rise in temperature because the tensile stress will diminish in the cementing phase. The transverse rupture strength should increase with temperature, and the compressive and transverse rupture strengths should approach each other. When stating these general trends, other factors must be kept in mind, however, which may alter the reaction slightly such as changes in modulus of elasticity with temperature, coefficient of thermal expansion and strength of the individual phases. All of the above trends have been observed by various individual experimenters working on specific problems. The greatest drawback to this theory is the lack of experimental proof of these stresses. Various experimenters have observed stresses in tungsten carbide-cobalt alloys by X-ray techniques, both line broadening and line shift, but they have failed to come

to any general agreement about either the magnitude or the sign of these residual stresses. Many of the experimenters have used as-sintered surface vs. a surface leached with an acid which will remove the cobalt and relieve the stresses on the tungsten carbide as their two conditions. An as-sintered surface cannot be characteristic of the bulk of the material. Others have used various surface preparations such as grinding, polishing, etc. None of these surfaces will be the same as the bulk material. It is easy to see why the experimental evidence for residual thermal stresses is so contradictory and that more work in this area is sorely needed. Another major failing of this theory is that it gives no specifics of the manner of failure on the right of the inflection point of the transverse rupture vs. cobalt percent curve.

Some success, of a qualitative nature, has been realized in this area of the transverse rupture curve vs. cobalt content by applying dispersion hardening theories. The data, however, will not differentiate between the theories of Orowan, and Ansell and Lenel. The dispersion hardening theory, with some slight modification, does work reasonably well for compression yield data as evidenced by the calculations of H. Doi, Y. Fujiwara, and K. Miyake(8).

They used the relationship that $r_s/R_s =$ volume fraction of tungsten carbide where r_s is the radius of the tungsten carbide particles and R_s is one-half the distance between the center of the tungsten carbide particles. This relationship is true subject to the assumption of uniform size and distribution of carbide particles (see Figure 6). Then upon using the dislocation by-pass model, as given by Ashby(9), the observed yield stresses show good linear relationship with respect to the calculated ones, but the former are several times larger (see Figure 7). In these calculations the shape, etc., of the particles are not taken into account. These should lower the particle spacing. To correct for this, Doi divided the calculated spacings by 6 and found excellent correlation between experimental and theoretical values of yield. This model is based on simple glide of dislocations in the binder phase by-passing the dispersed carbide particles. They further calculated the stresses necessary for breaking of the carbide bridges after the concept by Ansell and Lenel. These were found to be much greater than the Orowan stress for glide and it was concluded that this was of minor importance in the mechanical behavior of tungsten carbide-cobalt alloys.

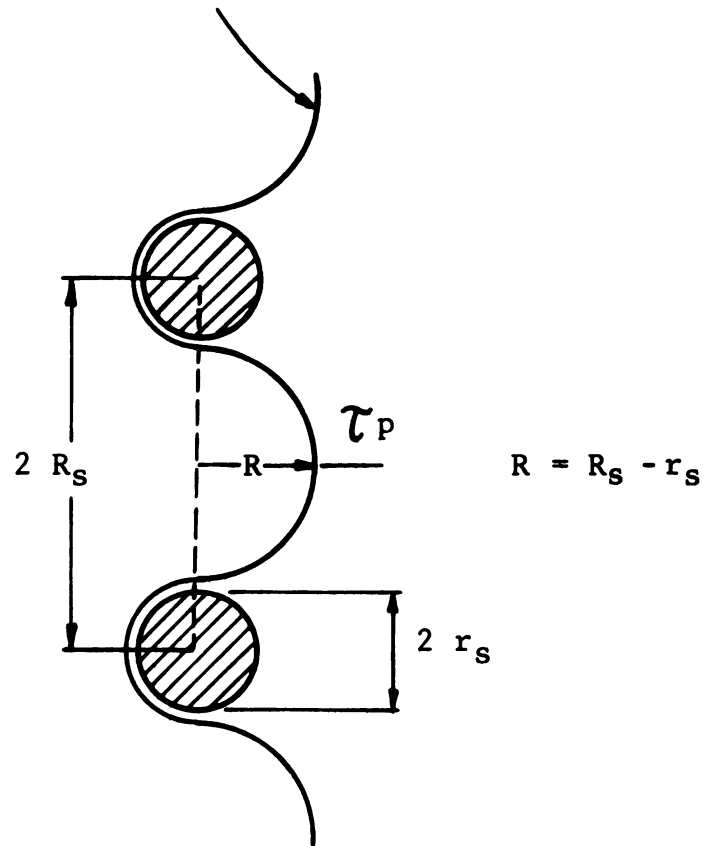
Drucker⁽¹²⁾ attacks this problem from a continuum mechanics

FIGURE 6

DISLOCATION BY-PASS MODEL FOR
CALCULATING OROWAN'S STRESS

τ_p gives the dispersed particle strengthening, and the distance represented by $2R$ is called the mean planar interparticle spacing.

Dislocation Bowing Out
Between Two Dispersed Particles



$$\tau_p = \frac{Gb}{4\pi} \cdot \frac{\Phi}{R_s - r_s} \cdot \ln \frac{R_s - r_s}{b}$$

Orowan's Stress: $\tau = \tau_s + \tau_p$

τ_s : Critical Shear Stress of Matrix
(Ashby)

FIGURE 6

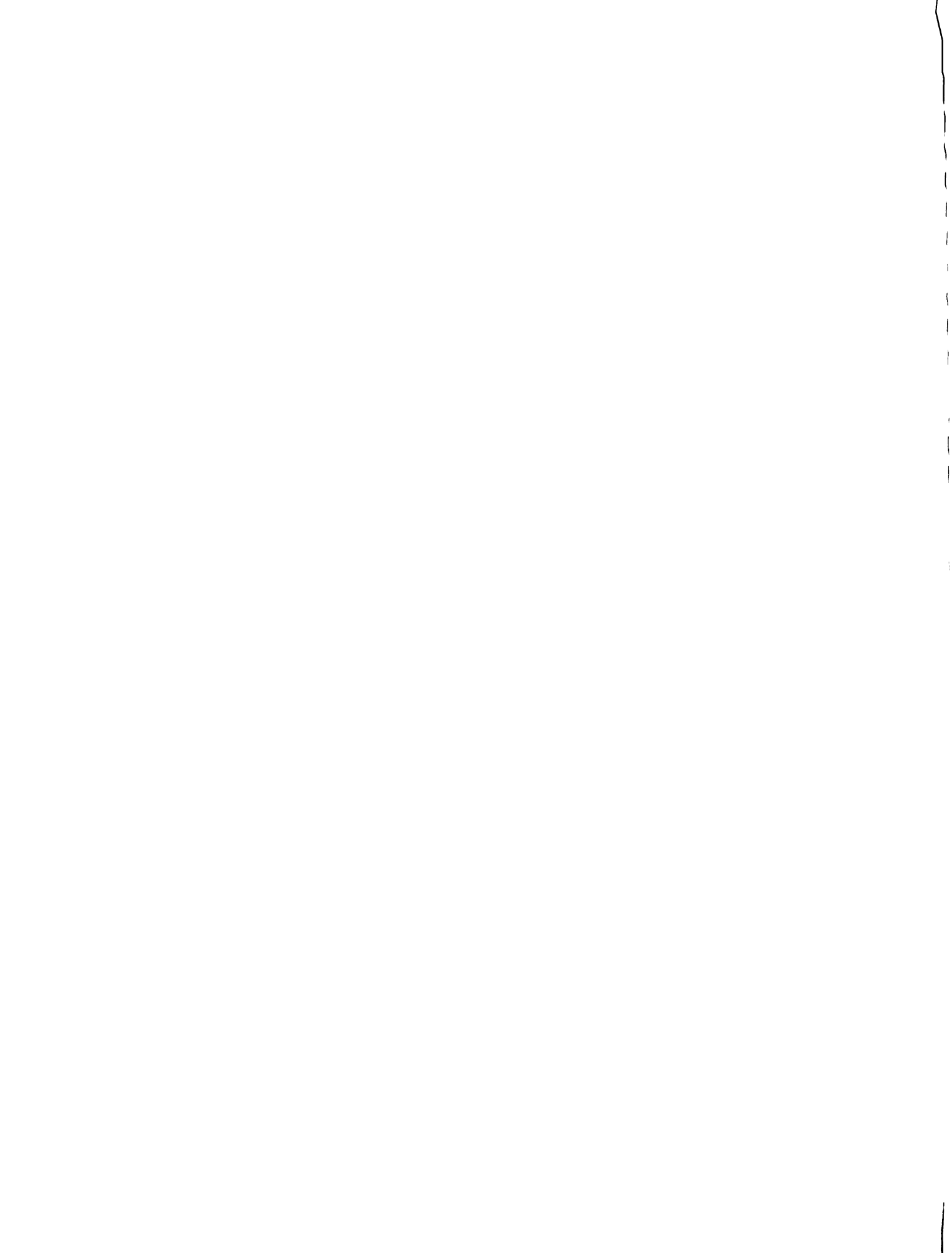


FIGURE 7

A COMPARISON OF THE OBSERVED YIELD STRESSES
IN SHEAR OF WC-Co ALLOYS WITH THE THEORETICAL
VALUES FOR THE DISPERSED PARTICLE STRENGTHENING

τ_p relates the observed yield stresses with theoretical values calculated on a basis of a simple assumption regarding the shape and distribution of the carbide particles, while τ'_p relates the observed yield stresses with the theoretical values which have been calculated after correcting the interparticle spacings.

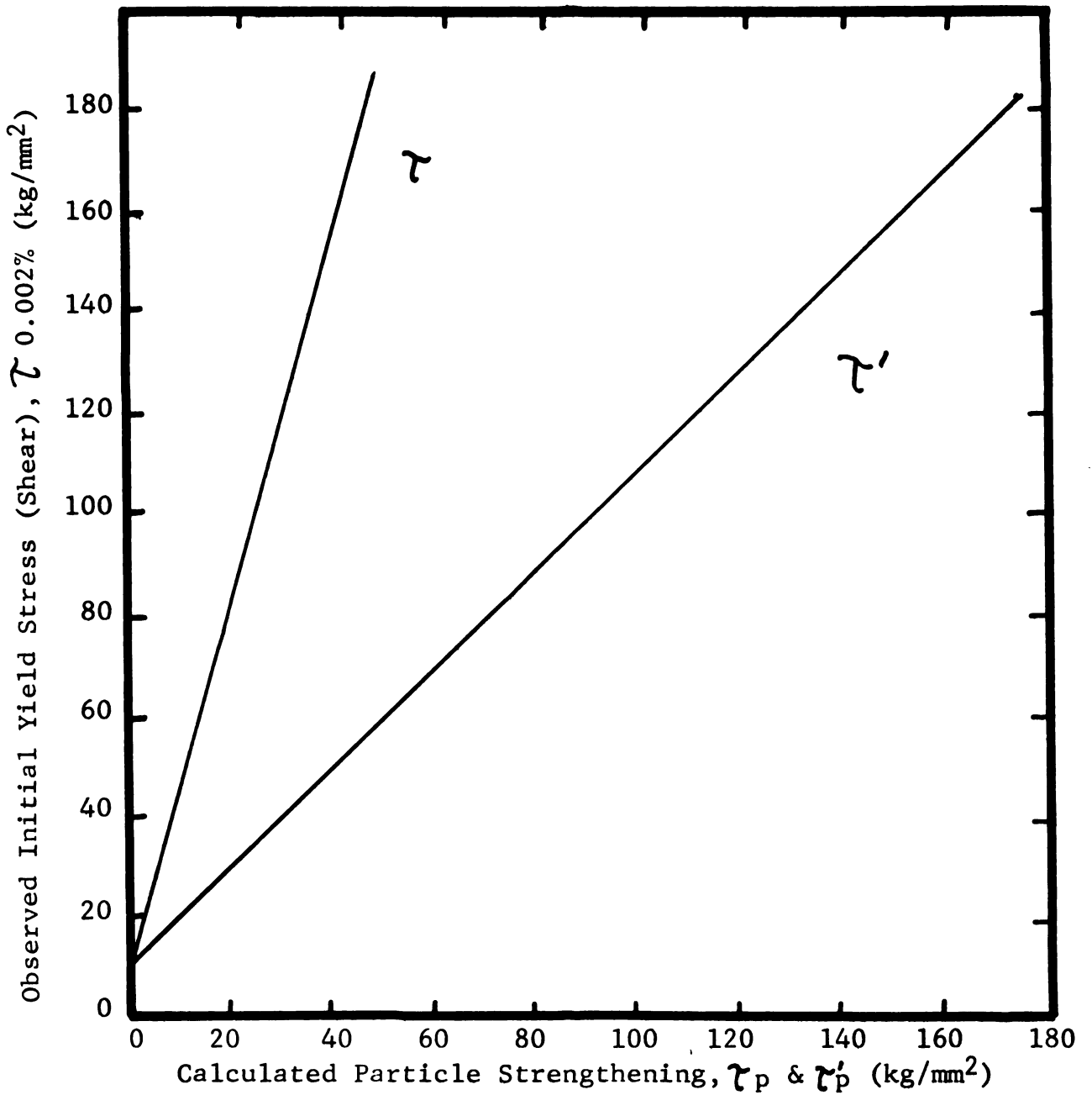


FIGURE 7

A COMPARISON OF THE OBSERVED YIELD STRESSES
IN SHEAR OF WC-Co ALLOYS WITH THE THEORETICAL
VALUES FOR THE DISPERSED PARTICLE STRENGTHENING

view using a two-dimensional array of regular hexagons to represent the tungsten carbide grains and the area between these to represent the cobalt phase. Using a viscous flow approach in vertical compression (hexagons in the vertical direction come closer together and squeeze out the cobalt) he calculates speed of flow with respect to speed of displacement of the hexagons letting the gradient of the pressure to cause flow be equal to the yield stress and using the velocity gradient times a viscosity coefficient to equal the yield stress in shear. Using these he converts velocity consideration to pressure consideration, then using pressure to balance applied stress and balancing these in the various channels he can calculate the stress which must be applied to the configuration in order to achieve such a flow. This stress is then in terms of the yield stress of the matrix material and the ratio of the size of the hexagon to the size of the channel. By using this approach he calculates a plastic constraint factor which is equivalent to the amount of stress necessary to cause flow divided by the yield stress of the material ($\sigma_{ave}/\sigma_0 = \frac{1}{2} (1 + \frac{2a}{3n} + \frac{n}{a})$ where "a" is the dimension of the side of the hexagon and "n" is the thickness of the channel. By varying these he can simulate the effect of

various cobalt contents and grain sizes. He states that his approximation is good only for $a/n > 3$ which makes it applicable to high cobalt alloys. (See Table 1 below for constraint factor.)

TABLE 1

STRENGTH OF TUNGSTEN CARBIDE-COBALT ALLOYS
ASSUMING COBALT TO GOVERN, NO SIZE EFFECT,
CARBIDE INFINITELY STRONG

Fraction WC	$\frac{a}{n}$	$\frac{\sigma_{ave}}{\sigma_o}$	Calculated Tensile Strength
.90	16.16	5.92	950,000
.81	7.93	3.21	510,000
.75	5.74	2.50	400,000
.69	4.39	2.07	330,000
.63	3.46	1.79	290,000
.50	2.22	1.46	230,000
.30	1.16	1.05	170,000

He then postulates that if a Griffith type theory is assumed with the likelihood of interior or surface flaws of dimension proportional to the diameter of the carbide particles, the average stress at fracture is then inversely proportional to the square root of the diameter

($\sigma = K / \sqrt{d}$), where K is independent of carbide volume

fraction and particle spacing. He then plots the data of Gurland for transverse rupture versus mean free path on the basis of transverse rupture strength versus particle diameter for all cobalt contents on the decreasing or right side of the maximum (see Figure 3). This, he believes, shows the validity of his assumption. For all of the points on the curve the cobalt is in a plastic or ductile state (see calculated tensile strength and constraint factor table) that is $\sigma_{ave} = \sigma_o X$ (constant factor). This leads to the conclusion that fracture in this area is due to fracture of the carbide particles first as their diameter would seem to control fracture strength. The fact that the transverse rupture strength drops as the cobalt content is lowered below some point is attributed to the cobalt being under such high constraint that it will not flow and thus the carbide particles will be under very high contact stresses which will increase in severity as the cobalt decreases, thus lowering the strength of the alloy with reduction in cobalt once this point is reached. This then means that in this region raising the cobalt's ductility will increase the composite strength. In this theory then the tungsten carbide phase is the real controlling factor in fracture of tungsten carbide-cobalt

alloys and the cobalt only controls the mechanisms by which the composite fractures. The total theory would then imply that if we raised the yield strength of the matrix in some manner then the alloys to the right of the maximum on the transverse rupture vs. cobalt curve would remain at approximately the same strength level as long as $\sigma_o X$ (constraint factor) $\leq \sigma_{TR}$ and that the equilibrium condition would be reached quicker, thus the maximum would be shifted to the right. The alloys to the left of the maximum for any given cobalt content would be subject to even less plastic flow, thus the strength should go down.

This effect is not observed in practice as Suzuki was able to raise the amount of tungsten in solution in the cobalt phase as a result of staying on the low carbon side of the equilibrium stoichiometric range of tungsten carbide. This would presumably raise the cobalt yield stress, the transverse rupture data he reports as illustrated in Figure 8. He states that no low carbon alloy was weaker than the higher carbon alloys. All alloys were in the stoichiometric range, thus the predictions of Drucker's theory are not borne out by experiment. Butler (1969 PhD thesis, Brown University), one of Drucker's students, carries this view further. With regard to the

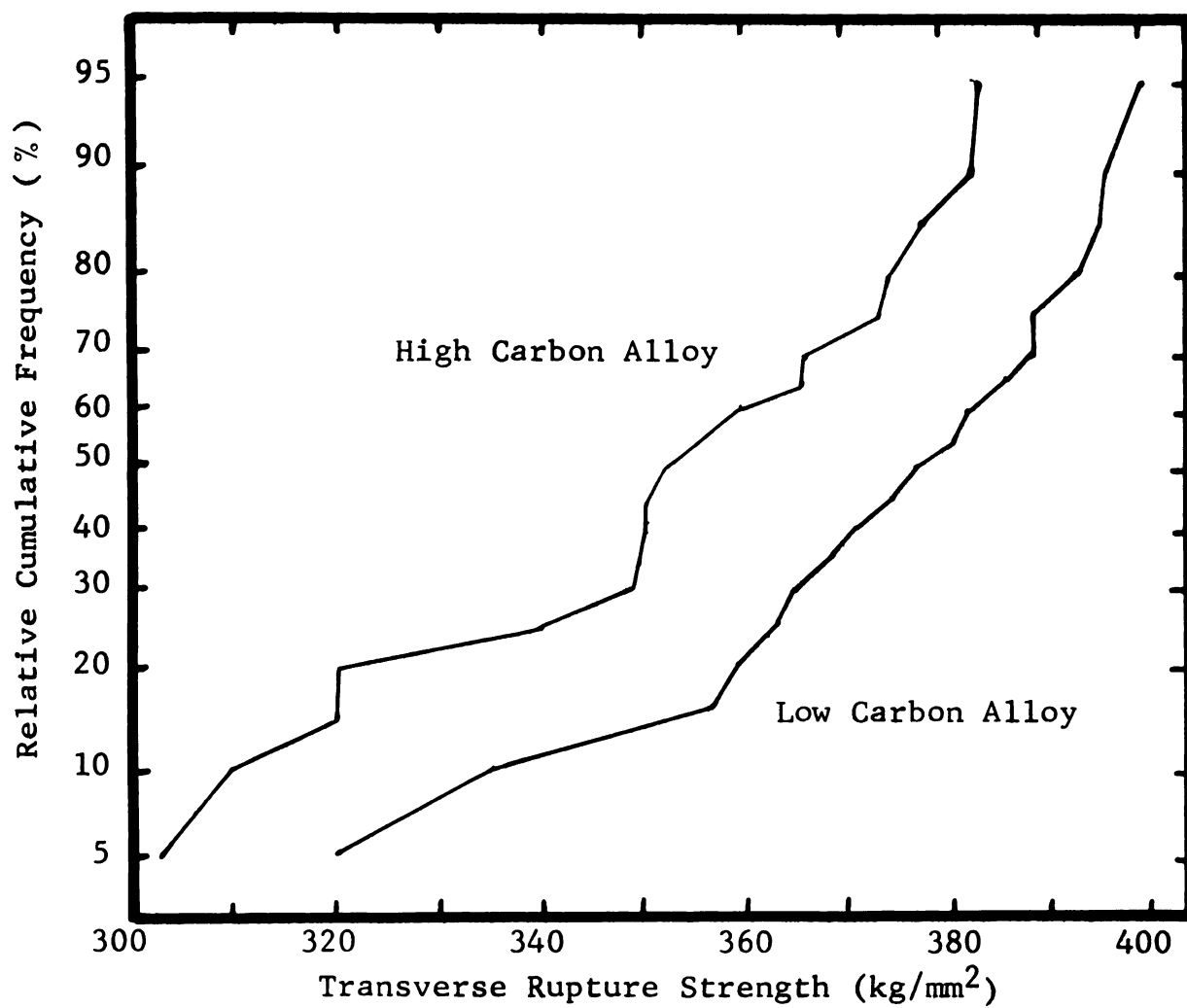


FIGURE 8

EFFECTS OF CARBON CONTENT ON THE STRENGTH OF WC
10% Co ALLOY HAVING MEAN GRAIN SIZE OF 2.2 MICRONS

transverse rupture data he presents similar views and adds (with regard to the "brittle" side of the transverse rupture vs. cobalt curve), "High peak stresses in the WC particles caused by stress concentrations are not smoothed out because of insufficient and highly constrained plastic deformation of the Co. As load is applied to a specimen, eventually either WC particles start to break or fracture takes place at the particle matrix interface or the bond fails. When this happens the fracture can then propagate relatively easily in a brittle fashion since there is little plastic deformation to blunt the propagating crack." With regard to the "ductile" side of the curve, he states, "Eventually as the stresses in both WC and cobalt increase, the weakest WC particles fracture. The cobalt behaves plastically, blunting any cracks. As stress is increased further, more and more WC particles fracture. Eventually the remaining cobalt and unbroken WC particles can no longer carry the load and the specimen ruptures." This would indicate two distinctly different modes of fracture. He extends this theory to account for compressive failure here. He concludes, "The compressive strength of WC-Co is limited by the same factors which control the bending and tensile strengths. Maximum compressive strengths are governed by

cross-tension stresses fracturing the WC particles or causing bond failures and are predicted by the continuum modes." It is interesting to note that he plots the compressive strength of a carbide assuming the cobalt strength governs, including the constraint effect, and also assuming infinitely strong carbide particles. He compares this to measured compressive strengths for the two cases of cobalt at 160 k psi ultimate and 200 k psi ultimate (see Figure 9). If we add to this plot the data of Lueth and Hale, we find very good agreement with the predicted values making opposite assumptions to those made by Butler. It seems then that this theory in its present form fails to account for experimental phenomena.

Kreimer⁽¹⁰⁾ presents a modified Griffith/Orowan theory to explain the behavior of tungsten carbide-cobalt composites. He applies this theory only to the ascending portion of the transverse rupture vs. cobalt curve. He assumes that on the left or ascending portion of this curve the yield strength of the cobalt is equal to the ultimate strength and to the right of the maximum the yield strength of the cobalt is below the ultimate strength. This is similar to the Drucker assumption. The data of Doi mentioned earlier with respect to dislocation damping studies,

FIGURE 9
COMPRESSIVE STRENGTH AS A
FUNCTION OF PERCENT WC (GURLAND)

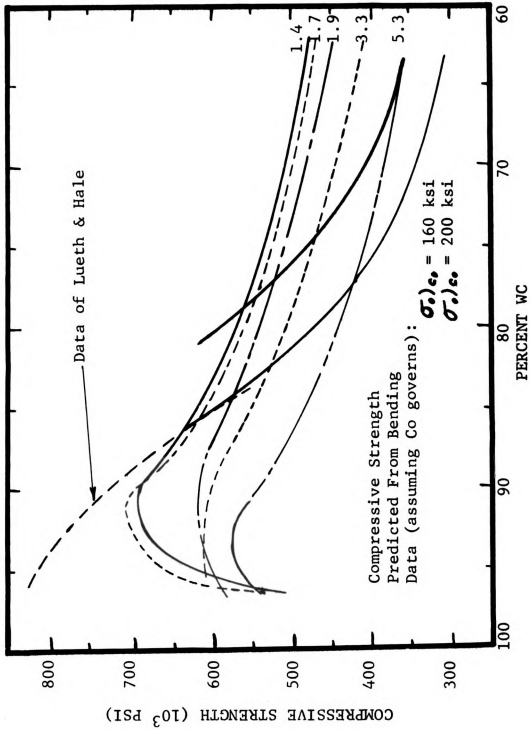


FIGURE 9

however, shows that there is considerable dislocation movement and multiplication even in very low cobalt alloys at stress levels much below the failure level. Kreimer further states that even during what is considered brittle fracture there is always some evidence of at least micro-plasticity (Orowan's modification to the Griffith theory of brittle fracture). This plastic deformation should be found mostly in the cobalt phase and thus the more cobalt phase showing on the fracture surface the larger amount the amount of energy necessary to fracture the material. Kreimer states that the area of the fracture which is composed of cobalt is proportional to the volume of the cobalt phase in the alloy and that the work of plastic deformation then is proportional to the cobalt content ($P = AC$ where P is plastic work, C is cobalt content and A is a constant).

In view of the general findings of other investigators that the amount of tungsten carbide vs. cobalt fracture is strongly grain size dependent and may be dependent on other factors such as speed of crack, etc., this would seem to be a rather strong assumption. The impact strength of tungsten carbide-cobalt alloys is composed of three parts; namely, work of elastic deformation, work of plastic deformation of the cobalt region adjacent to the fracture

surface, and the work expended in the formation of this surface $a_T = a_E + P + \gamma$. Kreimer believes that the first and last terms are to be neglected and that only the work of plastic deformation is important in fracture. He also assumes that the critical crack length is independent of cobalt content and that the ultimate strength of tungsten carbide-cobalt alloys is determined by the stress necessary for crack propagation, not the stress necessary for initiation. With these assumptions, the Griffith/Orowan equation can be written $\sigma^3 = AEC$ where A is a constant, E is the modulus of elasticity and C is cobalt content. He presents several plots of σ^3 (transverse rupture)² vs. EC - all of which form fairly straight lines. This fact would be expected as the modulus of elasticity changes little in this range (left of the TR vs. Co curve) and it is well known that the TR is dependent on cobalt content and tungsten carbide grain size. The final form of the equation for strength which he presents is $\sigma^3 = AEC + K$ where K is a constant which governs the grain size dependency of the strength. Many of these assumptions here are directly opposite to those of Drucker and others. This theory then says that as cobalt content goes down, it takes less energy to propagate existing cracks and thus the material is less

strong. This should hold in all forms of loading; however, the data of Lueth and Hale contradicts this theory for the case of compressive strength, and this proposal does not fit the available data in all respects.

Many theories of strength of tungsten carbide-cobalt alloys have been put forward; however, as yet none explain the total range of experimental data, rather each attempts to explain one small portion of the data. All have some validity but further work must be done to sort out those ideas which can best be used to further understand the alloys, and thus be able to put them to better and more extensive use.

There are other theories which try to explain the behavior of these alloys. It has been endeavored to review only those which have received the most complete acceptance, as many of the others have even more obvious flaws.

SUBJECT RESEARCH

Most of the theories of strength and behavior of tungsten carbide-cobalt alloys depend heavily on the initiation area--that is, tungsten carbide or cobalt on an interphase boundary and the propagation (which phase is traversed by the crack). Most of the studies of fracture of these alloys have been done on transverse rupture bars or similar tests in which the test is immediately catastrophic. Here the fracture is extremely fast and may not reflect the true nature of the initial crack which must start and propagate initially very slowly. To properly apply the Griffith/Orowan theory to the material, no assumptions should be made about the fracture until data have been provided to substantiate these assumptions. The purpose of this research is to obtain K_{Ic} and G_{Ic} values for the tungsten carbide-cobalt alloy system and to examine the implication that these parameters have on the proposed theories to explain the strength of cemented carbides. This was accomplished by a wedge loaded double cantilever beam system. Pertinent information of the applicability and mechanics of this test can be found in Appendix I.

EXPERIMENTAL PLAN

Nine alloys were used in this study with various cobalt contents and grain sizes. Nominal grain sizes and cobalt contents of these alloys are listed below.

<u>Alloy No.</u>	<u>Cobalt Content (Wt. %)</u>	<u>Nominal Grain Size (μ)</u>
1	3	1.5
2	3	3
3	6	7-8
4	9	1.5
5	9	3
6	9	7-8
7	15	1.5
8	15	3
9	15	7-8

These alloys were hydrogen sintered at appropriate temperatures and the carbon contents in the median range for the alloy. Photomicrographs of the structure with porosity and soundness ratings can be found in Appendix II.

The test bars were 3" x 1/8" x 1/2" with a 3/4" x .35 slot cut in one end and a 1/16" groove cut along the center the full length of the sample (see Figure 1, Appendix III). All grinding was done with a diamond grinding wheel of

100 grit and all grinding marks were parallel to the longitudinal axis of the specimen. The groove was necessary to prevent the crack from deviating from the center line of the specimen during propagation. The ungrooved side of the specimen was polished prior to testing to aid in observing the extent of the crack.

Testing was done in a specially designed fixture (see Figure 2, Appendix III) which allowed the advance of a carbide wedge (via a micrometer screw) into the slot provided in the sample. The arms of the double cantilever beam could then be displaced and this displacement measured via attached transducers. The length of the crack was measured through the use of a travelling stage (to which the total fixture was attached) and a microscope mounted above the sample. The data gathered then consisted of arm displacement and crack length. In order that this information be converted to the desired K_{Ic} and G_{Ic} data the compliance calibration of the system at any given crack length must be determined. The method of obtaining compliance is discussed in the next section (see Appendix I for mathematical development).

COMPLIANCE CALIBRATION

The strain energy release rate G is equal to

$$G = \left(\frac{\Delta^2}{2\lambda^2 b} \right) \left(\frac{\partial \lambda}{\partial(L)} \right)$$

where b is the width of the fractured surface.

In order to determine the strain energy release rate of any given material we must first determine the compliance λ of the material in the configuration of the test.

$$\lambda \text{ (Compliance)} = \frac{\Delta}{p}$$

This is essentially the inverse spring constant of the system.

λ must be determined for various crack lengths such that $\frac{\partial \lambda}{\partial L}$ may be determined at any given crack length.

The accuracy of the compliance can depend only on the accuracy of the measurement and since the compliance changes very little with crack length, the correctness and sensitivity of the measuring system is paramount.

LOAD MEASURING SYSTEM

To measure the load on the sample a transducer was built which consisted of tungsten carbide cobalt wedge with a groove machined along the mid line of the wedge (see figure 1, appendix III). Strain gages were placed at the bottom of the groove. These gages produce a signal when the wedge was loaded at the tip. Since the wedge was displaced into the machined portion of the specimen to

produce increasing displacements, and thus loads, the point of contact of the specimen on the wedge transducer would change; therefore, the wedge must be calibrated along its usable portion. This was accomplished via a fixture which allowed the wedge to be loaded by an exterior mechanism at any point on the usable part of the wedge (see figure 3, appendix III). This total apparatus was then placed on an Instron load cell and data on load versus output from the wedge was taken as a function of loading position. The wedge strain gage signal was read through a BAM 1 amplifier and a Barber Coleman recorder. The output was found to be linear with respect to load at any given point of application on the wedge. The slope of the load versus wedge output data were plotted against position on the wedge and this was also found to be linear. The load could be read to within $\pm .25$ lbs over a range of 50 lbs, or about $\pm .5\%$ error. From this information, the known starting point and the displacement read off of the micrometer the load could be determined on the specimen during compliance calibration in the test fixture.

DISPLACEMENT MEASURING SYSTEM

The displacement was measured via a Daytronic variable inductance transducer and read on a Daytronic transducer amplifier meter (see figure 2, appendix III). This system has a summing capability for the two transducers such that lateral displacement of the specimen, if any, will not be

recorded as displacement. This system allows measurement of five micro inches; however, readings were taken routinely of .0002", thus error here could only be attributed to positioning of probe and initial calibration of the instrument. An error of less than .5% is expected.

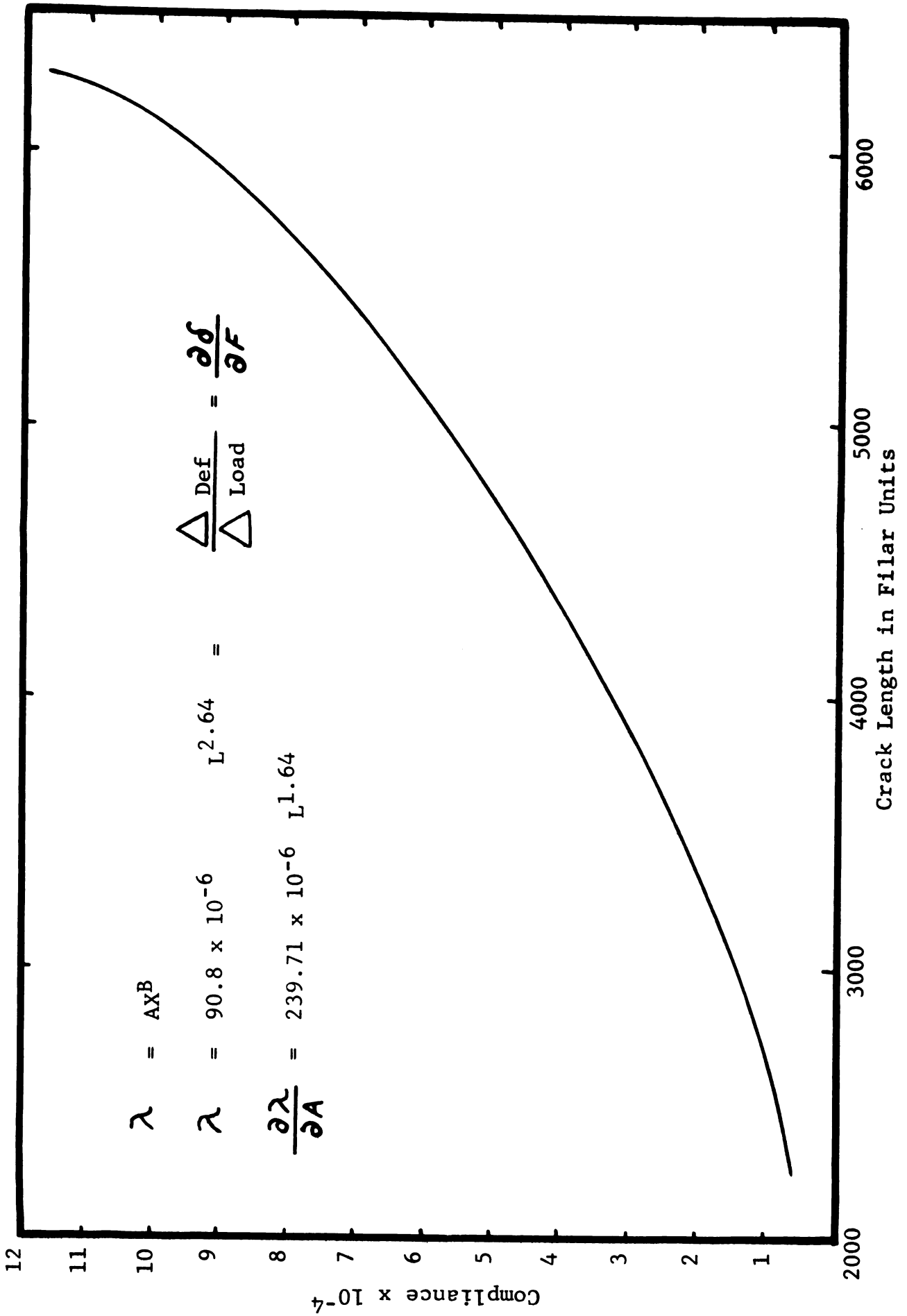
MEASUREMENT OF DATA AND TREATMENT

Load versus displacement data were taken and several samples were taken at crack length increments of $\approx .1$ " over the length of the specimens from 1" to 3". All these data were then plotted for each crack length and the compliance determined. The deflections were found to be linear with load as required. The compliance data from all samples and crack lengths were then plotted on a master curve (see figure 10) and as can be seen, all of these data correlated quite well. A regression analysis was performed on these data and equation of the form $Y = AX^B$ gave the best fit with an index of determination of .996. This result agrees well with theory. The displacement using the regular theory is

$$y = \frac{FL^3}{3EI} \quad \text{or} \quad \frac{\Delta}{p} = \frac{L^3}{3EI}$$

From the regression analysis $\frac{\Delta}{p} = 90.8 \times 10^{-6} L^{2.64}$. To obtain $\frac{\partial \lambda}{\partial L}$ the first derivative was taken of this equation in the normal manner. This procedure eliminated the need to determine experimentally the slope of the master plot at any point. With this information G for this material may be determined with only displacement and crack length measurements.

FIGURE 10
COMPLIANCE VERSUS CRACK LENGTH



EFFECT OF MODULUS ON COMPLIANCE

Since the elastic modulus of the several grades of carbide which were used in the study differ, the effect of this difference must be considered.

$$\lambda = \frac{\Delta}{p} = \frac{Y^2}{F}$$

From Gillis and Gillman

$$Y_o = \frac{FL^3}{3EI} + \frac{kFL(2(1+\nu))}{AE} + \frac{CL^2F}{EI}$$

$$Y_o E = \frac{FL^3}{3I} + \frac{2kFL(1+\nu)}{\Delta} + \frac{CL^2F}{I}$$

Observing that the right side of this equation depends only on sample configuration parameter and load except for a slight contribution due to change in ν then $Y_o E C = (f(\text{sample parameters}))P$

$$Y_o = f(\text{sample parameters}) \frac{P}{E_c}$$

$$f = \frac{Y_o E}{P} = \lambda_c E_c$$

since F is the same for all grades then.

$$f = \lambda_c E_c = \lambda_M E_M$$

$$\lambda_c E_c = \lambda_M E_M$$

$$\lambda_M = \frac{\lambda_c E_c}{E_M}$$

Therefore,

$$\frac{\partial \lambda_c}{\partial L} E_c = \frac{\partial \lambda_M}{\partial L} E_M$$

$$\frac{\partial \lambda_M}{\partial L} = \frac{\partial \lambda_c}{\partial L} \left(\frac{E_c}{E_M} \right)$$

$$G_M = \frac{\Delta^2}{2b\lambda_c^2 \left(\frac{E_c}{E_M} \right)} \left(\frac{\partial \lambda_c}{\partial L} \right) \left(\frac{E_c}{E_M} \right) = \frac{\Delta^2}{2b\lambda_c^2} \frac{\partial \lambda_c}{\partial L} \frac{E_M}{E_c}$$

Comparison of Standard Theory (unslotted beam) vs. experiment (slotted beam)

From simple beam theory

$$Y_o = \frac{FL^3}{EI}$$

for $L=1$

$$\lambda = \frac{2Y_o}{p} = \frac{2L^3}{3EI} = 57.71 \times 10^{-6}$$

From the more complex beam theory and using the results of Brown and Srawley

$$\frac{2Y_o}{F} = \lambda = \frac{2L^3}{3EI} \left(\left(1 + \frac{3/2H}{L^2} \right) + \frac{k(1+\nu)}{HE} \right)$$

$$\lambda = 57.71 \times 10^{-6} L^3 \left(1 + \frac{3/4(.69)}{.5175}\right) + \frac{(4)(2.183)(1.3) \times 10^{-6}}{(.79)}$$

$$\lambda = 57.71^{-6} (1.5175) L^3 + \frac{5.2(2.183) \times 10^{-6}}{.79}$$

for $L=1$

$$\lambda = 87.08 \times 10^{-6}$$

From compliance calibration

$$\lambda = 90.8 \times 10^{-6}$$

or about 3.5% difference

This could possibly be accounted for in some warping of the beam due to the fact that the bottom is not flat (due to slot).

It appears that the slot in the beam does not introduce serious deviation from standard double cantilever beam theory.

TEST PROCEDURE

The test samples were placed in the test fixture and the arms of the double cantilever beam displaced until a natural crack was initiated and arrested. The length of this precrack varied from 1/2" to 2" depending on the fracture toughness of the material. The total length of the crack was then measured (including the original diamond wheel notch) and the wedge withdrawn to close the natural crack. The displacement transducers were then zeroed prior to beginning the test. The arms of the wedge loaded double cantilever beam (hereafter referred to as WLDCB) were displaced until the crack began to move; data were then taken on total crack length and arm displacement. When ten readings had been taken in this manner the wedge was then withdrawn and the procedure repeated. This was done to eliminate any cumulative error which might result if all readings were taken in succession. Usually four to six sets of ten readings were taken on each sample. After completion of the test the fractured sample was examined to ascertain whether the crack had run off center into the thicker material on either side of the slot. If this had occurred those data points taken from the affected area were considered invalid and discarded. The consequences of a

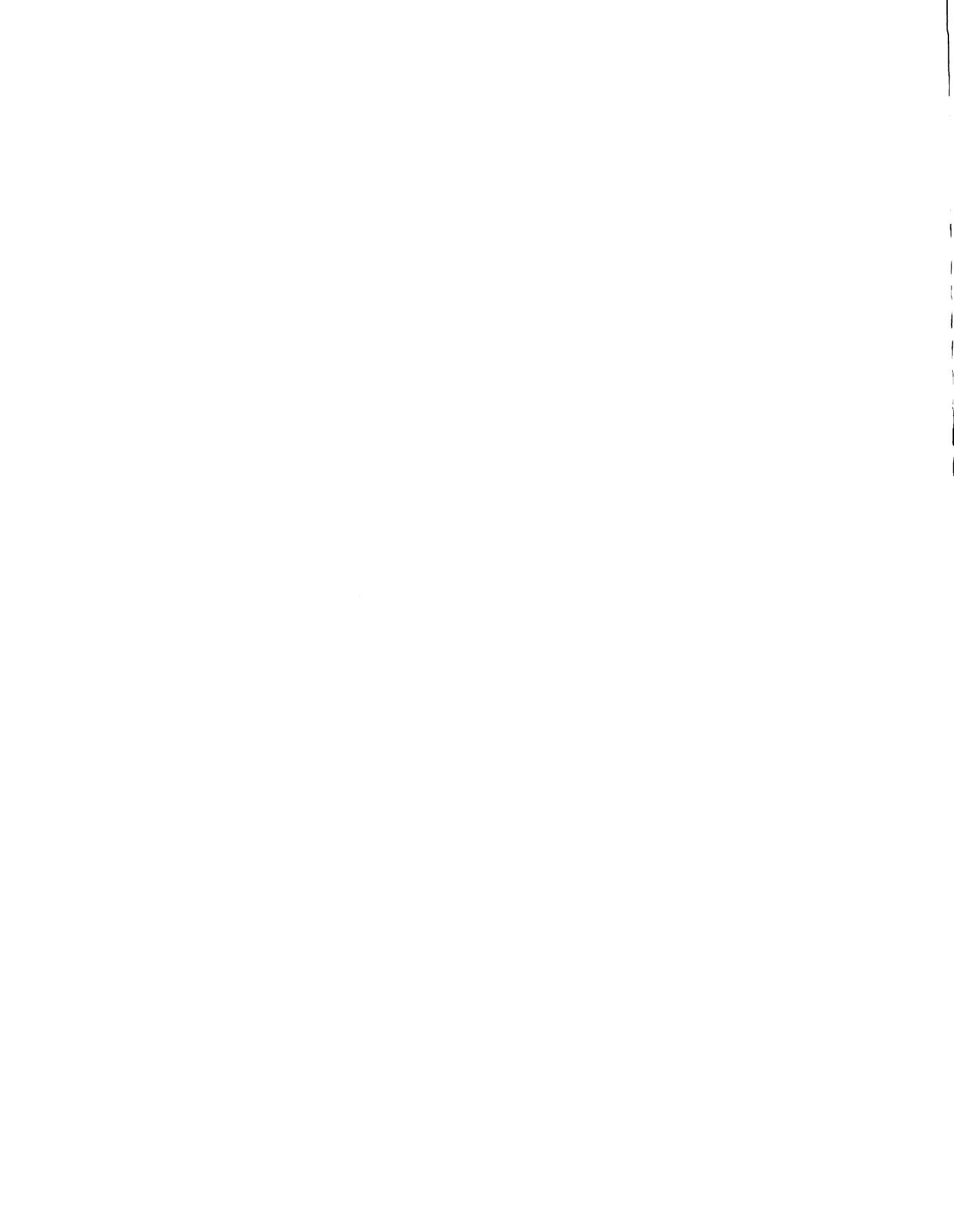
crack running off center would be to have the crack traversing a double thickness area (1/8" thick) and to make the arms of the beam unequal in thickness, thus negating the compliance calibration.

Samples were also prepared to obtain other pertinent physical property data such as transverse rupture strength, compressive strength, yield, and modulus of elasticity. The transverse rupture data were obtained from 1/4" x 1/4" bars broken in three point bending on 5/8" centers. The samples were ground using a 100 grit diamond wheel with the grinding marks running parallel to the longitudinal axis. The compression samples were prepared in a similar manner and were 1/4" x 1/4" x 1" with the ends ground parallel to better than .0003". The test was run with 1 mil steel shims top and bottom of the sample (see reference #7). The compression samples were also instrumented with two strain gages on opposing sides and the strain data used in the modulus of elasticity calculations were the average of these two gages. A typical stress strain curve can be seen in Figure 11; the yield strength was evaluated by the .002% offset method.

The arm displacement, crack length, and modulus of elasticity data were converted to G_{Ic} and K_{Ic} values using

FIGURE 11

**STRESS STRAIN CURVE FOR 15% Co
1.5 MICRON GRAIN SIZE ALLOY IN COMPRESSION**



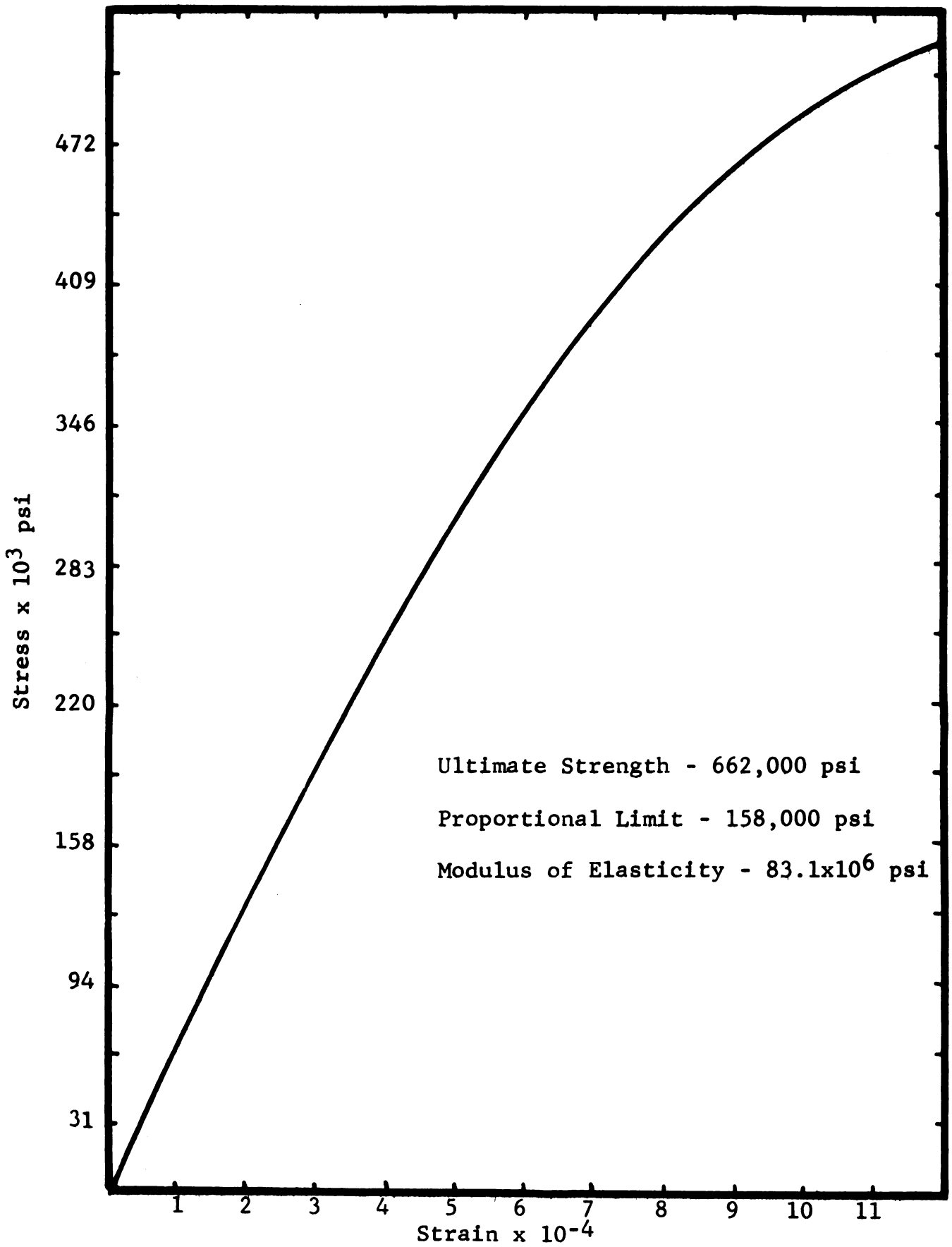


FIGURE 11

a computer program based on the compliance calibration and calculations on pages 120-121 of Appendix I. All of these physical property data along with binder film thickness are compiled in Table II.

RESULTS AND DISCUSSION

The critical strain energy release rate G_{Ic} for cemented carbides bears a near linear relationship to binder film thickness for the low to medium binder film thicknesses with some leveling out at the higher values of this parameter (see Figure 12). The energy which is absorbed during fracture (the controlling factor in the critical strain energy release rate) is controlled by the manner in which the material fractures.

The mode of fracture of the various alloys was studied by two techniques. First, motion pictures were taken through the microscope while the crack slowly propagated across the viewing field via the WLDCB method. Individual frames of this film were then printed and sequences of propagating cracks could then be studied. Magnifications of approximately 1000X were achieved in this way. Secondly, the fractured surfaces were studied via transmission electron microfractography (see Appendix IV). Both of these techniques indicate that in the fine grained alloys (grain size

TABLE II
PHYSICAL PROPERTY DATA

Wt. % Co	Grain Size in microns	Transverse Rupture Strength psi	Compressive Yield psi .002% offset	Ultimate Compressive Strength psi	Critical GI Strain Energy Release Rate in lbs/in ²	Critical Stress Intensity Parameter psi in Kf	Hardness Rockwell A	Modulus of Elasticity 10 ⁶ psi	Binder Film Thickness in microns
15	1.5	430,000	158,000	662,000	1.9	12,500	89.0	83.1	.29
	2.5-3	420,000	102,000	556,000	3.25	15,000	87.0	72.4	.65
	7-8	388,000	78,000	458,000	6.5	22,000	85.0	71.9	1.4
9	1.5	340,000	221,000	709,000	.88	8,400	90.5	81	.16
	2.5-3	306,000	212,000	631,000	1.7	11,600	88.9	79.2	.38
	7-8	340,000	142,000	515,000	4.78	19,000	87.3	76.0	1.05
3	1.5	196,000	420,000	860,000	.58	6,500 ^f	92.8	95.5	.09
	2.5-3	250,000	280,000	693,000	.98	9,600	91.3	94.7	.14
6	7-8	298,000	190,000	566,000	1.98	13,000	88.6	84.5	

FIGURE 12
CRITICAL STRAIN ENERGY RELEASE RATE
VERSUS BINDER FILM THICKNESS FOR WC-Co ALLOYS

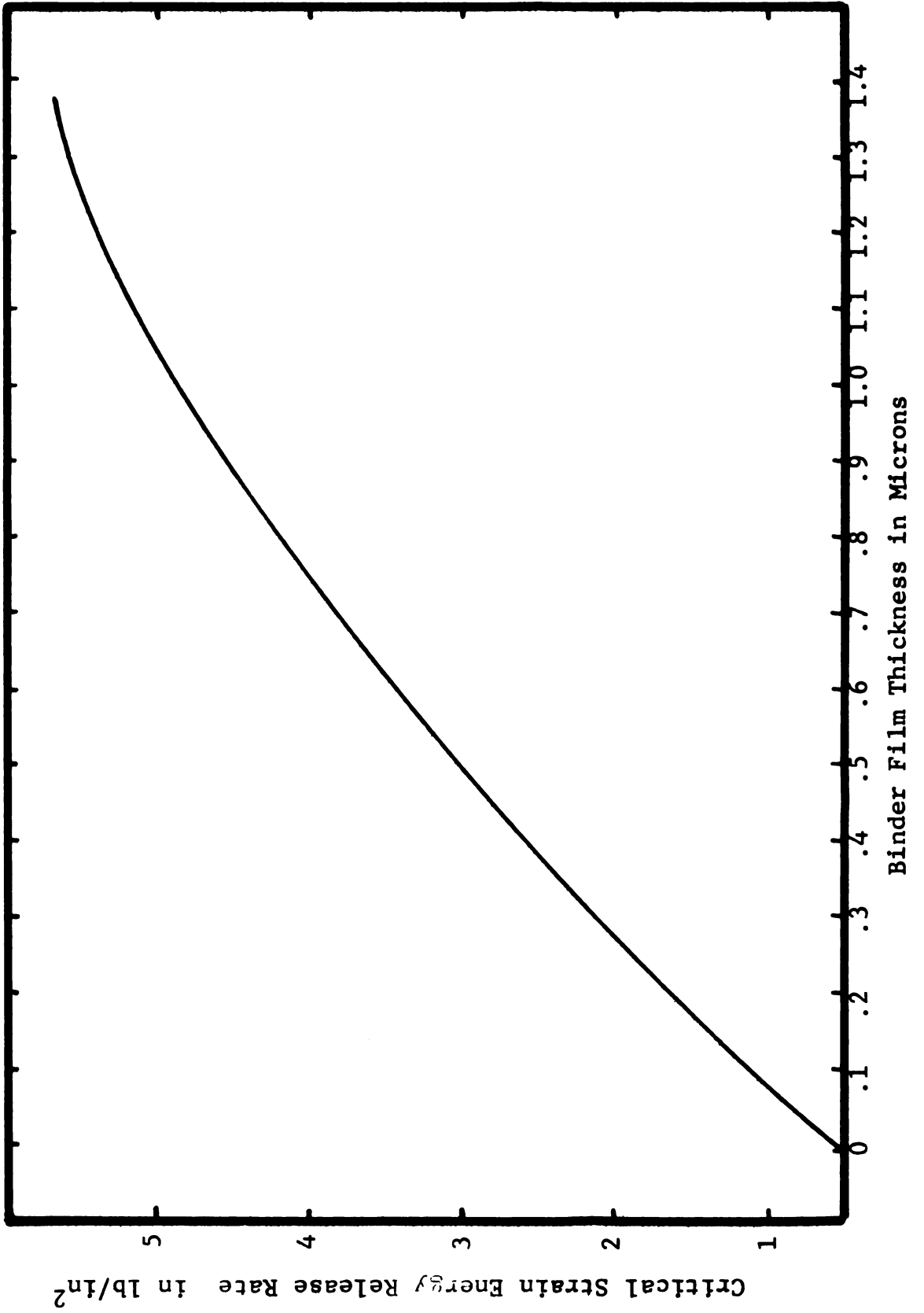


FIGURE 12

approximately 1.5 microns) the fracture travelled almost totally through the binder phase. From the electron microfractographs it can be seen that for the 3% and 9% alloys the mode of fracture was mainly a binder tungsten carbide particle interface separation, whereas in the 15% alloy there was a very ductile failure of the binder phase with some grain fracture (see Appendix IV). In the 15% and 9% large grained alloys (approximately 8 micron grain size) the fracture propagated by fracturing of the tungsten carbide particles with the linking up of these fractures later by the ductile fracture of the remaining binder ligaments. The alloy with 6% binder and large grains, however, again failed almost totally through the binder phase. This observation is contrary to the general feeling among other investigators that all tungsten carbide-cobalt alloys with grains larger than 5 microns will fail through particle fracture. The medium grain size alloys (grain size of 2.5-3 microns) failed with various amounts of all of the above mechanisms with the higher cobalt materials tending toward more grain fracture.

These observations of fracture mode pertain to slow fractures as occurs in the WLDCB test. Samples in which the fracture was propagated at a high velocity, such as an

impact test, reveal a considerably greater preponderance of fractured carbide grains than do the slowly fractured samples. The large grained 6% alloy was changed to nearly a complete tungsten carbide particle type of fracture and the fine grained alloys also show a considerable amount of grain fracture (see Appendix IV). This phenomenon may be responsible for the large number of conflicting statements in the literature about fracture path as the various investigators have used many types of samples in their studies. Some have used transverse rupture bars, other impact bars, and still others cracks at the corners of hardness impressions, all of which vary considerably in fracture speed. The kind of fracture which will give the most fruitful information must be the very slow fracture as a high speed fracture in itself indicates an excess of energy necessary to propagate the crack and in this case catastrophic failure is underway and will not be stopped; rather a study of the growth of a crack to critical proportions is most important and this indicates a slowly growing crack.

The fracture path of these alloys as well as the change in fracture toughness can be understood if we consider the distance about the crack tip where the material will have

reached yield. From McClintock and Irwin(11) the distance from the crack tip at which material will be yielded according to the Mises criterion is approximately

$$r_y = .4 \left(\frac{K_{Ic}}{\sqrt{\pi} \sigma_{YS}} \right)$$

where σ_{YS} is the yield strength of the material. The value of this parameter for the various alloys as well as mode of failure can be found in Table III. This equation was derived for an isotropic homogeneous material and may very well be optimistic due to the effect of the strong hard carbide particles. From Table III it is observed that those alloys with a calculated r_y of 1 or less grain diameters failed via the binder regardless of the grain size. The alloys of medium grain size and $r_y > 2$ grain diameters failed in a combination of grain fracture and binder failure with a larger amount of grain fracture as the binder content is increased. The fine grained alloys largely resist grain fracture regardless of the plastic zone size and the large grained alloys with $r_y > 2$ failed by grain fracture. The type of fracture which dominates in a given tungsten carbide-cobalt alloy is determined by several factors. As the binder at the tip of a crack yields, dislocation multiplication and migration occurs; if the zone over which this happens is large enough to include several tungsten carbide grains, then these

TABLE III
THE EFFECT OF PLASTIC ZONE SIZE ON MODE OF FRACTURE

Cobalt Wt. %	Grain Size in microns	r_y in microns	r_y in grain diameter	Mode of Fracture
15	1.5	11.1	7	Ductile binder failure
15	2.5-3	27.6	9	Failure of larger grains with considerable binder failure
15	8	29.5	7	Grain fracture
9	1.5	2.8	1	Interfacial and ductile binder failure
9	2.5-3	6.3	2	Ductile binder failure with some grain fracture
9	8	27.5	3	Grain fracture
3	1.5	.5	0	Interfacial and ductile binder failure
3	2.5-3	2	0	Interfacial and ductile binder failure
6	8	9.6	1	Ductile binder failure

dislocations will pile up against the tungsten carbide particles resulting in very high stress levels in the particles. The particle strength and perfection is related very strongly to size in the micron range with the smaller particles being considerably stronger than the large. Also the large particles >5 microns may not be monocrystalline and would thus have planes of weakness. If the particles are not strong enough to withstand this stress the particles in the plastic zone will fracture followed by the ductile failure of the remaining binder ligaments. If the zone over which plastic deformation occurs is not large enough to include the area one grain diameter away from the tip of the crack the plastic deformation will be largely confined to the one binder film where the crack tip is located. If this is the case the amount of plastic work will be considerably less than for alloys where larger areas have yielded, and the critical strain energy release rate will be much lower. This would be the case for the 3% alloys and the fine grained 9% alloy.

This dislocation migration and multiplication has been observed in tungsten carbide-cobalt alloys through internal friction studies by H. Doi, Y. Fujiwara and K. Miyake(13).

In their investigation they studied the effects of plastic deformation in compression on both the amplitude dependent and amplitude independent components of internal friction. They established that the fourth root of the plastic strain is proportional to the magnitude of the stress above yield.

$$\Delta\sigma = (\sigma - \sigma_{.00002}) = C_1 \sqrt[4]{\epsilon_p}$$

This was done using standard strain gage techniques. They also found that by normalizing the plastic strain with the volume % cobalt that the constant of proportionality is essentially independent of cobalt content or grain size. These relations have been found to hold in the present study (see figure 13) such that

$$\Delta\sigma = (\sigma - \sigma_{.00002}) = C_2 \sqrt[4]{\frac{\epsilon_p}{1-f}}$$

where f is the volume fraction of WC.

Using the Granato Lucke theory of dislocation damping, Doi found the distance between pinning points of the dislocations to be approximately .074 microns at room temperature. This was also found to be independent of plastic strain, cobalt content, or grain size.

They established that the relation between dislocation density and amount of plastic prestrain is:

FIGURE 13
COMPRESSIVE STRESS VERSUS THE FOURTH
ROOT OF PLASTIC STRAIN

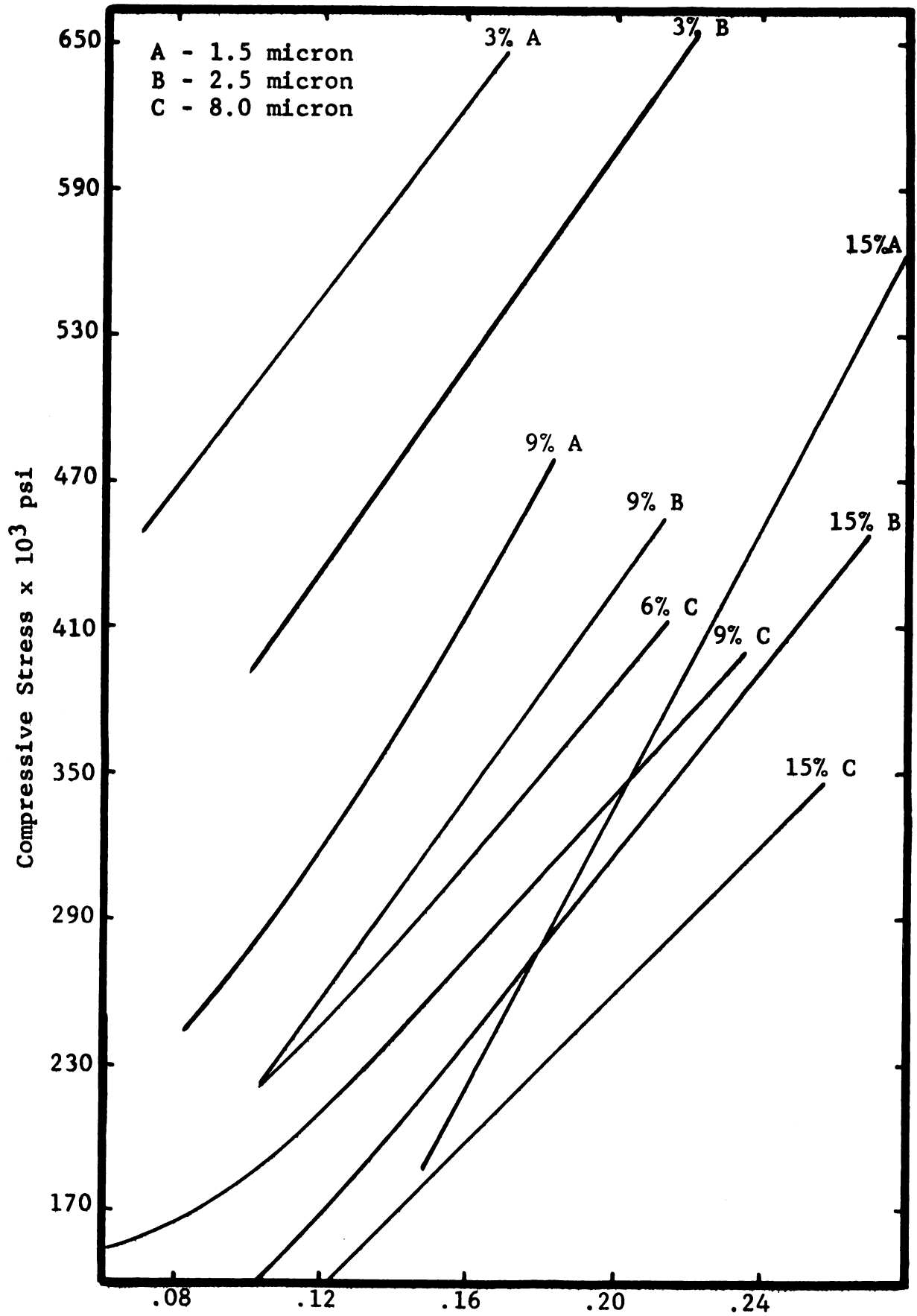


FIGURE 13

$$\rho \approx 2.7 \times 10^{10} \left(\frac{1}{B}\right) \left\{\frac{\epsilon_p}{1-f}\right\}^{1/2}$$

where B is a damping constant. (B for cobalt has not been directly measured and could range from 10^{-4} to 10^{-1} .)

From this relationship and the relation between stress above yield and plastic strain then

$$\Delta\sigma = (\sigma - \sigma_{.00002}) = C_2 \sqrt[4]{\frac{\epsilon_p}{(1-f)}}$$

$$(\Delta\sigma)^2 = (\sigma - \sigma_{.00002})^2 = C_2^2 \sqrt[4]{\frac{\epsilon_p}{(1-f)}}$$

$$\Delta\sigma^2 = C_2^2 \left[\frac{\rho B}{2.7 \times 10^{12}} \right]$$

or

$$\Delta\sigma^2 = K\rho$$

where K is a constant.

First consider the effects of these dislocations on the WC particles. Ansel and Lenel (Reference # 14) show that the stress on a precipitate particle (WC grain) is $\tau = n\sigma$ where σ is the stress applied to the sample and n is the number of dislocations which are being forced against the particle. They then derive the relation that the number of dislocations is equal to

$$n = \frac{2\lambda\sigma}{\mu b}$$

where σ is the applied stress, λ is the free distance between particles (binder film thickness) and b is the burgers vector of the dislocation. They then assume that the limiting stress which a particle can withstand is proportional to the modulus of the material; then if U_e^* is the modulus of the carbide particle

$$\tau_{\text{for fracture}} = \frac{\sqrt{\mu b U_e^*}}{2\lambda C}$$

or is proportional to $\sqrt{\frac{1}{\lambda}}$.

Calculations show that this form of a relationship is invalid in either compression or tension for WC cobalt alloys. The relationship which Ansell and Lenel derive for the average number of dislocations around a particle with respect to the applied stress in this case is of doubtful validity, since the equation was derived for a two dimensional model of a single pile up crystal. If we use the results of Doi (Reference # 8), however, then the dislocation density, and thus the average number of dislocations on any particle, is proportional to the stress above yield to the second power or

$$\Delta\sigma^2 = K\rho$$

The stress on a WC particle is

$$\sigma_{wc} = C\rho\sigma = K_2 \Delta\sigma^2 \sigma_{ULT}$$

where C and K_2 are constants.

Since K_2 is independent of cobalt content and grain size, then

$$\sigma_{wc} \left\{ \Delta\sigma^2 \sigma_{ULT} \right.$$

for all alloys.

If we calculate this parameter from the compression data of the alloys used in this study, the stress on a WC particle at failure is found to be constant for a given grain size regardless of cobalt content (see table IV).

TABLE IV
 COMPRESSIVE STRENGTH DATA

Cobalt	Grain Size μ	Compressive Yield Strength psi	Ultimate Compressive Strength psi	Factor Proportional to Stress on Particle
3	1.5	420,000	860,000	1665
9	1.5	221,000	709,000	1688
15	1.5	158,000	662,000	1681
3	2.5-3	280,000	693,000	1180
9	2.5-3	212,000	631,000	1107
15	2.5-3	102,000	556,000	1146
6	8	190,000	566,000	798
9	8	142,000	515,000	716
15	8	78,000	458,000	652

An implicit assumption in this statement is that the relationships which Doi derives are true in the total plastic range. This assumption has not been verified. The data presented here are, however, a strong argument for the correctness of this assumption. The compressive strength of tungsten carbide-cobalt alloys is then dependent on the yield strength of the binder and the strength of the tungsten carbide particles. The yield of these alloys has been explained by Doi on a dislocation bypass model of Ashby's and the strength of the tungsten carbide particles is very size dependent. From the above and Table IV the stress on a tungsten carbide particle of a 15% 1.5 micron grain size alloy which fails at 660,000 psi is the same as the stress on the tungsten carbide particles in a 3% 1.5 micron grain size alloy which fails at 860,000 psi, or a 9% 1.5 micron grain size alloy which fails at 710,000 psi. The 3% alloy is stronger than the others due to the thin binder film which impedes dislocation movement and multiplication and results in a high yield. Thus there will be fewer dislocations piled against the tungsten carbide particles at any given stress level and the composite will withstand a higher nominal stress than the high binder alloys. This explains why the compression strength of the

alloys continue to increase as the binder content goes down even though the fracture toughness value goes down. For this to occur, the material must have no flaws large enough to propagate in a compressional mode. The reason for this is that any surface flaws, as well as flaws perpendicular to the longitudinal axis of the specimen, will tend to close on compression and thus the effect will be minimal. The fracture toughness then is not consequential in the compression strength of this material unless a flaw of critical dimensions is present. The data shown in Table IV also reveal that the strength of the 1.5 micron particles is approximately twice that of the 8 micron grain size with the 3 micron particles in between.

The transverse rupture strength of these alloys is determined by the factors of strength of the tungsten carbide particles, the yield level of the binder, the size of flaws present on the surface, and the strain energy release rate. For the low binder materials the transverse rupture strength is below or close to the yield (3% 1.5 and 3 micron grain size, 9% 1.5 micron grain size alloys and 6% 8 micron grain size alloys) and the materials will fail when the strain energy release rate for crack propagation becomes critical for the flaw sizes which are present.

The surface flaws on the 3% 1.5 micron grain size and 9% 1.5 micron grain size materials which result from grinding should be approximately the same size and as a result the transverse rupture strength of the 9% alloy is about 33% higher due to the 33% higher strain energy release rate (the modulus of these two materials being fairly close). The 3% alloys with 3 micron grain size should have a larger inherent flaw size (assuming that the inherent flaws from grinding, etc. are proportional to the grain size of a given alloy) than the 9% 1.5 micron grain size alloy, and since they have approximately the same critical strain energy release rates, the 3% alloy is less strong in the transverse rupture sense. The 6% 8 micron grain size alloy would have the greatest flaw size of these alloys but also the greatest critical strain energy release rate, and as a result the transverse rupture strength is in the same range as the other alloys in this group.

For the alloys whose transverse rupture strength is below the yield strength the critical flaw size with respect to its critical strain energy release rate must be present. That is, no crack growth is necessary as the binder has not yielded and the grains in these alloys are not broken during fracture. Thus an increase in binder yield for these

alloys would not affect an increase in transverse rupture.

In the materials which show a transverse rupture strength above the yield strength, the transverse rupture strength is controlled by different mechanisms. For these alloys the strain energy release rate is such that the critical flaw sizes are not present. As these materials are loaded, dislocation motion and multiplication occur in the binder much as they do in the compression test. If the strength of the tungsten carbide particles is not sufficient to withstand the dislocation pressure the grains will fracture and lead eventually to a critical size flaw. This mechanism operates in the large grained higher cobalt alloys, especially where the critical strain energy release rate is high and the grain strength is low. In materials where the grain strength is sufficient to withstand the stresses imposed on them (15% 1.5 micron grain size) the binder itself must fail in a normal ductile manner until the critical flaw size is reached, then catastrophic failure will occur. For alloys of medium grain size all of these mechanisms can work, depending on the specific cobalt content and grain size. For this type of alloy, strengthening the binder should raise the transverse rupture strength and lower the critical strain energy release rate.

Considering some of the earlier theories of the strength of cemented carbides in the light of the views presented here we find some great differences. The skeleton theory has been viewed very differently by the various authors. In fact, some attribute the strength of cemented carbide to this theory and others the weakness of the alloys to the same theory. Generally it is agreed that the lower the cobalt content and the finer the grain size, the more complete the skeleton will be. There has not been conclusive proof of either the presence or absence of a carbide skeleton. However, if we assume it to exist, then for the low cobalt, small grain size alloys (such as the 3% 1.5 micron alloy in this study) during fracture there would be a large number of broken grains. This would be a necessary result of a continuous skeleton. The less complete the skeleton the smaller the number of broken grains. This would occur as we go to higher cobalt contents. The evidence presented in this study, however, indicates the opposite occurs; that is, as we lower the cobalt content fewer fractured grains are observed. The reasons for this have been described earlier. These observations hold for all grain sizes and make the existence of a skeleton of any completeness doubtful.

On the question of residual thermal stresses as a result of differences in the thermal coefficient of expansion, the major drawbacks to this theory are the lack of experimental agreement of not only the magnitude but also the sign of these stresses, the fact that this view does not explain the different modes of failure, the qualitative nature of the theory, and the lack of three dimensional calculations. The calculations presented here with regard to the stresses on the tungsten carbide particles of grain size during ultimate compressive failure indicate that if these thermal stresses are present, they have no great effect. The values of the numbers, as derived in this study, which are proportional to tungsten carbide particle stress at failure in ultimate compression are the same for a given grain size regardless of cobalt content, whereas thermal stresses certainly would not be. The calculations of Doi, Fujiwara and Miyake also indicate that these stresses must be low as they have had success in calculating the yield stress of tungsten carbide-cobalt alloys on the dislocation bypass model of Ashby's. This would not be possible if residual stresses played a major role in this material. The theory which Drucker and Butler propose fails to explain many of the phenomena which occur with respect to

the failure of cemented carbides. With regard to the left hand side of the transverse rupture vs. mean free path curve, they propose that an increase in the tungsten in solution in the cobalt would reduce the transverse rupture strength of the material. For a large part of this curve the opposite effect is observed (see Reference #4). With regard to the right side of this curve their contention is that by applying a Griffith type approach the average stress of fracture is inversely proportional to the square root of the particle diameter, or $\sigma_{ave} = K / \sqrt{d}$.

It is then proposed that K is independent of carbide volume or clear spacing. This proposal would necessitate that the strain energy release rate G_I times the modulus of elasticity of tungsten carbide-cobalt alloys would be a constant with regard to cobalt content or free spacing. This is obviously in error as Figure 13 will indicate - the G_I in alloys of this kind varies by a factor of 3 whereas the modulus varies little. With regard to compressive loading, Butler states that "As volume fraction of Co is decreased, eventually there will not be enough Co to wet the WC during sintering and completely cover all or most of the WC particles. When this happens there is not enough Co to smooth out peaks of stress due to WC-WC

contacts and early fracture occurs." This statement also must be questioned as the fracture strength in compression of tungsten carbide-cobalt alloys is found to increase as the cobalt is decreased (see reference #7). Also, the dislocation bypass model of Ashby as applied by Doi works well with these materials even in the low cobalt range; this would not be possible if there was a shortage of cobalt to cover the surface of the tungsten carbide particles. Kreimer, in developing his theory involving a Griffith approach, made several assumptions which in the light of this work do not seem justified. He assumes:

- 1) On the left, or ascending, portion of the cobalt content vs. transverse rupture curve that the yield strength of the cobalt is equal to the ultimate strength.
- 2) The more cobalt phase showing on the fracture the larger the amount of energy necessary to fracture the material.
- 3) The area of fracture composed of cobalt is proportional to the volume of the cobalt phase in the alloy; thus the plastic work is proportional to cobalt content.

All of these assumptions have been found to be in error

as a result of the information presented in this work.

The theories of Griffith and Orowan can be fruitfully applied to tungsten carbide-cobalt alloys. However, in the past they have been diluted with various unfounded assumptions about material behavior. In this work no assumptions about the material have been made.

CONCLUSIONS

The mode of failure of a tungsten carbide-cobalt alloy can vary widely depending on several compositional and microstructural factors. The failure mode of these alloys under tensile loading depends on the plastic zone size at the tip of the crack and the carbide grain size of the alloy. If the plastic zone radius is less than one grain diameter, then the alloy will fail through the cobalt binder regardless of the carbide grain size. If the plastic zone size is large enough to include several grains, then the failure mode will depend on the carbide grain strength. That is, the larger grained alloys (weak grains) will fail through grain fracture; the smaller grained alloys will fail through ductile binder failure. Medium grain size alloys with large plastic zone sizes will fail with various amounts of these modes, depending on cobalt content and grain size. The higher the cobalt content and the larger the grain size the more the fracture will tend to be transgranular.

The strength of these alloys in tension depends on the inherent flaw size and the fracture toughness. The shape of the transverse rupture strength vs. binder film thickness curve is a necessary result of these factors.

The compressive strength of these alloys is dependent on carbide grain strength and dislocation density in the cobalt at ultimate failure load. The stress imposed on the grains of tungsten carbide-cobalt alloys has been found to be constant for a given grain size regardless of cobalt content, and as a result the compressive strength will rise as the binder film thickness goes down for a given grain size.

The approach to the strength of cemented carbides presented here allows much of what was considered anomalous behavior of tungsten carbide-cobalt alloys in both the laboratory and the field to be recognized as a necessary result of the nature of tungsten carbide-cobalt alloys.

BIBLIOGRAPHY

BIBLIOGRAPHY

- 1 Schwartzkopf and Kieffer, Cemented Carbides, The MacMillan Co., New York
- 2 W. Dawihl and T. Hinnuber, Kolloid, Vol. 20, No. 104, p. 233 (1943)
- 3 V. A. Ivensen, O. N. Eiduk, and L. Pivovavov, Poroshkovaya Met., Vol. 22, No. 4 (1969)
- 4 Suzuki, Hayashi, and Kawakatsa, Nippon Kinzoku Gakkaishi, Vol. 4, No. 33, p. 504 (1969)
- 5 J. Gurland and J. T. Norton, Jour. of Metals, Vol. 4, No. 10, p. 1051 (1952)
- 6 W. Spath, Metall., Vol. 12, p. 925 (1958)
- 7 R. C. Lueth and T. E. Hale, Materials Research and Standards MTRSA, Vol. 10, No. 2, p. 23
- 8 H. Doi, Y. Fujiwara, and K. Miyake, Transactions of the Metallurgical Society of AIME, Vol. 245, pp. 1457-1470, July 1969
- 9 M. Ashby, 2 Metall. 1964, Vol. 55, pp. 5-17
- 10 G. S. Kreimer, "Strength of Hard Alloys," translation from Russian by Consultants Bureau, 1968, Plenum Publishing Corp., N.Y., N.Y.
- 11 F. A. McClintock and G. R. Irwin, "Plasticity Aspects of Fracture Mechanics," Fracture Toughness Testing and Its Applications, ASTM STP 381

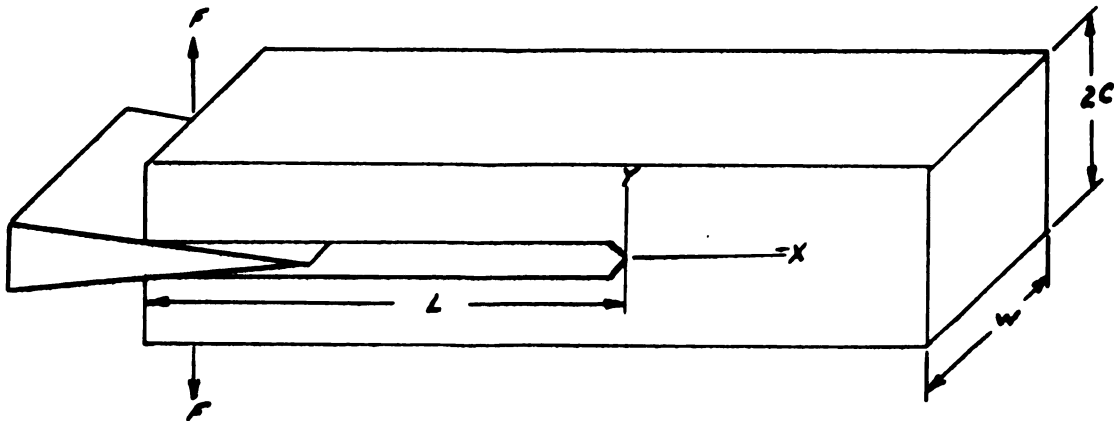
- 12 D. C. Drucker, "Engineering and Continuum Aspects of High Strength Materials," High Strength Materials, Ed. by Zakey 1965, John Wiley & Sons, Inc., N.Y., N.Y.
- 13 J. C. Fischer, E. W. Hart, and R. H. Pry, Acta Met., Vol. 1, p. 336 (1953)
- 14 G. S. Ansell and F. V. Lenel, Acta Met., Vol. 9, No. 8, p. 612 (1960)

APPENDICES

APPENDIX I

ANALYSIS OF THE DOUBLE CANTILEVER BEAM TEST

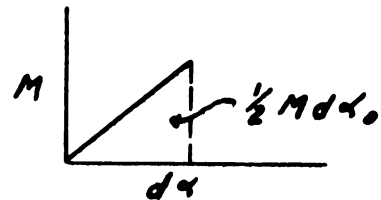
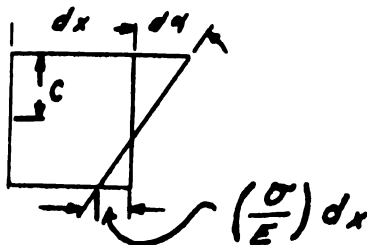
THE DOUBLE CANTILEVER BEAM TEST



Treating this system as a simple cantilever beam, the bending moment at any cross section is

$$M(x) = F(L-x) \quad , \quad 0 \leq x < L$$

Using a simple strength of materials approach and observing one small element of the beam dx , the moment on this section is $M(x)$. This moment causes one face of the element dx to rotate through an angle $d\alpha$ with respect to the other face.



If this deformation is linear, then the internal work produced by M is $1/2 M d\alpha$. If we consider the angular deformation small, then

$$d\alpha = \tan d\alpha = \frac{\left(\frac{\sigma}{E}\right) dx}{c} \quad (\text{see Fig. 1})$$

where σ is the stress at the distance c from the neutral axis. Therefore,

$$\sigma = \frac{Mc}{I} \quad ; \quad d\alpha = \left(\frac{M}{EI}\right) dx$$

The strain energy of an element at length dx is then

$$U_{dx} = \frac{1}{2} M d\alpha = \frac{1}{2} \frac{M^2 dx}{EI}$$

The total strain energy in the beam is then

$$U_T = \frac{1}{2EI} \int_0^L M^2(x) dx = \frac{1}{2EI} \int_0^L (F(L-x))^2 dx = \frac{F^2 L^3}{6EI}$$

To determine the deflection, we use Castigliano's theorem

$$\delta_o = \left. \frac{U}{F} \right|_{x=L} = \frac{FL^3}{3EI}$$

Squaring both sides

$$\delta_o^2 = \frac{F^2 L^6}{9E^2 I^2} = \frac{F^2 L^3}{6EI} \left(\frac{2L^3}{3EI}\right)$$

Substituting in above we get

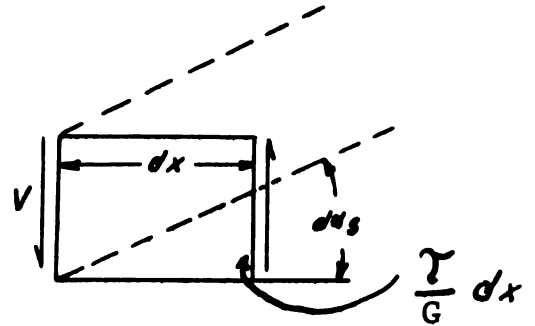
$$\delta_0^2 = U \left(\frac{2L^3}{3EI} \right) \quad \text{or} \quad U = \frac{3EI \delta_0^2}{2L^3}$$

This is the strain energy of one beam in terms of the deflection.

There is a contribution to the deflection due to shear of the beam. The development of this is as follows:

The shear stress at any point is $\frac{F}{tw} = \frac{V}{tw}$. The shear force = V . This causes one face of an element dx to rotate through an angle $d\alpha_s$, the internal work due to this is

$$U_s = \frac{1}{2} V d\alpha_s$$



If $d\alpha_s$ is considered small, then

$$- d\alpha_s = \tan d\alpha_s = \frac{\tau}{G} dx/dx = \frac{\tau}{G} = \frac{V/tw}{G}$$

Total energy then equals

$$U_s = \int_0^L \frac{1}{2} \frac{V^2}{Ga} dx = \int_0^L \frac{1}{2} \frac{F^2}{Ga} dx = \frac{F^2 L}{2Gtw}$$

$$\frac{\partial U}{\partial F} = \frac{FL}{GtW} = \delta_{o_s} = \frac{3Et^2}{GL^2} \delta_{o_M}$$

$$\frac{3E}{G} \left(\frac{t}{L}\right)^2 \approx \frac{t^2}{L^2}$$

This error for long thin beams can be neglected for $t/L > 0.1$. The error would then be 1% by neglecting this.

At the instant that the crack begins to propagate the surface energy of the crack must be provided by the strain energy and the work done by the applied force. This is essentially the Griffith criterion.

$$\frac{\partial S}{\partial L} = - \frac{\partial U}{\partial L} + \frac{\partial W}{\partial L}$$

That is, the rate at which surface energy is used per unit crack extension must equal the strain energy release rate plus the work done by the external forces. In the system to be used here the loading is via a wedge, and thus the displacement of the force is controlled and is taken as zero as the crack begins to propagate. Thus,

$$\frac{\partial S}{\partial L} = - \frac{\partial U}{\partial L} \quad \text{or} \quad S = U$$

$$S = \gamma Lw \quad ; \quad U = \frac{3EI}{2L^3} \delta_o^2$$

$$S = \gamma Lw = U = \frac{3Ewt^3 \frac{1}{12} \delta_o^2}{2L^3}$$

$$S = \gamma W L = \frac{3E \frac{1}{12} t^3 \delta_o^2}{2L^3}$$

$$\gamma L = \frac{3E \frac{t^3}{12} \delta_o^2}{2L^3}$$

$$\frac{\partial S}{\partial L} = \gamma = - \frac{\partial U}{\partial L} = \frac{3E \frac{1}{12} t^3 \delta_o^2 6L^2}{4L^6}$$

$$\frac{\partial U}{\partial L} = \frac{3E t^3 \delta_o^2}{8L^4} = G$$

This is the strain energy release rate. From this we can calculate the stress intensity parameter for this configuration

$$K_I = (G E)^{1/2}$$

$$K_I = \frac{\sqrt{3} E t^{3/2} \delta_o}{2 \sqrt{2} L^2}$$

The derivation of this parameter and its relation to G will now be derived, starting with the equilibrium and compatibility equations of plane extension elasticity.

$$\frac{\partial \sigma_x}{\partial x} + \frac{\partial \tau_{xy}}{\partial y} = 0 \quad ; \quad \frac{\partial \tau_{xy}}{\partial x} + \frac{\partial \sigma_y}{\partial y} = 0$$

$$\nabla^2 (\sigma_x + \sigma_y) = 0$$

and assuming an Airy type stress formulation

$$\sigma_x = \frac{\partial^2 \phi}{\partial y^2} \quad ; \quad \sigma_y = \frac{\partial^2 \phi}{\partial x^2} \quad ; \quad \tau_{xy} = - \frac{\partial^2 \phi}{\partial x \partial y}$$

we obtain a biharmonic nature for ϕ or $\nabla^4 \phi = 0$. Choosing

$$\phi = \psi_1 + X\psi_2 + Y\psi_3$$

will satisfy equation

$$\nabla^4 \phi = 0$$

if each is harmonic, that is

$$\nabla^2 \psi_i = 0$$

using

$$Z = x + iy$$

and a function $\bar{Z}(z)$ and its derivatives

$$\frac{\partial \bar{Z}}{\partial z} = \bar{z} \quad ; \quad \frac{\partial \bar{Z}}{\partial \bar{z}} = z \quad ; \quad \frac{\partial Z}{\partial z} = z'$$

have harmonic real and imaginary parts if the function is analytic.

if $\bar{Z} = \text{Re}\bar{Z} + i\text{Im}\bar{Z}$ then $\nabla^2(\text{Re}\bar{Z}) = \nabla^2(\text{Im}\bar{Z}) = 0$

This is a result of the Cauchy-Riemann condition, that is

$$\frac{\partial \operatorname{Re} \bar{Z}}{\partial x} = \frac{\partial \operatorname{Im} \bar{Z}}{\partial y} = \operatorname{Re} Z \quad ; \quad \frac{\partial \operatorname{Im} \bar{Z}}{\partial x} = - \frac{\partial \operatorname{Re} \bar{Z}}{\partial y} = \operatorname{Im} Z$$

If we let

$$\phi_I = \operatorname{Re} \bar{Z}_I + y \operatorname{Im} \bar{Z}_I$$

this automatically satisfies equilibrium and compatibility.

The resulting stresses are

$$\sigma_x = \operatorname{Re} Z_I - y \operatorname{Im} Z_I'$$

$$\sigma_y = \operatorname{Re} Z_I + y \operatorname{Im} Z_I'$$

$$\tau_{xy} = - y \operatorname{Re} Z_I'$$

Then any function

$$Z_I = \frac{g(z)}{[(z+b)(z-a)]^{1/2}}$$

will solve crack problems for a crack allowing the x axis from $x = -b$ to $x = a$ ($y = 0$), if $g(x)$ is well behaved, since the stresses σ_y and τ_{xy} , along the interval are zero provided that

$$\operatorname{Im} g(x) = 0 \quad \text{for} \quad (-b < x < a)$$

Substituting the variable $\rho = (z-a)$, then

$$Z_I = \frac{f(\rho)}{\rho^{1/2}} \quad ; \quad Z_I \Big|_{|\rho| \rightarrow 0} = \frac{K_I}{(2\pi\rho)^{1/2}}$$

using polar coordinates $\rho = re^{i\theta}$, the crack tip stress field is:

$$\sigma_x = \frac{K_I}{(2\pi r)^{1/2}} \cos \frac{\theta}{2} \left[1 - \sin \frac{\theta}{2} \sin \frac{3\theta}{2} \right]$$

$$\sigma_y = \frac{K_I}{(2\pi r)^{1/2}} \cos \frac{\theta}{2} \left[1 + \sin \frac{\theta}{2} \sin \frac{3\theta}{2} \right]$$

$$\tau_{xy} = \frac{K_I}{(2\pi r)^{1/2}} \sin \frac{\theta}{2} \cos \frac{\theta}{2} \cos \frac{3\theta}{2}$$

The strain in the y direction can be written in terms of displacements and stresses by Hooke's Law:

$$\epsilon_y = \frac{\partial V}{\partial y} = \frac{\sigma_y}{E} - \frac{\nu}{E} (\sigma_x + \sigma_z)$$

for plain strain $\epsilon_z = 0$ and

$$\sigma_z = \nu(\sigma_x + \sigma_y)$$

This leads to

$$V = \frac{1+\nu}{E} [2(1-\nu) \text{Im}\bar{Z}_I - y\text{Re}Z_I]$$

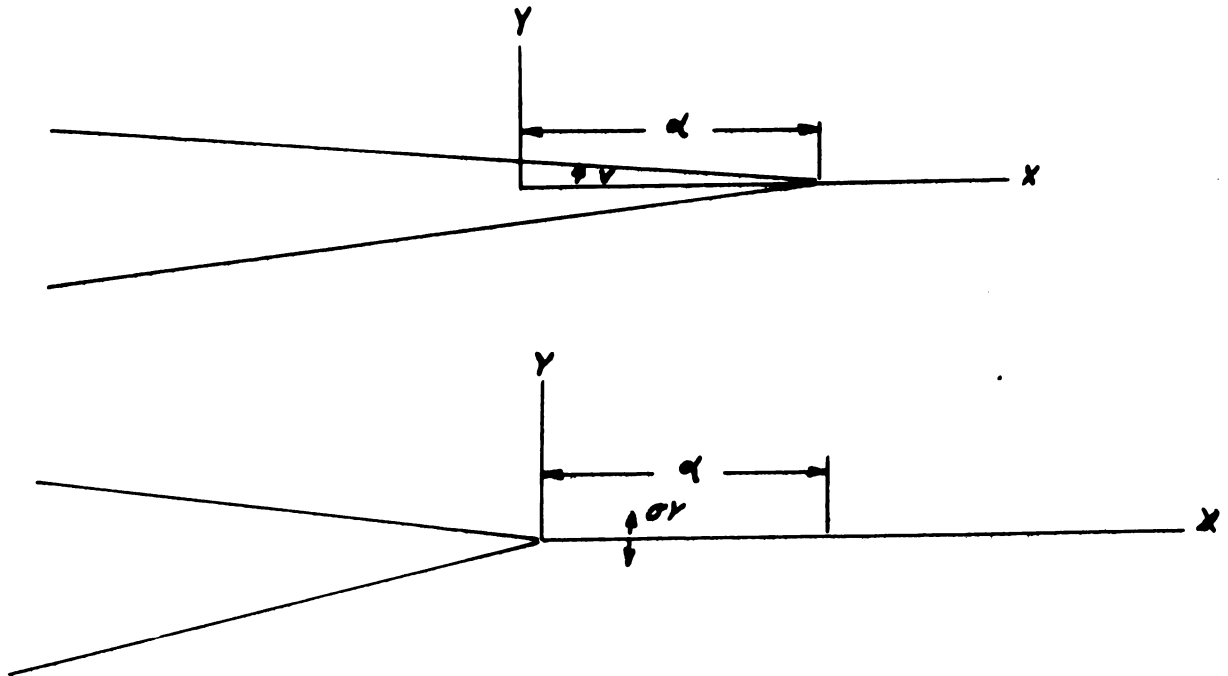
using

$$Z_I \Big|_{|\rho| \rightarrow 0} = \frac{K_I}{(2\pi\rho)^{1/2}} \quad ; \quad \rho = re^{i\theta}$$

$$V = \frac{2K_I}{E} (1+\nu) \left(\frac{r}{2\pi}\right)^{1/2} \sin \frac{\theta}{2} [2 - 2\nu - \cos^2 \frac{\theta}{2}]$$

or for $\theta = \pi$

$$V = \frac{2K_I}{E} (1-\nu^2) \sqrt{2} \frac{r}{\pi}$$



Now, to compute the work necessary to close an increment of the crack adjacent to the crack tip. This work is recoverable upon reopening and is the energy available for that increment of crack extension: Taking unit thickness the work per unit area done in closing the crack increment is:

$$G = \lim_{\alpha \rightarrow 0} \frac{2}{\alpha} \int_0^{\alpha} \frac{\sigma_y V}{2} dx$$

$$\sigma_y \text{ for } \theta = \pi = \frac{K_I}{(2\pi x)^{1/2}}$$

$$G = \lim_{\alpha \rightarrow 0} \frac{2}{\alpha} \int_0^{\alpha} \frac{2K_I}{2(2\pi x)^{1/2}} \left(\frac{K_I(1-\nu^2)}{E} \left(\frac{2(\alpha-x)}{\pi} \right)^{1/2} \right) dx$$

$$G = \lim_{\alpha \rightarrow 0} \frac{2K_I^2(1-\nu^2)}{\alpha E} \int_0^{\alpha} \sqrt{\frac{2(\alpha-x)}{\frac{\pi}{2\pi x}}} dx$$

$$G = \lim_{\alpha \rightarrow 0} \frac{2K_I^2(1-\nu^2)}{\alpha E} \int_0^{\alpha} \frac{1}{\pi} \left(\frac{\alpha-x}{x} \right)^{1/2} dx$$

$$G = \lim_{\alpha \rightarrow 0} \frac{2K_I^2}{\pi \alpha E} (1-\nu^2) \int_0^{\alpha} \left(\frac{\alpha-x}{x} \right)^{1/2} dx$$

$$G = \lim_{\alpha \rightarrow 0} \frac{(1-\nu^2)2K_I^2}{\pi \alpha E} \left((\alpha-x)^{1/2} (x)^{1/2} + \alpha \sin^{-1} \frac{x}{\alpha} \right) \Big|_0^{\alpha}$$

$$G = \lim_{\alpha \rightarrow 0} \frac{(1-\nu^2)2K_I^2}{\pi \alpha E} \left(\alpha \frac{\pi}{2} \right) = \frac{K_I^2(1-\nu^2)}{E}$$

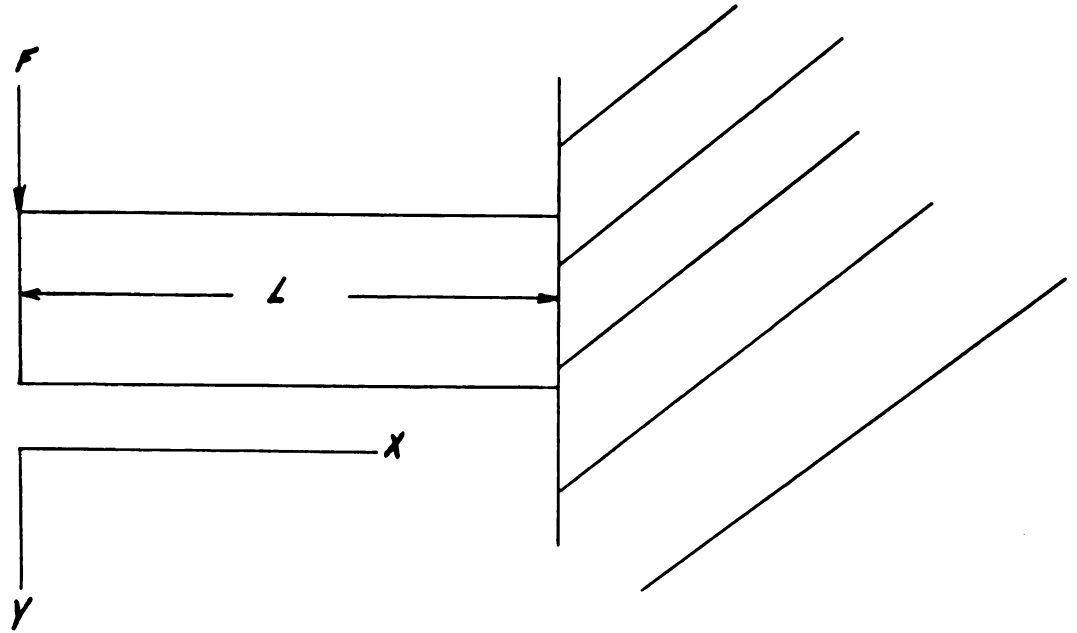
The above equation is a direct relation between the stress intensity parameter and the strain energy release rate G. Thus both approaches are equivalent and lead to the same

result whether by energy consideration or stress consideration. Both result in material parameters which are indicative of the material's ability to resist propagation at existing flows.

The above discussion lays the basic groundwork for the proposed work; however, several things must be considered further. First, when using a simple cantilever approach to the D.C.B. type specimen, we are subject to all the assumptions implicit in the strength of materials such as no deflection or rotation at the base of the beam. However, this does not hold in our case as the two beams are really part of a larger system and there will be a contribution to the strain energy in the section past the base of the legs. Also the fact that the beam is finite will change this contribution as the crack approaches the end of the sample. Another area which must be looked at is the effect of the axial load applied during wedge loading as the system which will be used in this investigation is a wedge loaded D.C.B. specimen.

Gillis and Gillman (Ref. 1) have attempted to take these effects into consideration in a strength of materials approach by allowing rotations due to shear and an arbitrary rotation due to the strains past the crack tip.

According to Gillis and Gillman:



The bending moment at any cross section is

$$M = -Fx$$

The shearing force is

$$V = -F$$

The bending curvature relation is

$$\frac{\partial^2 y}{\partial x^2} = -M/EI + k/AG \frac{\partial V}{\partial X}$$

where k is a constant close to 1, A is the cross sectional area, assuming all sections are free from warp

$$\frac{\partial y}{\partial x} = \frac{Fx^2}{2EI} - \frac{kF}{AG} + C_1$$

Using this condition to allow some arbitrary rotation at the base $C_1 = -\theta$, then

$$\frac{\partial y}{\partial x} = -F(L^2 - x^2)/2EI - (kF/AG) - \theta$$

This allows some rotation due to shear and some due to energy past the crack tip. Then

$$y = -F(3L^2x - x^3)/6EI - (kFx/AG) - \theta x + C_2$$

due to symmetry

$$y = 0 \quad \text{at} \quad x = L$$

and

$$Y = [F(2L^3 - 3L^2x + x^3)/6EI) + (kF(L-x)/AG) + \theta(L-x)]$$

and

$$y_0 = (FL^3/3EI) + (kFL/AG) + \theta L$$

Now the strain energy in the beam is given by

$$U_b = \int_0^L \frac{M^2 dx}{2EI} + \int_0^L \frac{kV^2}{2AG} dx$$

$$U_b = F^2 L^3 / 6EI + kF^2 L / 2AG$$

By Castigliano's theorem

$$Y_o = \left(\frac{\partial U}{\partial F} \right) = \frac{\partial U_b}{\partial F} + \frac{\partial U_a}{\partial F}$$

where U_a is the energy past the crack tip. From this we obtain

$$\frac{\partial U_a}{\partial F} = \theta L$$

Under adiabatic conditions of crack initiation

$$dQ = dE + dW = 0 \quad ; \quad dQ = 0$$

$$dE = dS_{\text{surface}} + dU_{\text{strain energy}} \quad ; \quad dW = - Fdy_o$$

$$dS + dU = Fd'y_o$$

surface energy = γbL where γ is the specific surface energy.

Choosing F and L as independent variables

$$\frac{\partial U}{\partial F} = F \left(\frac{\partial Y_o}{\partial F} \right) \quad ; \quad \frac{\partial U}{\partial L} + \gamma b = F \frac{\partial Y_o}{\partial L}$$

$$U = U_b + U_a = F^2 L^3 / 6EI + kF^2 L / 2AG + \theta LF$$

$$Y_o = FL^3 / 3EI + kFL / AG + \theta L$$

$$\begin{aligned}\frac{\partial U}{\partial F} &= \frac{FL^3}{3EI} + \frac{kFL}{AG} + \theta L = F \left(\frac{\partial y_o}{\partial F} \right) \\ &= \frac{FL^3}{3EI} + \frac{kFL}{AG} + FL \frac{\partial \theta}{\partial F}\end{aligned}$$

This requires that θ be dependent linearly on F , that is

$$\theta = CF$$

This also implies that y_o must depend linearly on F . If this is true, then from conservation of energy

$$Fy_o/2 = U_a + U_b$$

$$F^2L^3/6EI + kF^2L/2AG + CF^2L/2 = \frac{F^2L^3}{6EI} + \frac{kF^2L}{2AG} + \theta FL$$

$$\theta = CF \quad ; \quad U_a = CF^2L/2$$

assume

$$C = C_1 L^n / EI$$

then

$$\frac{\partial U}{\partial L} + \gamma b = F \left(\frac{\partial y_o}{\partial L} \right)$$

and

$$\gamma = (F^2L^2/2EIb)[1 + (kEI/AGL^2) + (n+1) C_1 L^{n-2}]$$

In this theory the values of n , k , C are not known. Two ways to obtain these will now be discussed. First, however, consider the term in the last bracket:

$$\left[1 + \frac{kEI}{AGL^2} + (n+1) C_1 L^{(n-2)}\right] = \left[1 + \frac{k(1+\nu)H^2}{6L^2} + (n+1) C_1 L^{(n-2)}\right]$$

The first term is the contribution of the bending moment, the second is that due to shear, the third is that due to rotation at the end of the beam. The shear term is proportional to H^2/L^2 , so for $k \approx 1$ this term is approximately

$$\frac{1}{6} \left(\frac{H}{L}\right)^2$$

and for $H/L < .2$. This is less than 1% of the bending term. The third term will be negligible only if C_1 is very small and if $n \leq 2$.

The first method to explain these constants is the solution to the problem by a boundary collocation of the Williams function for a wedge when the wedge angle is 180° . First starting with the Mitchell Solution of the biharmonic equation

$$\nabla^2 \nabla^2 \phi = 0$$

in polar coordinates

$$\left(\frac{\partial^2}{\partial r^2} + \frac{1}{r} \frac{\partial}{\partial r} + \frac{1}{r^2} \frac{\partial^2}{\partial \theta^2}\right)^2 \phi = 0$$

Here we want a solution which allows separation of variables.
Choosing ϕ of the form

$$\phi = f(r) e^{\beta\theta}$$

Substituting into the above equation

$$\left[f^{1v} + \frac{2f^{1111}}{r} - (1-2\beta^2) \frac{f^{11}}{r^2} + (1-2\beta^2) \frac{f^1}{r^3} + \beta^2(4+\beta^2) \frac{f}{r^4} \right] e^{\beta\theta} = 0$$

Let $r = e^\zeta$; then

$$\left[\frac{d^4 F}{d\zeta^4} - 4 \frac{d^3 F}{d\zeta^3} + (4+2\beta^2) \frac{d^2 F}{d\zeta^2} - 4\beta^2 \frac{dF}{d\zeta} + \beta^2(4+\beta^2)F \right] e^{\beta\theta} = 0$$

Taking the solution F in the form

$$F = e^{a\zeta}$$

then we have a 4th-order differential equation with constant coefficients, and the characteristic equation for "d" is

$$a^4 - 4a^3 + (4+2\beta^2)a^2 - 4\beta^2 a + \beta^2(4+\beta^2) = 0$$

This yields

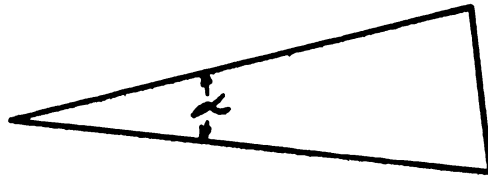
$$(a^2 + \beta^2) (a^2 - 4a + 4 + \beta^2) = 0$$

then

$$\beta = ia \qquad \beta = i(a-2)$$

$$\beta = -ia \qquad \beta = -i(a-2)$$

Mitchell then chose $\beta = in$ where n is an interger to obtain periodicity in θ . For our purposes we cannot expect periodicity in θ , however, as our domain does not cover the entire region.



We will therefore set $a = \lambda$, which we set no condition on; then

$$\phi = Ce^{a\zeta} e^{\beta\theta} \quad ; \quad \text{from above } \zeta = \ln r$$

$$e^{a \ln r} = e^{\ln r^a} = r^a$$

$$\phi = r^\lambda [Ae^{i\lambda\theta} + Be^{-i\lambda\theta} + Ce^{i(\lambda-2)\theta} + Ee^{-i(\lambda-2)\theta}]$$

$$\begin{aligned} \phi = r^\lambda [& A(\cos\lambda\theta + i\sin\lambda\theta) + B(\cos\lambda\theta - i\sin\lambda\theta) + C(\cos(\lambda-2)\theta \\ & + i\sin(\lambda-2)\theta + E(\cos(\lambda-2)\theta - i\sin(\lambda-2)\theta)] \end{aligned}$$

$$\begin{aligned} \phi = r^\lambda [& \cos\lambda\theta(A+B) + \sin\lambda\theta(i(A+B)) + \cos(\lambda-2)\theta(C+E) \\ & + \sin(\lambda-2)\theta(i(C-E))] \end{aligned}$$

$$\text{Let} \quad (A+B) = C_1 \quad ; \quad i(A-B) = C_2$$

$$(C+E) = C_3 \quad ; \quad i(C-E) = C_4$$

$$\phi = r^\lambda [C_1 \cos \lambda \theta + C_2 \sin \lambda \theta + C_3 \cos(\lambda-2)\theta + C_4 \sin(\lambda-2)\theta]$$

The wedge must be stress free at $\theta = 0$, $\theta = \alpha$

$$\sigma_{\theta\theta} = \frac{\partial^2 \phi}{\partial r^2} = \lambda(\lambda-1) r^{(\lambda-2)} [C_1 \sin \lambda \theta + C_2 \cos \lambda \theta + C_3 \sin(\lambda-2)\theta + C_4 \cos(\lambda-2)\theta]$$

$$\sigma_{r\theta} = - \frac{\partial}{\partial r} \left(\frac{1}{r} \frac{\partial \phi}{\partial \theta} \right) = - (\lambda-1) r^{(\lambda-2)} [C_1 \lambda \cos \lambda \theta - C_2 \lambda \sin \lambda \theta + C_3 (\lambda-2) \cos(\lambda-2)\theta - C_4 (\lambda-2) \sin(\lambda-2)\theta]$$

$$\text{at} \quad \theta = 0$$

$$\text{from} \quad \sigma_{\theta\theta} = 0 \quad ; \quad C_2 = - C_4$$

$$\text{from} \quad \sigma_{r\theta} = 0 \quad ; \quad \lambda C_1 = - (\lambda-2) C_3$$

from the conditions at $\theta = \alpha$

$$\frac{-(\lambda-2)C_3}{\lambda} \sin \lambda \alpha + C_3 \sin(\lambda-2)\alpha + (-\cos \lambda \alpha + \cos(\lambda-2)\alpha) C_4 = 0$$

$$C_3 \left[\sin(\lambda-2)\alpha - \frac{(\lambda-2)}{\lambda} \sin \lambda \alpha \right] + C_4 [\cos(\lambda-2)\alpha - \cos \lambda \alpha] = 0$$

$$C_3 [(\lambda-2) \cos(\lambda-2)\alpha - (\lambda-2) \cos \lambda \alpha] - C_4 [(\lambda-2) \sin(\lambda-2)\alpha - \lambda \sin \lambda \alpha] = 0$$

By Cramer's rule to satisfy these homogeneous equations λ must be the root of the transcendental equations obtained by expanding the determinate of the coefficients and equating this to zero

$$\sin(\lambda+1)\alpha = \pm \frac{\sin\alpha}{\alpha} (\lambda+1)\alpha$$

Let $\lambda + 1 = \gamma$

$$\sin\gamma\alpha = \pm \gamma\sin\alpha$$

When $\alpha = 2\pi$ this corresponds to the case of a crack with stress free surfaces and

$$\sin\gamma 2\pi = 0$$

or $\gamma = n/2$

This yields the stress function

$$\phi = r^{\gamma+1} [C_1 \sin(\gamma+1)\theta + C_2 \cos(\gamma+1)\theta + C_3 \sin(\gamma-1)\theta + C_4 \cos(\gamma-1)\theta]$$

This will satisfy stress free edges along

$$\theta = 0 \quad ; \quad \theta = \alpha \quad \text{for } n = 1, 2, 3, \dots$$

$$\phi = r^{(n/2+1)} [C_1 \sin(\frac{n}{2}+1)\theta + C_2 \cos(\frac{n}{2}+1)\theta + C_3 \sin(\frac{n}{2}-1)\theta + C_4 \cos(\frac{n}{2}-1)\theta]$$

From the general definition of the stress function

$$\sigma_r = \frac{1}{r^2} \frac{\partial^2 \phi}{\partial \theta^2} + \frac{1}{r} \frac{\partial \phi}{\partial \theta} \quad ; \quad \tau_{r\theta} = -\frac{1}{r} \frac{\partial^2 \phi}{\partial r \partial \theta} + \frac{1}{r^2} \frac{\partial \phi}{\partial \theta}$$

$$\sigma_\theta = \frac{\partial^2 \phi}{\partial \theta^2}$$

both σ_θ and $\tau_{r\theta}$ must vanish at $\theta = 0$ and $\theta = 2\pi$

from the above equation this can be done by requiring

$$F(\theta) = 0 \quad \text{at} \quad \theta = 0, 2\pi \quad \text{and} \quad F''(\theta) = 0 \quad \text{at} \quad \theta = 0, 2\pi$$

or

$$[C_1 \sin(\frac{n}{2}+1)\theta + C_2 \cos(\frac{n}{2}+1)\theta + C_3 \sin(\frac{n}{2}-1)\theta + C_4 (\frac{n}{2}-1)\theta]$$

$$\text{at} \quad \theta = 0$$

$$[C_2 + C_4] = 0 \quad \text{or} \quad C_4 = -C_2$$

and

$$C_1 (\frac{n}{2}+1) \cos(\frac{n}{2}+1)\theta - C_2 (\frac{n}{2}+1) \sin(\frac{n}{2}+1)\theta + (\frac{n}{2}-1) C_3 \cos(\frac{n}{2}-1)\theta$$

$$- (\frac{n}{2}-1) C_4 \sin(\frac{n}{2}-1)\theta \quad \text{at} \quad \theta = 0$$

$$C_1 (\frac{n}{2} + 1) = - (\frac{n}{2} - 1) C_3 \quad \text{or} \quad C_1 = - \frac{n-2}{n+2} C_3$$

Therefore,

$$\phi = r^{(n/2+1)} \left[\left[C_3 \left(\sin\left(\frac{n}{2}-1\right)\theta - \frac{n-2}{n+2} \sin\left(\frac{n}{2}+1\right)\theta \right) \right] \right. \\ \left. + C_4 \left[\cos\left(\frac{n}{2}-1\right)\theta - \cos\left(\frac{n}{2}+1\right)\theta \right] \right]$$

Writing the equation in terms of the bisector angle

$$\psi = \theta - \pi$$

$$\phi = r^{(n/2+1)} \left[C_3 \left[\sin\left(\frac{n}{2}-1\right)(\psi+\pi) - \frac{n-2}{n+2} \sin\left(\frac{n}{2}+1\right)(\psi+\pi) \right] \right. \\ \left. + C_4 \left[\cos\left(\frac{n}{2}-1\right)(\psi+\pi) - \cos\left(\frac{n}{2}+1\right)(\psi+\pi) \right] \right]$$

$$\phi = r^{(n/2+1)} \left[C_3 \left[\overset{(1)}{\sin\left(\frac{n}{2}-1\right)\psi} \overset{(2)}{\cos\left(\frac{n}{2}-1\right)\pi} + \overset{(3)}{\cos\left(\frac{n}{2}-1\right)\psi} \overset{(4)}{\sin\left(\frac{n}{2}-1\right)\pi} \right] \right. \\ \left. - \frac{n-2}{n+2} \left[\overset{(5)}{\sin\left(\frac{n}{2}+1\right)\psi} \overset{(6)}{\cos\left(\frac{n}{2}+1\right)\pi} + \overset{(7)}{\cos\left(\frac{n}{2}+1\right)\psi} \overset{(8)}{\sin\left(\frac{n}{2}+1\right)\pi} \right] \right] \\ + C_4 \left[\overset{(7)}{\cos\left(\frac{n}{2}-1\right)\psi} \overset{(8)}{\cos\left(\frac{n}{2}-1\right)\pi} + \overset{(5)}{\sin\left(\frac{n}{2}-1\right)\psi} \overset{(6)}{\sin\left(\frac{n}{2}-1\right)\pi} \right] \\ - \overset{(7)}{\cos\left(\frac{n}{2}+1\right)\psi} \overset{(8)}{\cos\left(\frac{n}{2}+1\right)\pi} - \overset{(5)}{\sin\left(\frac{n}{2}+1\right)\psi} \overset{(6)}{\sin\left(\frac{n}{2}+1\right)\pi} \right]$$

for $n = 1, 3, 5, 7, \dots$ terms (1), (3), (5), (7) will drop out

for $n = 2, 4, 6, 8, 10, \dots$ terms (2), (4), (6), (8) will drop out

Then, for terms (1), (3), (5), (7) let $n = 2N$

for terms (2), (4), (6), (8) let $n = 2N-1$

Then,

$$f(2N)_{N=1,2,3} + f(2N-1)_{N=1,2,3} = f(n)_{n=1,2,3}$$

in $f(2N)$ all odd terms will appear

in $f(2N-1)$ all even terms will appear

or

$$\begin{aligned}\phi &= r^{N+1} [C_3 [\sin(N-1)\psi(-1)^{N-1} - \frac{N-1}{N+1} [\sin(N+1)\psi(-1)^{N-1}]] \\ &\quad + C_4 [\cos(N-1)\psi(-1)^{N-1} - \cos(N+1)\psi(-1)^{N-1}] \\ &\quad + r^{(N+1/2)} [C_3 [\cos(N-\frac{3}{2})\psi(-1)^N - \frac{2N-3}{2N+1} [\cos(N+\frac{1}{2})\psi(-1)^N]] \\ &\quad + C_4 [\sin(N-\frac{3}{2})\psi(-1)^N - \sin(N+\frac{1}{2})\psi(-1)^N]]\end{aligned}$$

$$\begin{aligned}\phi &= r^{(N+1)} (-1)^N [C_3 [-\sin(N-1)\psi + \frac{N-1}{N+1} [\sin(N+1)\psi]] \\ &\quad + C_4 [-\cos(N-1)\psi + \cos(N+1)\psi]] \\ &\quad + r^{(N+1/2)} (-1)^N [C_3 [\cos(N-\frac{3}{2})\psi - \frac{2N-3}{2N+1} [\cos(N+\frac{1}{2})\psi]] \\ &\quad + C_4 [\sin(N-\frac{3}{2})\psi - \sin(N+\frac{1}{2})\psi]]\end{aligned}$$

Breaking this into even and odd parts

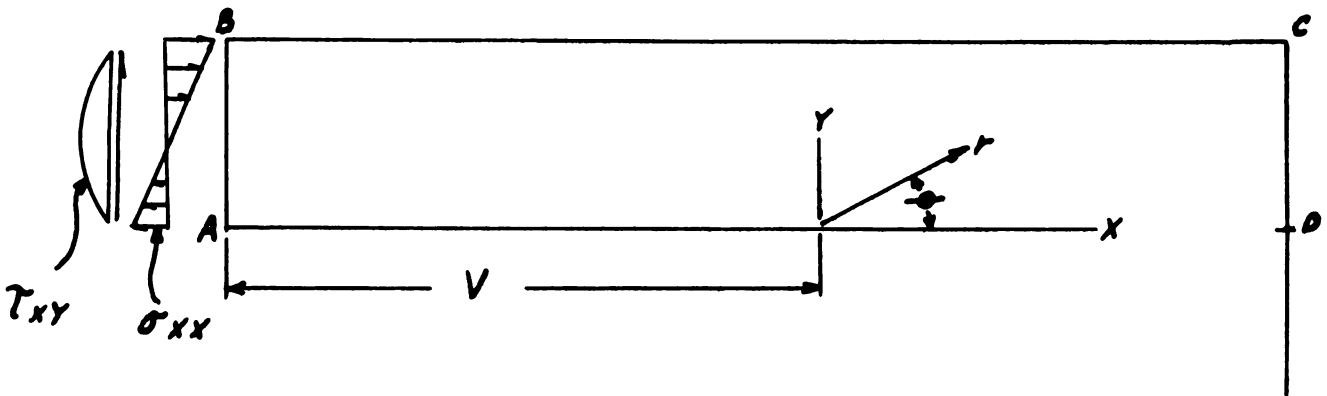
$$\begin{aligned}\phi_e &= (-1)^N r^{(N+1/2)} [C_{3(2N-1)} [\cos(N-\frac{3}{2})\psi - \frac{2N-3}{2N+1} [\cos(N+\frac{1}{2})\psi]] \\ &\quad + [C_{4_{2N}} r^{(N+1)} (-1)^N [-\cos(N-1)\psi + \cos(N+1)\psi]]]\end{aligned}$$

$$\begin{aligned}\phi_o &= (-1)^N r^{(N+1)} [C_{3_{2N}} [-\sin(N-1)\psi + \frac{N-1}{N+1} \sin(N+1)\psi] \\ &\quad + C_{4(2N-1)} r^{(N+1/2)} (-1)^N [\sin(N-\frac{3}{2})\psi - \sin(N+\frac{1}{2})\psi]]\end{aligned}$$

In this case due to symmetry only ϕ_e is used

$$\phi_e = (-1)^{N-1} r^{N+1/2} C_{3(2N-1)} \left[-\cos\left(N-\frac{3}{2}\right)\psi + \frac{2N-3}{2N+1} \cos\left(N+\frac{1}{2}\right)\psi \right] \\ + (-1)^N r^{N+1} C_{4(2N)} \left[-\cos(N-1)\psi + \cos(N+1)\psi \right]$$

The biharmonic equation and the boundary conditions are satisfied all along a crack by the above equations. Assuming the stress distribution below, at some point Brown & Srawley solve the problem as follows:



by applying the boundary collocation procedure at n stations we can force the above function to match the boundary conditions of the problem. Here they set the boundary conditions on ϕ rather than using the stresses

$$\begin{aligned}\sigma_{yy} &= \frac{\partial^2 \phi}{\partial x^2} = \frac{\partial^2 \phi}{\partial r^2} \cos^2 \theta - 2 \frac{\partial^2 \phi}{\partial \theta \partial r} \frac{\sin \theta \cos \theta}{r} + \frac{\partial \phi}{\partial r} \frac{\sin^2 \theta}{r} \\ &\quad + 2 \frac{\partial \phi}{\partial \theta} \frac{\sin \theta \cos \theta}{r^2} + \frac{\partial^2 \phi}{\partial \theta^2} \frac{\sin^2 \theta}{r^2}\end{aligned}$$

$$\begin{aligned}\sigma_{xx} &= \frac{\partial^2 \phi}{\partial y^2} = \frac{\partial^2 \phi}{\partial r^2} \sin^2 \theta + 2 \frac{\partial^2 \phi}{\partial \theta \partial r} \frac{\sin \theta \cos \theta}{r} + \frac{\partial \phi}{\partial r} \frac{\cos^2 \theta}{r} \\ &\quad - 2 \frac{\partial \phi}{\partial \theta} \frac{\sin \theta \cos \theta}{r^2} + \frac{\partial^2 \phi}{\partial \theta^2} \frac{\cos^2 \theta}{r^2}\end{aligned}$$

$$\begin{aligned}-\tau_{xy} &= \frac{\partial^2 \phi}{\partial x \partial y} = \frac{\partial^2 \phi}{\partial r^2} \sin \theta \cos \theta + \frac{\partial^2 \phi}{\partial r \partial \theta} \frac{\cos 2\theta}{r} - \frac{\partial^2 \phi}{\partial \theta^2} \frac{\sin \theta \cos \theta}{r^2} \\ &\quad - \frac{\partial \phi}{\partial r} \frac{\sin \theta \cos \theta}{r} - \frac{\partial \phi}{\partial \theta} \frac{\cos 2\theta}{r^2}\end{aligned}$$

These boundary conditions are as follows

along AB $\frac{\phi}{P} = -\frac{6(a-v)}{Bh^3} \left(\frac{y^3}{3} - \frac{hy^2}{2} \right)$ -- this corresponds to the normal stress

$\frac{\partial \phi}{\partial x} = -\frac{6P}{Bh^3} \left(\frac{y^3}{3} - \frac{hy^2}{2} \right)$ -- this corresponds to the shear stress condition

along BC $\frac{\phi}{P} = \frac{x+a}{B}$ -- this corresponds to $\sigma_{yy} = 0$

$\frac{\partial \phi}{\partial y} = 0$ -- this corresponds to $\tau_{xy} = 0$

along CD $\frac{\phi}{P} = \frac{a}{B}$

$\frac{\partial \phi}{\partial x} = 1$

the last four conditions assure continuity of the ϕ function at the corners of the sample

By doing this they have assigned properties or values to the functions and constants of integration and thus have warped the function in its x-y space as ϕ , $\frac{\partial \phi}{\partial x}$ varies as $(\frac{y^3}{3} - \frac{hy^2}{2})$ along AB or a parabolic variance

along BC ϕ varies as x to the first power and $\frac{\partial \phi}{\partial y} = 0$

and ϕ is constant as we move in the y direction

along the crack ϕ and $\frac{\partial \phi}{\partial x}, \frac{\partial \phi}{\partial y} = 0$ or $\phi = \text{constant}$ as we move on both the x and y direction

along CD $\phi = \frac{qP}{B}$ and is constant as we move in the y direction

$\frac{\partial \phi}{\partial x} = \frac{P}{B}$ and is constant as we move in the x direction

Thus ϕ is considerably warped in 2 dimensional space; whether or not this affects the solution to the problem has not been determined.

Using the above ϕ and boundary condition, if we choose n boundary station and set the appropriate function $\phi, \frac{\partial \phi}{\partial x}, \frac{\partial \phi}{\partial y}$ equal to the value of the boundary condition at that point, we obtain

$$\sum_{n=1,2,3,\dots} F \phi = \text{value of boundary condition at point } l$$

Therefore, for all boundary points

$$\begin{array}{ccccccc}
 a_1 & \left| \begin{array}{c} \phi_1 \\ \phi_2 \\ \phi_3 \\ \phi_4 \\ \cdot \\ \cdot \\ \cdot \\ \phi_{2n} \end{array} \right| & + a_2 & \left| \begin{array}{c} \phi_1' \\ \phi_2' \\ \phi_3' \\ \phi_4' \\ \cdot \\ \cdot \\ \cdot \\ \phi_{2N}' \end{array} \right| & + a_3 & \left| \begin{array}{c} \phi_1'' \\ \phi_2'' \\ \phi_3'' \\ \phi_4'' \\ \cdot \\ \cdot \\ \cdot \\ \phi_N'' \end{array} \right| & \dots\dots\dots = & \left| \begin{array}{c} bC_1 \\ bC_2 \\ bC_3 \\ bC_4 \\ \cdot \\ \cdot \\ \cdot \\ bC_{2N} \end{array} \right|
 \end{array}$$

We obtain $2n$ simultaneous algebraic equations corresponding to known values of

$$\phi \quad \text{and} \quad \frac{\partial \phi}{\partial x}, \quad \frac{\partial \phi}{\partial y}$$

Solving these the first $2n$ coefficients of the Williams stress function are obtained

$$\begin{aligned}
 \sigma_{yy} = & \frac{\partial^2 \phi}{\partial r^2} \cos^2 \theta - 2 \frac{\partial^2 \phi}{\partial \theta \partial r} \frac{\sin \theta \cos \theta}{r} + \frac{\partial \phi}{\partial r} \frac{\sin^2 \theta}{r} \\
 & + 2 \frac{\partial \phi}{\partial \theta} \frac{\sin \theta \cos \theta}{r^2} + \frac{\partial^2 \phi}{\partial \theta^2} \frac{\sin^2 \theta}{r^2}
 \end{aligned}$$

Let $A(r) = r^{N+1/2}$

$$A(\theta) = -\cos(N-\frac{3}{2})\psi + \frac{2N-3}{2N+1} \cos(N+\frac{1}{2})\psi$$

$$B(r) = r^{(n+1)}$$

$$B(\theta) = -\cos(N-1)\psi + \cos(N+1)\psi$$

$$\phi = (-1)^{N-1} A(r) C_{3(2N-1)} [A(\theta)] + (-1)^N B(r) C_{4(2N)} [B(\theta)]$$

$$\text{Let } A'(r) = (N + \frac{1}{2}) r^{(N-1/2)}$$

$$A''(r) = (N + \frac{1}{2})(N - \frac{1}{2}) r^{(N-3/2)}$$

$$A'(\theta) = (N - \frac{3}{2}) \sin(N - \frac{3}{2})\psi - \frac{(2N-3)(N+1/2)}{(2N+1)} \sin(N + \frac{1}{2})\psi$$

$$A''(\theta) = (N - \frac{3}{2})^2 \cos(N - \frac{3}{2})\psi - \frac{(2N-3)(N+1/2)^2}{(2N+1)} \cos(N + \frac{1}{2})\psi$$

$$B'(r) = (N+1) r^N$$

$$B''(r) = N(N+1) r^{(N-1)}$$

$$B'(\theta) = (N-1) \sin(N-1)\psi - (N+1) \sin(N+1)\psi$$

$$B''(\theta) = (N-1)^2 \cos(N-1)\psi - (N+1)^2 \cos(N+1)\psi$$

$$\begin{aligned} \sigma_{yy} = & [A''(r)A(\theta)(-1)^{N-1}C_{3(2N-1)} + B''(r)B(\theta)(-1)^N C_{4(2N)}] \cos^2 \theta \\ & - 2[A'(r)A'(\theta)(-1)^{N-1}C_{3(2N-1)} \\ & + B'(r)B'(\theta)(-1)^N C_{4(2N)}] \frac{\sin \theta \cos \theta}{r} \\ & + [A'(r)A(\theta)(-1)^{N-1}C_{3(2N-1)} + B'(r)B(\theta)(-1)^N C_{4(2N)}] \frac{\sin^2 \theta}{r} \\ & + 2[A(r)A'(\theta)(-1)^{N-1}C_{3(2N-1)} \\ & + B(r)B'(\theta)(-1)^N C_{4(2N)}] \frac{\sin \theta \cos \theta}{r^2} \\ & + [A(r)A''(\theta)(-1)^{N-1}C_{3(2N-1)} + B(r)B''(\theta)(-1)^N C_{4(2N)}] \frac{\sin^2 \theta}{r^2} \end{aligned}$$

For areas very close to the crack tip observe that for $n = 1$ the B terms will have no r dependency. The A term will all have a $\frac{1}{\sqrt{r}}$ dependency. For $n > 1$ all terms will depend on a positive power of r . Thus for areas very close to the crack tip the $n = 1$ A terms will dominate.

$$\begin{aligned}\sigma_{yy}_{r \rightarrow 0} &= A''(r)A(\theta)C_{3(1)} \cos^2 \theta - 2A'(r)A'(\theta)C_{3(1)} \frac{\sin \theta \cos \theta}{r} \\ &+ A'(r)A(\theta)C_{3(1)} \frac{\sin^2 \theta}{r} + 2A(r)A'(\theta)C_{3(1)} \frac{\sin \theta \cos \theta}{r^2} \\ &+ A(r)A''(\theta)C_{3(1)} \frac{\sin^2 \theta}{r^2}\end{aligned}$$

$$\begin{aligned}\sigma_{yy} &= \frac{3}{4} \frac{C_{3(1)}}{\sqrt{r}} \left[-\cos\left(\frac{-\psi}{2}\right) - \frac{\cos(3/2\psi)}{3} \right] \cos^2 \psi \\ &- 2 \left[\frac{3}{2}\sqrt{r} C_{3(1)} \left[-\frac{1}{2} \sin\left(\frac{-\psi}{2}\right) + \frac{3/2}{3} \sin\left(\frac{3}{2}\psi\right) \right] \right] \frac{\sin \psi \cos \psi}{r} \\ &+ \frac{3}{2}\sqrt{r} C_{3(1)} \left[-\cos\left(\frac{-\psi}{2}\right) - \frac{\cos(3/2\psi)}{3} \right] \frac{\sin^2 \theta}{r} \\ &+ 2 \left[r^{3/2} C_{3(1)} \left[-\frac{1}{2} \sin\left(\frac{-\psi}{2}\right) + \frac{3/2}{3} \sin\left(\frac{3}{2}\psi\right) \right] \right] \frac{\sin \psi \cos \psi}{r^2} \\ &+ \left[r^{3/2} C_{3(1)} \left[\frac{1}{4} \cos\left(\frac{-\psi}{2}\right) + \frac{9/4}{3} \cos\left(\frac{3}{2}\psi\right) \right] \right] \frac{\sin^2 \psi}{r^2}\end{aligned}$$

$$\begin{aligned}
\sigma_{yy} = & \frac{C_{3(1)}}{\sqrt{r}} \left[\left[\left(\cos \frac{\psi}{2} \left(-\frac{3}{4} \cos^2 \psi + \frac{1}{4} \sin^2 \psi \right) - \frac{6}{4} \sin^2 \psi \right) \right] \right. \\
& + \cos \frac{3\psi}{2} \left[-\frac{1}{3} \cos^2 \psi - \frac{1}{2} \sin^2 \psi + \frac{3}{4} \sin^2 \psi \right] \\
& + \sin \left(\frac{-\psi}{2} \right) \left[\frac{3}{2} \sin \psi \cos \psi - \sin \psi \cos \psi \right] \\
& \left. + \sin \left(\frac{3\psi}{2} \right) \left[\sin \psi \cos \psi - \sin \psi \cos \psi \right] \right]
\end{aligned}$$

After considerable algebra

$$\sigma_{yy} = - \frac{C_{3(1)}}{\sqrt{r}} \cos \frac{\psi}{2} \left(1 + \sin \frac{\psi}{2} \sin \psi \frac{3}{2} \right)$$

from the Westerguard analysis previously discussed (at the tip of the crack)

$$\sigma_{yy} = \frac{K_I}{\sqrt{2\pi r}} \cos \frac{\theta}{2} \left[1 - \sin \frac{\theta}{2} \sin \frac{3\theta}{2} \right]$$

Therefore,

$$- C_{3(1)} = \frac{K_I}{\sqrt{2\pi}}$$

$$K_2 = - C_{3(1)} \sqrt{2\pi}$$

Thus, the first term of the series in the solution to the problem by a boundary collocation of the Williams function is proportional to the stress intensity factor. From the first approximation to the strain energy release rate regarding the specimens as a pair of built in cantilever beams

$$K_I = \frac{2\sqrt{3} P_a}{bH^{3/2}}$$

This approach, however, has neglected some effects occurring in the specimen. Brown and Srawley have carried out calculations for various H_s and a_s height and crack length. The $2\sqrt{3}$ in the above equation has been found to be a limiting coefficient as $H/a \rightarrow 0$. They determined that

$$\frac{K_I BH^{3/2}}{P_a} = 3.46 + 2.38 \frac{H}{A}$$

or

$$K_I = \frac{P_a}{BH^{3/2}} [3.46 + 2.38 \frac{H}{a}]$$

By squaring the quantity in brackets and taking the square root

$$K_I = \frac{P_a}{BH^{3/2}} [12 + (6.92)(2.38) \frac{H}{L} + (2.38)^2 (\frac{H}{L})^2]^{1/2}$$

from Gillis and Gillman

$$\gamma = (F^2 L^2 / 2EIB) [1 + (kEI/AGL^2) + (n+1)C_1 L^{n-2}]$$

$$\gamma = F^2 L^2 / 2EB^2 H^3 [12 + \frac{kEBH^3}{BGL^2} + 12(N+1)C_1 L^{N-2}]$$

$$E\gamma = \frac{F^2 L^2}{2B^2 H^3} \left[12 + \frac{2kH^2(1+\nu)}{L^2} + 12(n+1)C_1 L^{n-2} \right]$$

At conditions of crack initiation

$$\partial S = \partial U$$

$$2\gamma = G$$

$$2GE = \frac{F^2 L^2}{2B^2 H^3} \left[12 + \frac{2kH^2(1+\nu)}{L^2} + (n+1)12C_1 L^{(n-2)} \right]$$

$$K_I = \sqrt{GE} = \left[\frac{FL}{BH^{3/2}} \left[12 + 2k(1+\nu) \left(\frac{H}{L}\right)^2 + (n+1)12C_1 L^{(n-2)} \right] \right]^{1/2}$$

Let C depend on H

$$\text{or } C_1 = C_2 H$$

and let $n = 1$; then

$$K_I = \frac{FL}{BH^{3/2}} \left[12 + 2k(1+\nu) \frac{H^2}{L^2} + 24C_2 \frac{H}{L} \right]^{1/2}$$

Comparing this with Brown and Srawley's result

$$K_I = \frac{FL}{BH^{3/2}} \left[12 + (6.92)(2.38) \frac{H}{L} + (2.38)^2 \frac{H^2}{L^2} \right]^{1/2}$$

$$2k(1+\nu) = (2.38)^2 \quad ; \quad k = 2.183$$

$$24C_2 = (6.92)(2.38) \quad ; \quad C_2 = .69$$

$$12 - \text{bending term} \quad ; \quad 2k(1+\nu) \frac{H^2}{L^2} \text{ shear term} \quad ;$$

$$2C_2 \frac{H}{L} \text{ energy past crack tip term}$$

The shear term will be unimportant when $\frac{H}{L} < \frac{1}{50}$. The tip energy terms, however, will be important until $\frac{H}{L} < \frac{1}{300}$.

Thus, for accurate values of K_I both these factors must be taken into account. The second factor which enters into the system is the force parallel to the axis of the sample. Gillis and Gillman have explored the effect of a compressive force applied to this type of sample.

They solved the case of bending only with no end rotation and even though the error using this approach could be 30% to 40% these results indicate that for our sample the error due to end force will be very small

$$\text{as} \quad P = F \tan(\psi + \phi)$$

where ψ = angle of friction and ϕ = wedge angle

$$P \approx F \tan 30^\circ \approx F(.5)$$

Therefore,

$$\frac{P_e}{FL} \approx \frac{R}{L} (.5)$$

$$e \approx .125$$

$$L \approx 2$$

$$\frac{P_e}{FL} \approx \frac{.5}{16} \approx \frac{1}{32} \approx .03$$

Looking at the graph of the solution the error due to the end force is vanishingly small.

It appears, then, that the major effects that will cause error from the standard strength of **materials** approach is the shear and energy past the crack tip. Both of these and the effect of end force can be accounted for by using compliance techniques.

During an increment of crack extension which creates new crack surface dA the work done by the loading force is $Pd\Delta$ where Δ is the displacement of the force in its own direction. The stored energy V is always positive and contributes $-dV$ during crack extension. Therefore,

$$\therefore G = \frac{Pd\Delta}{dA} - \frac{dV}{dA}$$

Load is related to displacement by $\Delta = \lambda P$ where λ is the inverse spring constant.

The strain energy can be written as the work done during loading at constant crack length.

$$V = \frac{P\Delta}{2} = \frac{\lambda P^2}{2}$$

$$G = P \frac{\partial(\lambda P)}{\partial A} - \frac{\partial\left(\frac{\lambda P^2}{2}\right)}{\partial A}$$

$$G = P\left[P \frac{\partial \lambda}{\partial A} + \lambda \frac{\partial P}{\partial A}\right] - \lambda P \frac{\partial P}{\partial A} - \frac{P^2}{2} \frac{\partial \lambda}{\partial A}$$

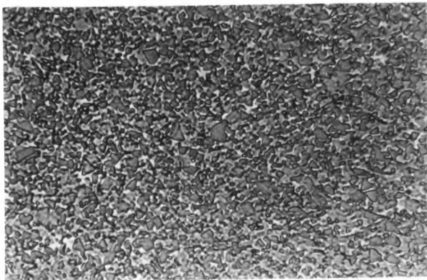
$$G = \frac{P^2}{2} \frac{\partial \lambda}{\partial A} = \frac{\Delta^2}{2\lambda^2} \frac{\partial \lambda}{\partial A} = \frac{\Delta^2}{2\lambda^2} \frac{\partial \lambda}{\partial(Lb)} = \frac{\Delta^2}{2\lambda^2 b} \frac{\partial \lambda}{\partial(L)}$$

From this G for the particular sample used in this investigation can be obtained and compared with that calculated from the other methods. The effect of the slot can then be determined.

APPENDIX II
MATERIALS USED

TABLE V
MATERIAL STRUCTURE DATA

Material Wt. % Cobalt	Grain Size Desired μ	Hardness Rockwell A	Density gm/cc	Porosity	Structure
3	1.5	92.8	15.27	A1 B1 macro voids	Heavy concentration 1-2 μ
3	2.5-3	91.3	15.34	A1	Heavy concentration 2-3 μ Small concentration 5-7 μ
6	7-8	88.6	14.89	A1 B1	Light concentration 1-3 μ Heavy concentration 6-10 μ
9	1.5	90.5	14.64	A1	Uniform grain size 1/2-2 μ
9	2.5-3	88.9	14.62	A1 B1	Heavy concentration 2-3 μ Some 3-4 μ
9	7-8	87.3	14.64	A1 B1	Heavy concentration 6-10 μ Light concentration 1-5 μ
15	1.5	89.0	14.01	A1	Heavy concentration 1-2 μ
15	2.5-3	87.0	14.03	A1	Heavy concentration 2-3 μ Some 3-4 μ
15	7-8	85.0	13.99	A1	Heavy concentration 5-9 μ Some >10 μ



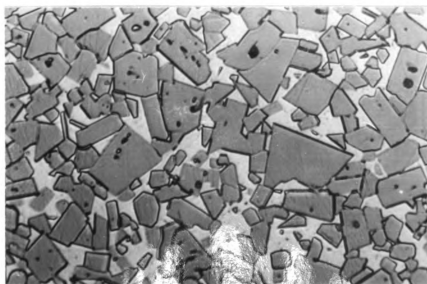
15% Cobalt

1.5 μ GS



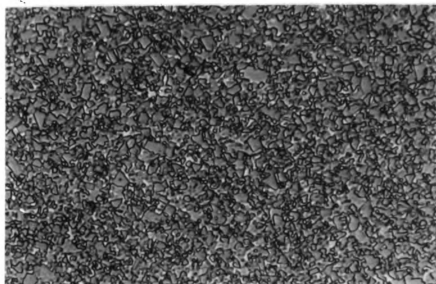
15% Cobalt

2.5-3 μ GS



15% Cobalt

8 μ GS



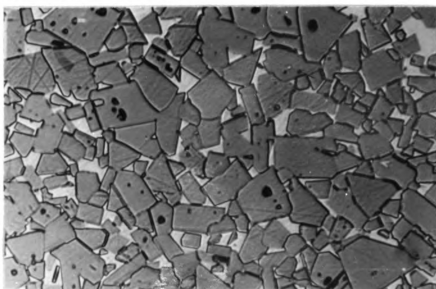
9% Cobalt

1.5 μ GS



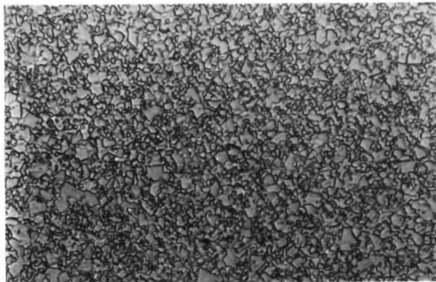
9% Cobalt

2.5-3 μ GS



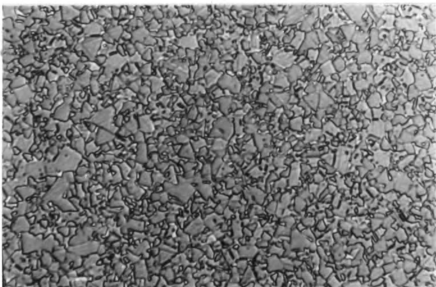
9% Cobalt

8 μ GS



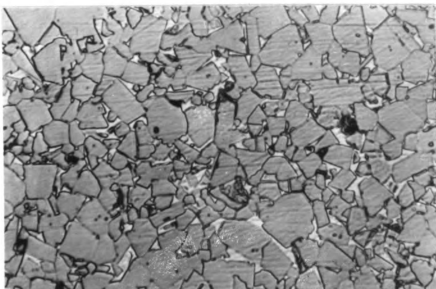
3% Cobalt

1.5 μ GS



3% Cobalt

2.5-3 μ GS



6% Cobalt

8 μ GS

APPENDIX III
APPARATUS AND SETUP

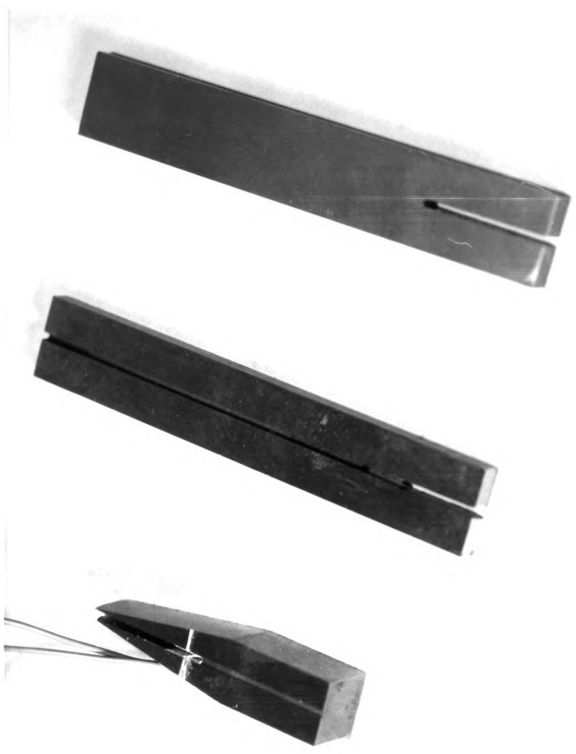


Figure 1

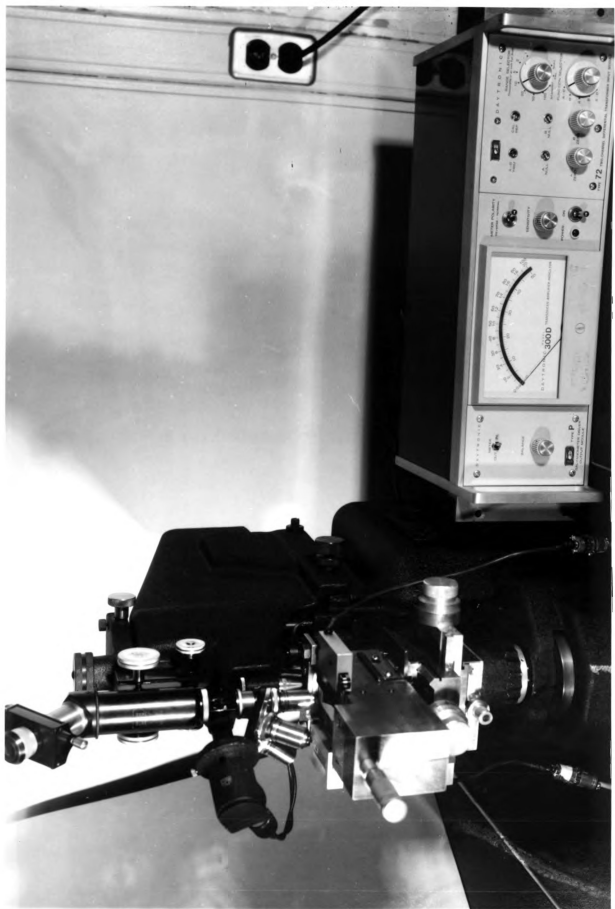


Figure 2

FIGURE 3

APPARATUS FOR CALIBRATION OF INSTRUMENTED WEDGE

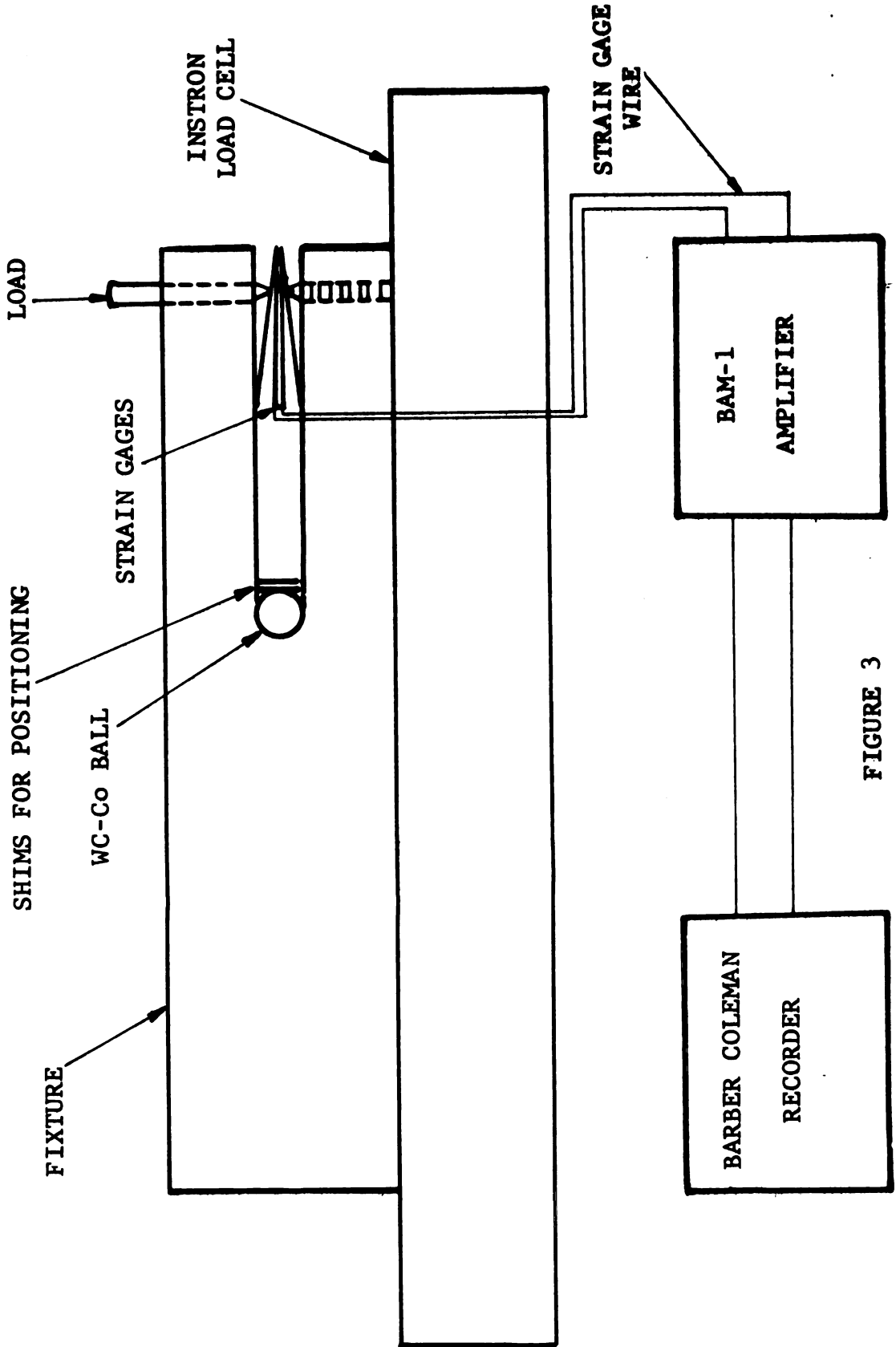


FIGURE 3

APPENDIX IV
FRACTOGRAPHS

D C B

SLOW FRACTURES 5000X





15% Cobalt

1.5 μ GS

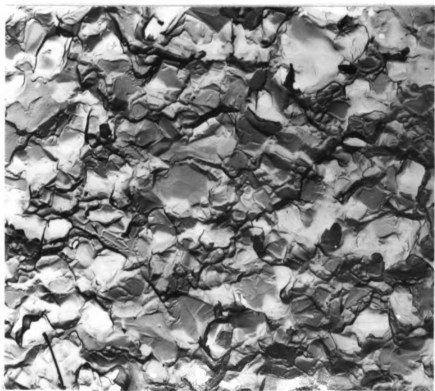


15% Cobalt

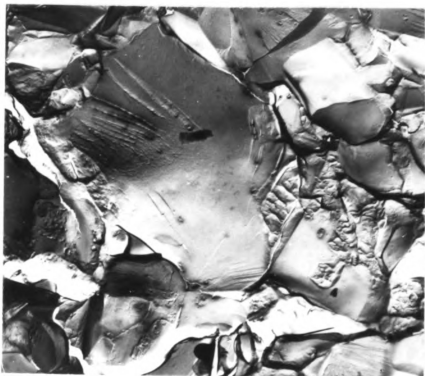
1.5 μ GS



15% Cobalt
2.5-3 μ GS



15% Cobalt
2.5-3 μ GS



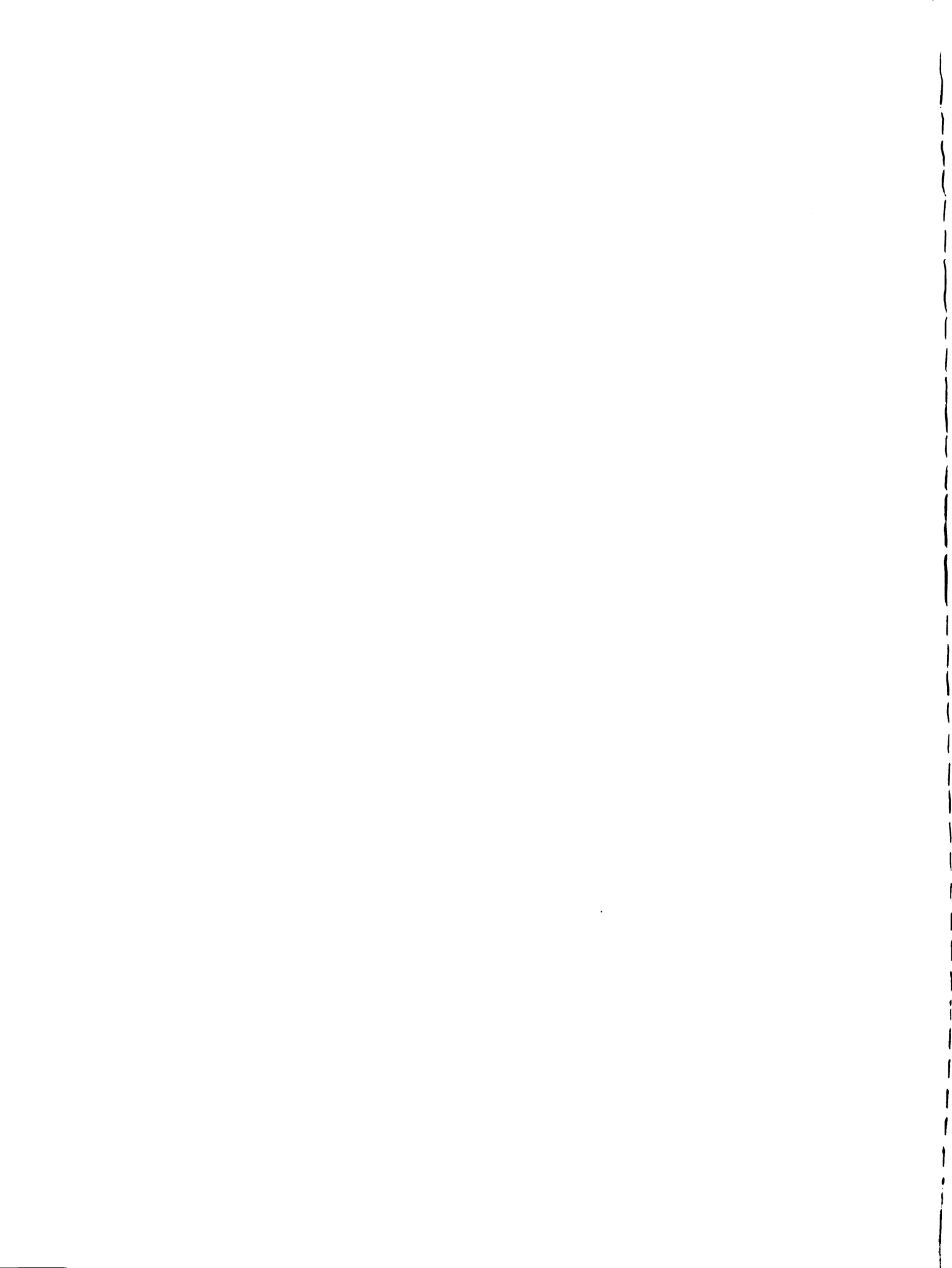
15% Cobalt

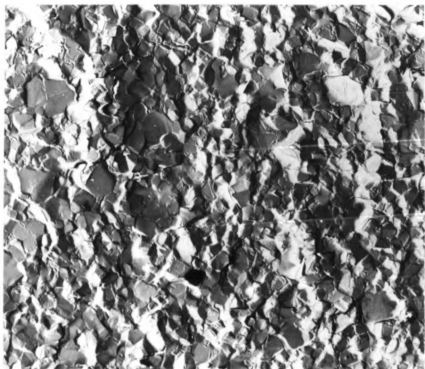
8 μ GS



15% Cobalt

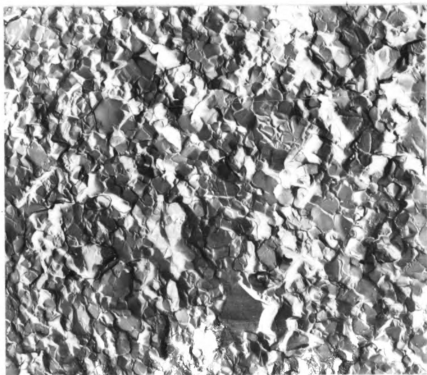
8 μ GS





9% Cobalt

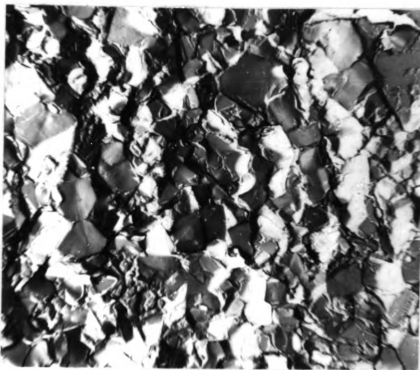
1.5 μ GS



9% Cobalt

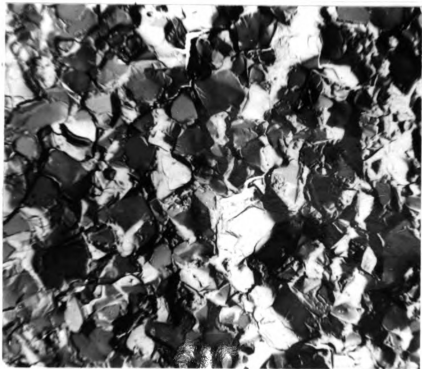
1.5 μ GS





9% Cobalt

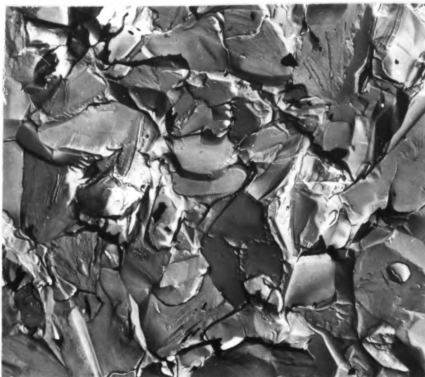
2.5-3 μ GS



9% Cobalt

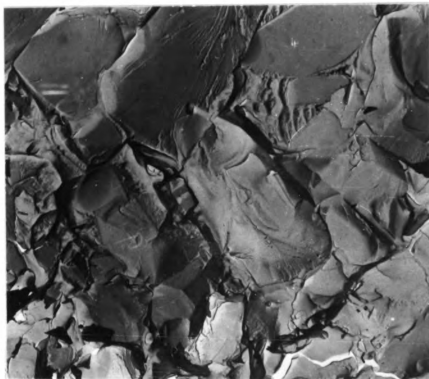
2.5-3 μ GS





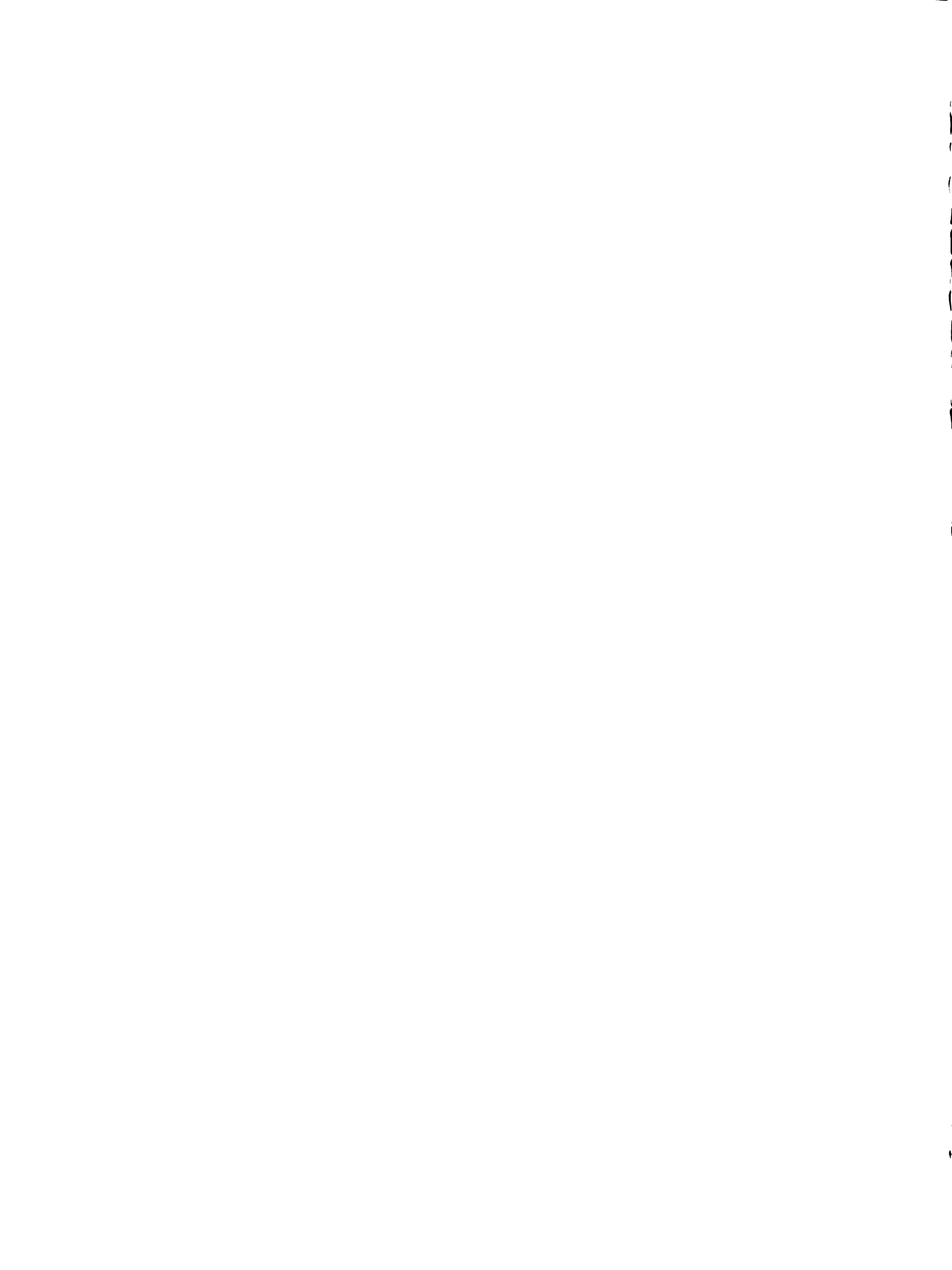
9% Cobalt

8 μ GS



9% Cobalt

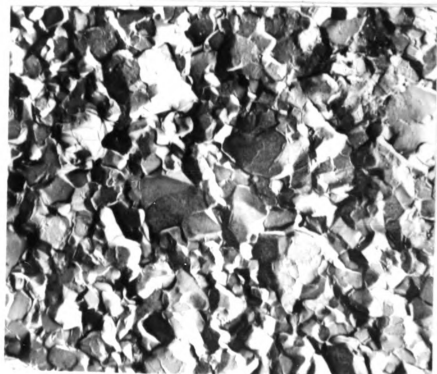
8 μ GS





3% Cobalt

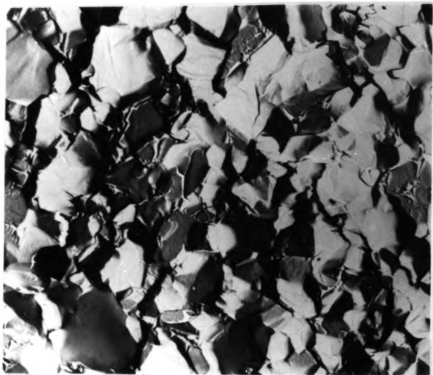
1.5 μ GS



3% Cobalt

1.5 μ GS





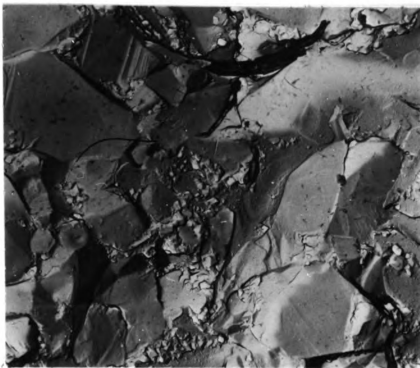
3% Cobalt

2.5-3 μ GS



3% Cobalt

2.5-3 μ GS



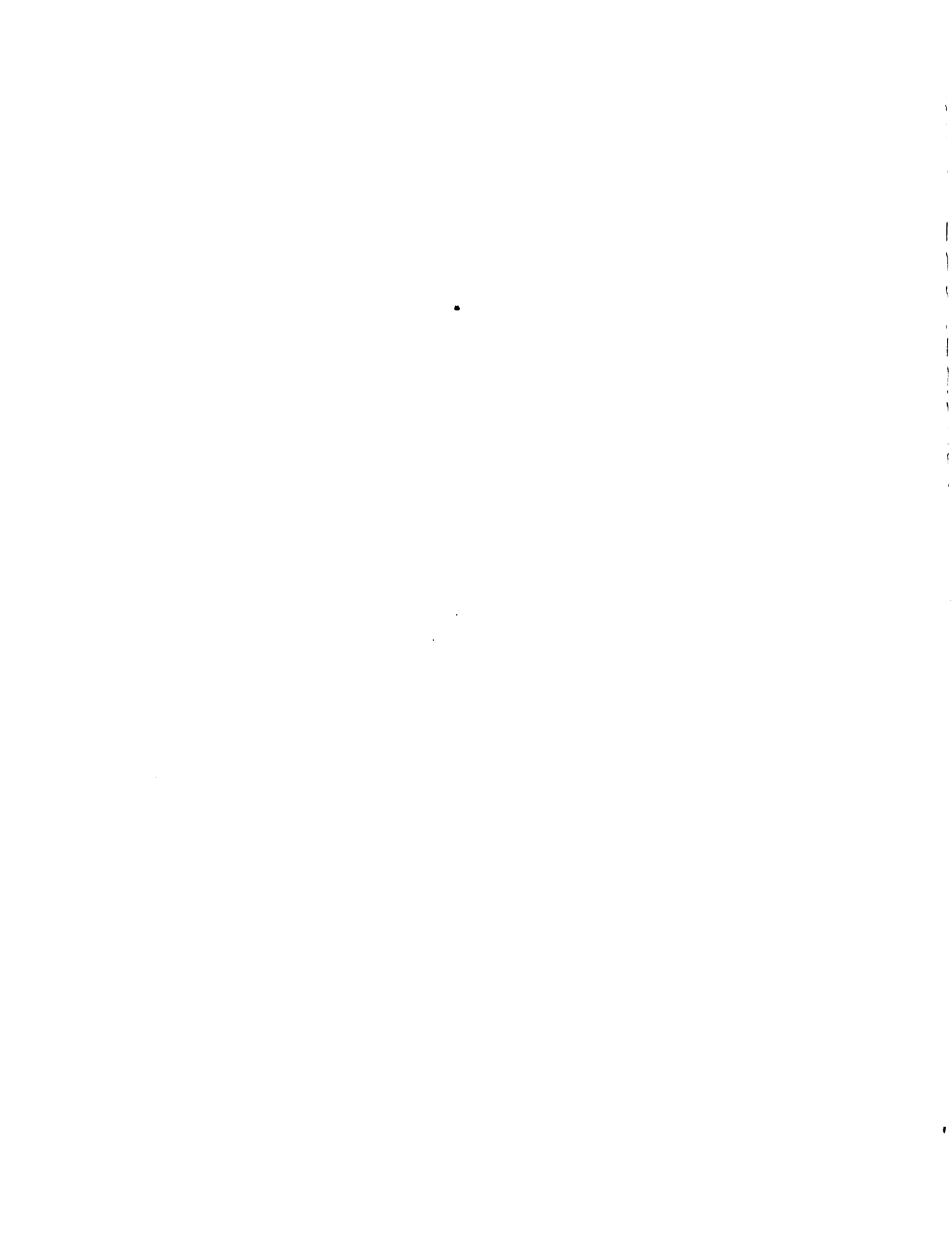
6% Cobalt

8μ GS



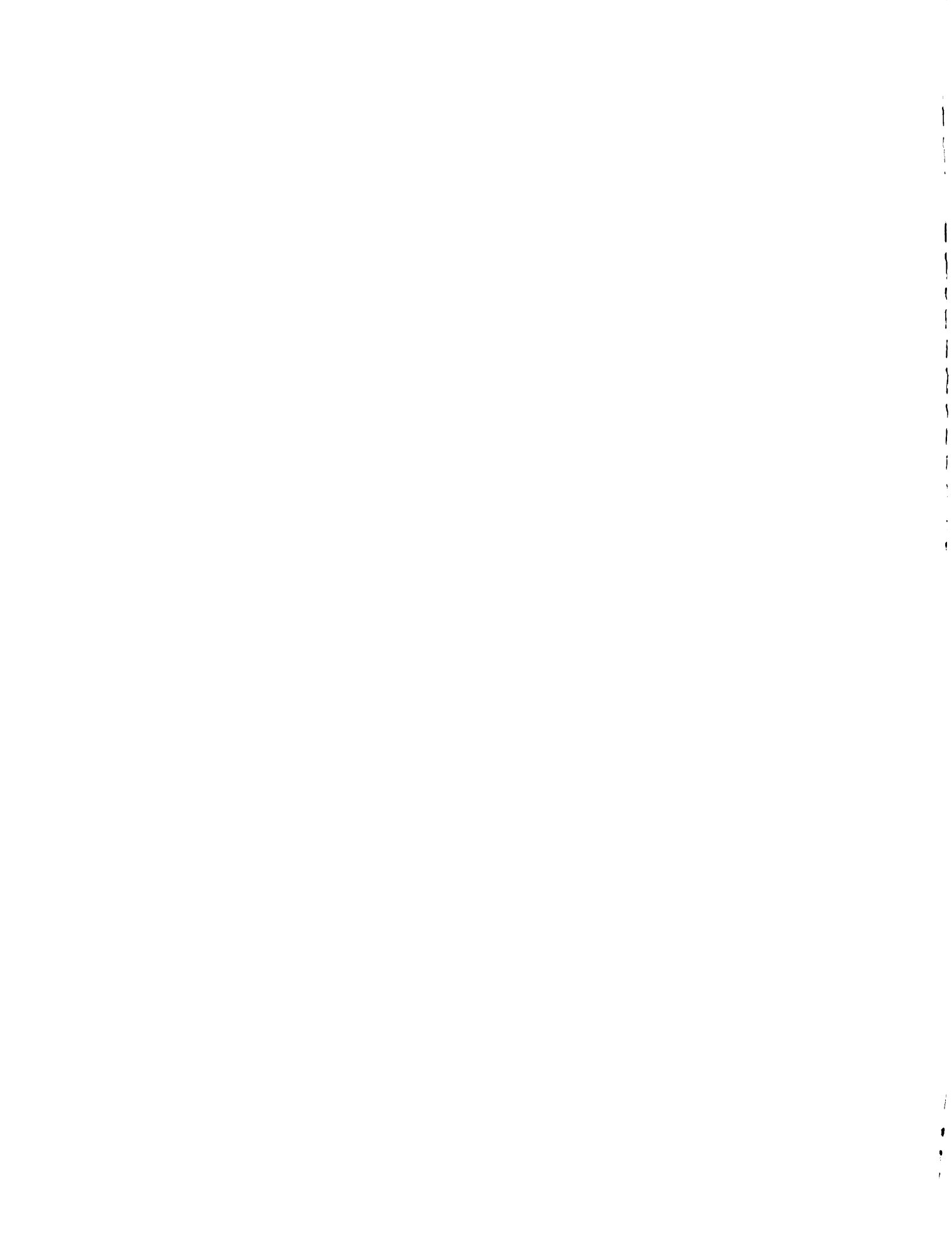
6% Cobalt

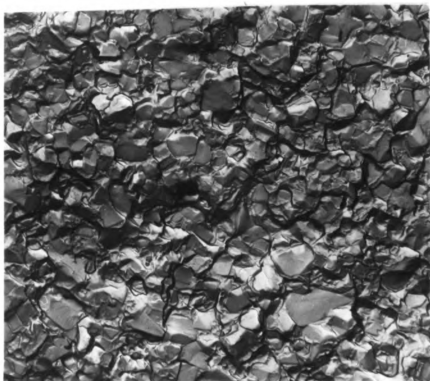
8μ GS



IMPACT

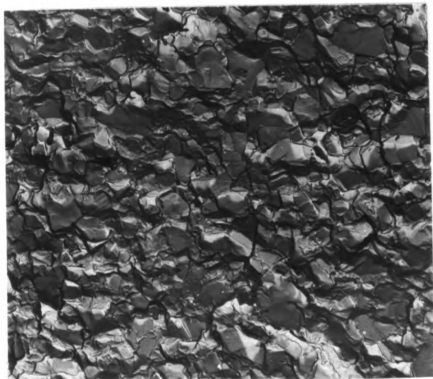
FAST FRACTURES 5000X





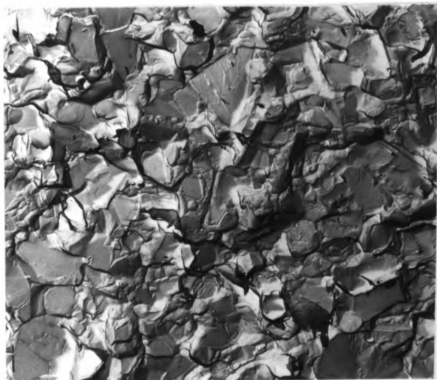
15% Cobalt

1.5 μ GS



15% Cobalt

1.5 μ GS



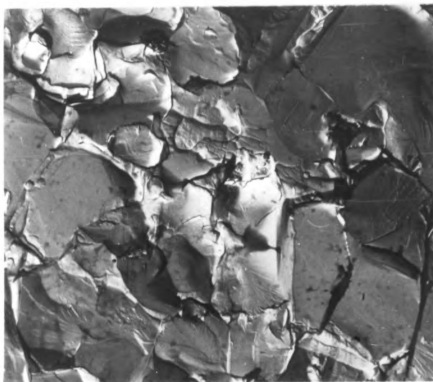
15% Cobalt

2.5-3 μ GS



15% Cobalt

2.5-3 μ GS



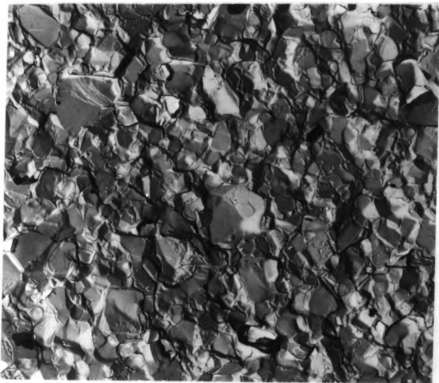
15% Cobalt

8 μ GS



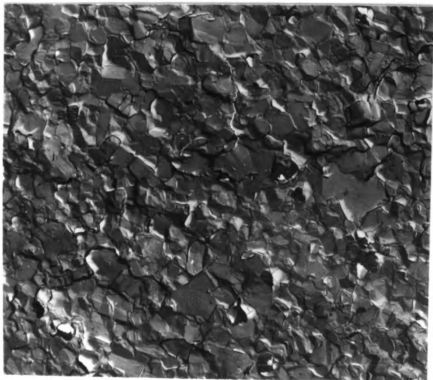
15% Cobalt

8 μ GS



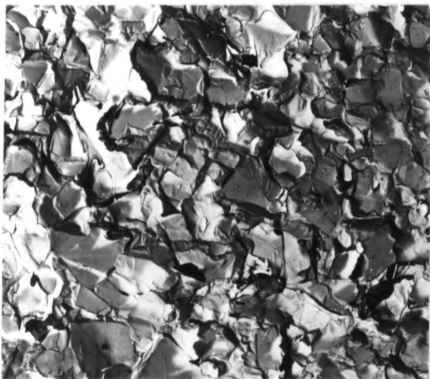
9% Cobalt

1.5 μ GS



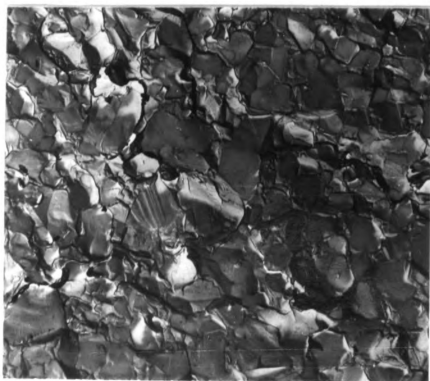
9% Cobalt

1.5 μ GS



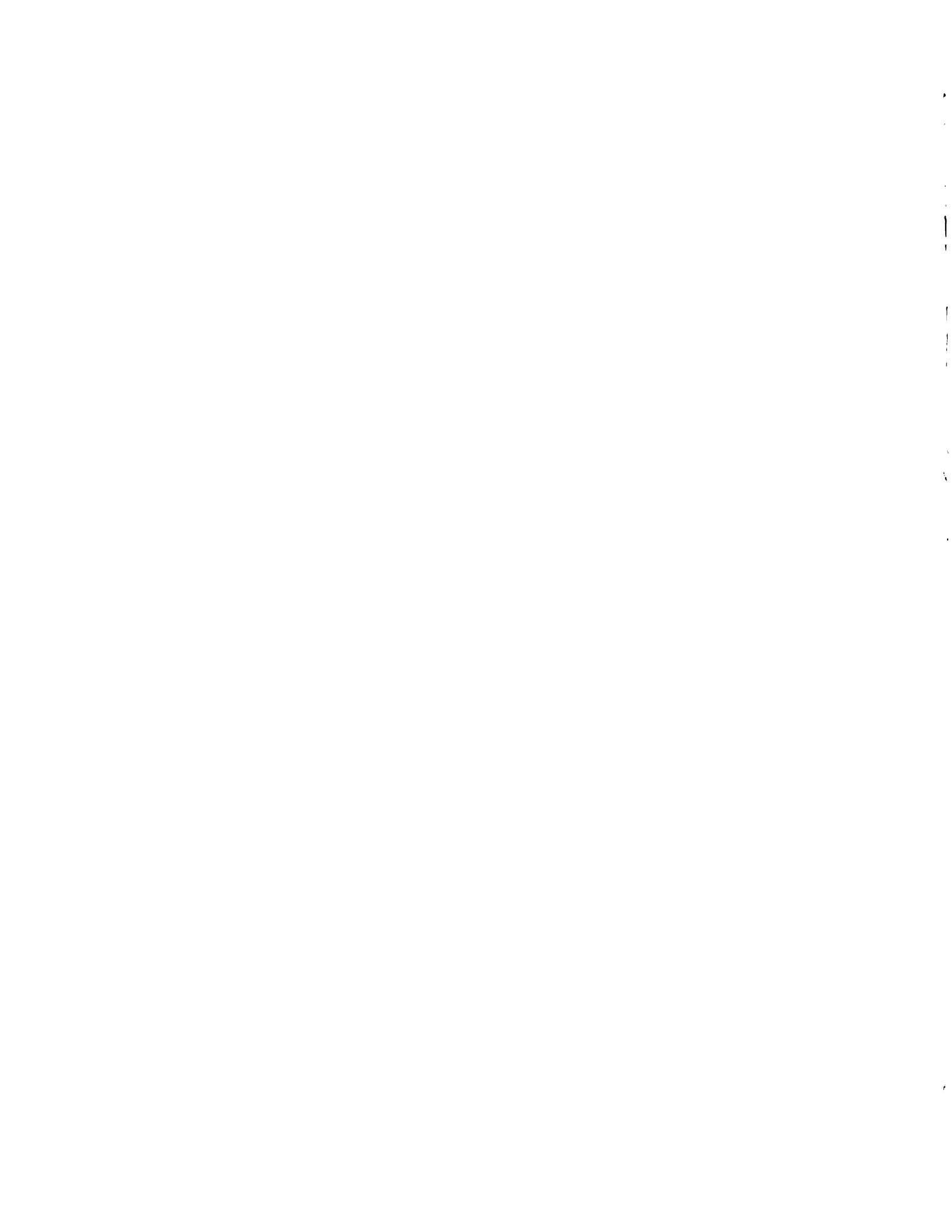
9% Cobalt

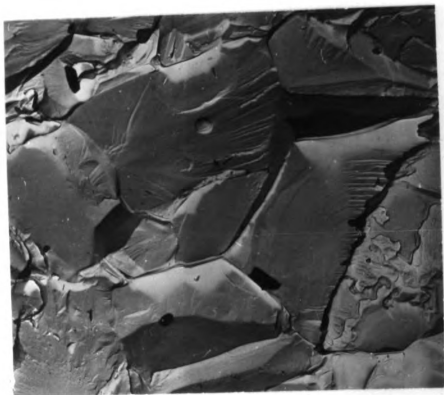
2.5-3 μ GS



9% Cobalt

2.5-3 μ GS





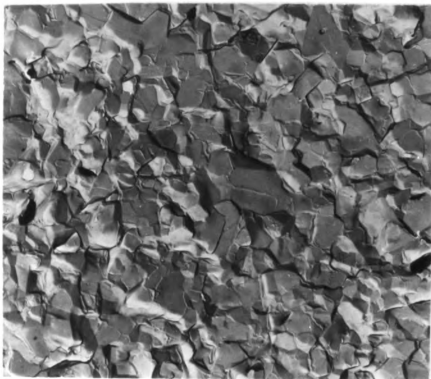
9% Cobalt

8 μ GS



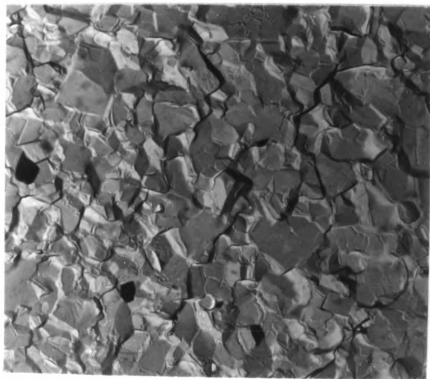
9% Cobalt

8 μ GS



3% Cobalt

1.5 μ GS



3% Cobalt

1.5 μ GS



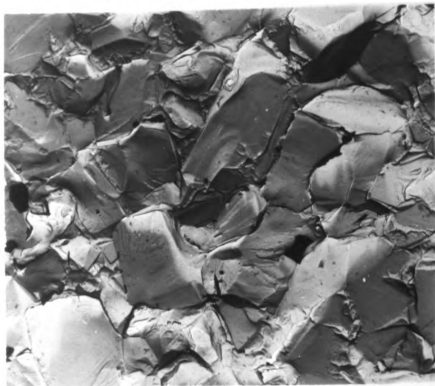
3% Cobalt

2.5-3 μ GS



3% Cobalt

2.5-3 μ GS



6% Cobalt

8 μ GS



6% Cobalt

8 μ GS

MICHIGAN STATE UNIVERSITY LIBRARIES



3 1293 03145 9237